NOTE TO USERS

This reproduction is the best copy available.

uOttawa

L'Université canadienne
Canada's university

FACULTÉ DES ÉTUDES SUPÉRIEURES ET POSTOCTORALES

uOttawa

L'Université canadienne
Canada's university

FACULTY OF GRADUATE AND POSDOCTORAL STUDIES

Benu Sethi

AUTEUR DE LA THÈSE / AUTHOR OF THESIS

M.A.Sc. (Biomedical Engineering)

GRADE / DEGREE

Department of Chemical and Biomedical Engineering

FACULTÉ, ÉCOLE, DÉPARTEMENT / FACULTY, SCHOOL, DEPARTMENT

Developing Novel Micro-Structured Biodegradable Hollow Fiber Channels for Functional Recovery After Spinal Cord Injuries

TITRE DE LA THÈSE / TITLE OF THESIS

Xudonp Cao

DIRECTEUR (DIRECTRICE) DE LA THÈSE / THESIS SUPERVISOR

CO-DIRECTEUR (CO-DIRECTRICE) DE LA THÈSE / THESIS CO-SUPERVISOR

EXAMINATEURS (EXAMINATRICES) DE LA THÈSE / THESIS EXAMINERS

Donald Russell

Michel Labrosse

Gary W. Slater

Le Doyen de la Faculté des études supérieures et postdoctorales / Dean of the Faculty of Graduate and Postdoctoral Studies

DEVELOPING NOVEL MICRO-STRUCTURED BIODEGRADABLE HOLLOW FIBER CHANNELS FOR FUNCTIONAL RECOVERY AFTER SPINAL CORD INJURIES

Benu Sethi

Thesis submitted to the

Faculty of Graduate and Postdoctoral Studies

In partial fulfillment of the requirements

For the MASc degree in Biomedical Engineering

Department of Chemical and Biological Engineering

Ottawa-Carleton Institute for Biomedical Engineering

Faculty of Engineering

University of Ottawa

Your file Votre référence
ISBN: 978-0-494-61186-9
Our file Notre référence
ISBN: 978-0-494-61186-9

Abstract

Traumatic spinal cord injury (SCI) is a devastating clinical condition that affects approximately 2.5 million patients across the world with 130,000 new injures being reported each year. Advances in research have provided better understanding of the complex pathophysiology after spinal cord injury, but so far no effective treatment has been able to provide functional recovery. Utilizing principles of tissue engineering, incorporation of a tubular implant at site of injury has gained considerable attention in recent years. The mechanical strength of the tubular implant, proposed for incorporation at site of injury, is very important for efficacy of the implant. In this project we have fabricated different types of hollow fiber channels (HFCs) with a porous morphology using dip-coating and sub-critical CO_2 process. The HFCs have been characterized, their mechanical properties have been tested *in vitro* and their degradation behaviour over time has been analyzed.

Among the different types of HFCs tested for mechanical properties, single layered, double layered and reverse porosity, presence of porosity gradient and its orientation plays an important role towards establishing the mechanical strength of the HFC. The porosity gradient results from the difference in pore sizes between the inner and the outer layer of the HFC. During our study we were able to satisfy two crucial parameters regarding the mechanical strength of the HFC. Firstly, it is important for the HFC to match its mechanical strength with that of spinal cord tissue and secondly, the ability of the HFC to possess optimal weight to avoid damage to the already injured tissue. Thus we were able to fabricate a tubular implant that has desired mechanical properties to be used after SCI.

Résumé

Les traumatismes médullaires bouleversent la vie de 2.5 millions de personnes à travers le monde. À chaque année, 130 000 nouveaux cas sont signalés. Aujourd'hui, la physiopathologie complexe de ce type de blessure est beaucoup mieux comprise. Malgré cette meilleure compréhension, aucun traitement efficace n'a été découvert qui permet une récupération fonctionnelle du patient. L'incorporation d'un implant tubulaire au niveau du site de la blessure, en utilisant les techniques de génie des tissus, a été un sujet d'intérêt majeur ces dernières années. La force mécanique de l'implant tubulaire, destiné à l'implantation, est essentielle pour l'efficacité de l'implant. Lors de ce projet, nous avons fabriqué par un dépôt par trempage et un procédé de CO_2 sous-critique différents types de canaux creux fibreux (Hollow fiber channels, HFC) dont la morphologie était poreuse. Les HFC ont été caractérisés, leurs propriétés mécaniques testées *in vitro* et leur dégradation au fil du temps analysée.

Parmi les différents types de HFC dont les propriétés mécaniques ont été caractérisées : monocouche, bicouche et porosité inverse, la présence d'un gradient de porosité et son orientation jouent des rôles importants dans l'établissement de la force mécanique du HFC. Les dimensions des pores de la couche intérieure et de la couche extérieure du HFC sont différentes créant le gradient de porosité. Lors de notre étude nous avons réussi à satisfaire aux deux paramètres primordiaux à la force mécanique du HFC. Premièrement, il est important que le HFC correspond à la force mécanique des tissues de la moelle épinière. Deuxièmement, le poids du HFC doit être optimisé afin de ne pas endommager les tissus affectés par les blessures. Nous avons réussi à fabriquer un implant

tubulaire avec les propriétés mécaniques désirées pour être utilisé après un traumatisme médullaire.

Acknowledgement

I would like to express gratitude towards my supervisor, Prof. (Dr.) Xudong Cao for providing guidance and support during the course of this research project. I am indebted to him for providing me with an opportunity to work in the pioneering field of spinal cord injuries.

I would also like to thank Dr. Jianqun Wang of Carleton University for providing necessary help while working on the SEM. Gratitude is also due to the staff members of the Machine Shop of Chemical and Biological Engineering Department for providing the necessary equipment for the project.

I am also indebted to the management of University of Ottawa for providing me the scholarship, without which it was not possible to complete the Graduate Studies.

I am also thankful to my colleagues for the whole-hearted support they have extended from time to time.

Last but not the least, I am also thankful to my family for the motivation and constant encouragement.

Table of Contents

List of Figures

List of Tables

Abbreviations

ASTM	American society for testing and materials
BBB	Blood-brain barrier
BDNF	Brain-derived neurotrophic factor
BSA	Bovine serum albumin
CE	Conformit Europe
CNS	Central nervous system
CSF	Cerebrospinal fluid
DMSO	Dimethylsulphoxide
FDA	US Food and Drug Administration
HEMA	2-hydroxy ethyl methacrylate
HFC	Hollow fiber channels
HFM	Hollow fiber membranes
MA	Methacrylate
MMA	Methyl methacrylate
NaCl	Sodium Chloride
NGF	Nerve growth factor
Ni-Cr	Nickel-Chromium
NSC	Neural stem cells
PAN/PVC	Poly(acrylonitrile-co-vinylchloride)

PBS	Phosphate buffer saline (physiological media)
PCL	Poly (ε-caprolactone)
PEG	Poly(ethylene glycol)
PGA	Poly(glycolic acid)
PHA	Poly(hydroxy-alkanoates)
PHB	Poly(β-hydroxybutyrate)
PHEMA	Poly(2-hydroxyethyl methacrylate)
PHEMA-MMA	Poly(2-hydroxy-ethyl methacrylate-co-methyl methacrylate)
PHPMA	Poly[N-(2-hydroxypropyl)methacrylamide]
PLA	Poly(lactic acid)
PLCL	Poly (lactide-co- ε-caprolactone)
PLGA 50:50	Poly (DL lactide-co-glycolide) with 50:50 monomer ratio
PNS	Peripheral nervous system
rhEGF	Recombinant human epidermal growth factor
$scCO_2$	Supercritical CO_2
SCI	Spinal cord injury
SEM	Scanning electron microscope
THF	Tetrahydrofuran
TIPS	Thermally induced phase separation
WPI	Wet phase inversion

Symbols

Symbol	Name	Unit
d_o	Outer diameter of HFC	mm
d_i	Initial diameter of HFC	mm
d_f	Final diameter of HFC	mm
E^*	Modulus of elasticity of foamed HFC	kPa
E_s	Modulus of elasticity of solid polymer	MPa
I	Second moment of area	mm^4
I.V.	Inherent Viscosity	dL/g
kPa	Kilo Pascal	kPa
l	Length of HFC	mm
l_i	Initial length of HFC	mm
l_f	Final length of HFC	mm
$l_{DoubleLayered}$	Length of the entire double layered HFC	mm
M_i	Initial mass of the HFC without the bag	
	at Week0	g
M_0	Mass of the HFC enclosed in the bag at Week0	g
$m_{DoubleLayered}$	Mass of the entire double layered HFC	g
$m_{InnerLayer}$	Mass of inner layer of PLGA 50/50	g
$m_{OuterLayer}$	Mass of outer layer of PLCL/PCL_3/1 blend	g

M_t	Mass of the HFC enclosed in the bag at Week t	
	(t refers to time point such as Week 1, 2, 3 ... 10)	g
M_w	Molecular weight	g/mol
N	Newton- unit of force	N
r_o	Outer radii of the double layered HFC	mm
r_i	Inner radii of the double layered HFC	mm
r_6	Denotes the radii of entire inner layer	
	of PLGA 50/50 (since there are 6 dip coats)	mm
t_f	face thickness of cell member in the	
	foamed structure of HFC	μm
t_e	edge thickness of cell member in the	
	foamed structure of HFC	μm
T_g	Glass Transition Temperature	°C
$V_{InnerLayer}$	Volume of inner layer of PLGA 50/50	mm^3
V_{PLGA}	Volume of single layered HFC	mm^3
$V_{OuterLayer}$	Volume of outer layer of PLCL/PCL_3/1 blend	mm^3
w	Weight of HFC	g
w/v	Weight/volume ratio of the polymer/solvent	g/ml
w/w	Weight/weight ratio of the polymer/polymer	-
α' and β'	constants of proportionality	-
ρ^*	Density of foamed HFC	g/ mm^3

ρ_s	Density of unfoamed HFC	g/ mm^3
ρ_{PLGA}	Density of single layered HFC	g/ mm^3
ε	Strain	-

1. Introduction

1.1 Spinal Cord Injury (SCI)

All over the world approximately 2.5 million patients live with spinal cord injuries (SCI) [1] and it has been estimated that 130,000 new injuries are reported each year [4] with an average of 10,000 cases being reported from the United States alone [5]. Some of the main factors that cause spinal cord injury are road accidents, diving injuries, accidental falls and gunshot wounds. Patients suffering from SCI have a low quality of life, are restricted to bedside and due to loss of income, often have accumulated financial burdens given the high costs associated with primary clinical care. As a result of loss of sensory and motor functions beyond the site of injury, the patients suffer from loss of limb function, multiple health problems such as urinary tract infection, pressure sores and other cardiac and respiratory disorders. SCI patients have reduced life expectancy and require extensive care for their daily living which is both challenging and exhaustive. It has been estimated that the total cost involved for all SCI cases in the US is to the tune of $7.736 billion [5] per year and poses an enormous burden on the health care system that provides for the basic necessities of these patients.

Advances in research in the field of SCI during the last twenty years [4, 6] has forged better understanding of the physiological conditions after injury and has enabled emergence of several regenerative strategies that seem promising. These strategies involve application of intricate principles of tissue engineering that involve combination of some or all elements such as tubular implants [7-10], neutralization of molecules that inhibit tissue regeneration [1, 11, 12], introduction of conducive cells and growth factors to provide a permissive

environment for tissue regeneration and eventually help reverse some of the devastation of SCI. However given the complex pathophysiology of SCI, functional recovery has remained elusive so far.

In our project, we hope to take a step in the right direction by proposing a strategy that may help in obtaining functional recovery after the SCI. Before suggesting our approach, a brief understanding of the anatomy of the nervous system and changes introduced within it after SCI is necessary. The knowledge of complex mechanism at play after the SCI is important to prepare one for the challenges that are faced while dealing with body's inherent response to spinal cord injury.

1.2 Nervous System in the Human Body, its Injury and Regeneration

The nervous system in the human body helps in coordinating activities within the different systems of the body by permitting communication, control and integration of bodily functions [13]. Homeostasis, the normal condition of the human body, is maintained successfully by the nervous system as it detects the changes that occur in the external and internal environment of the body, known as stimulus, evaluates the information received, assesses it and thereby provides an appropriate response to this stimulus. Based on the anatomy, different parts of nervous system that work in coordination with each other [14-16], are described below and shown in Figure 1.1:

i) Central Nervous System (CNS): As suggested by its name, CNS provides a central functionality within entire nervous system by behaving as the

principal integrator of sensory input and motor output. The CNS is responsible for receiving sensory information, evaluating it and then initiating an outgoing response. The CNS is comprised of the brain and the spinal cord that are protected by bony and membranous coverings along with the presence of cushioning fluid known as cerebrospinal fluid (CSF) [14]. Besides protecting it, the CSF also circulates in CNS along with blood, to monitor changes in the internal environment. Within CNS the barrier of cellular membranes that separates brain tissue and CSF from being in direct contact with blood is known as the blood-brain barrier (BBB). Structurally it is constituted of tight sheaths formed between astrocytes projections and endothelial cells of brain capillaries. The BBB maintains a stable environment that is required for normal functioning of the brain [16].

Spinal cord within the CNS has the important responsibility of providing routes to conduct information being transmitted in form of nerve impulses to and from the brain. Spinal cord accomplishes this task with help of two types of tracts essentially composed of bundles of axons (axons are discussed in detail in the next section) known as ascending and descending tracts. Ascending tracts conduct sensory impulses up the cord to the brain and descending tracts conduct motor impulses down the cord from the brain. Spinal Cord also serves as the reflex centre for all spinal reflexes [13].

ii) Peripheral Nervous System (PNS): This part of the nervous system is named as such since it consists of all the nerve tissues that lie within the peripheral

regions of the nervous system, outside the CNS. The PNS consists of cranial nerves that originate from the brain and carry impulses to and from it, and the spinal nerves that originate from the spinal cord and carry messages to and from it [13].

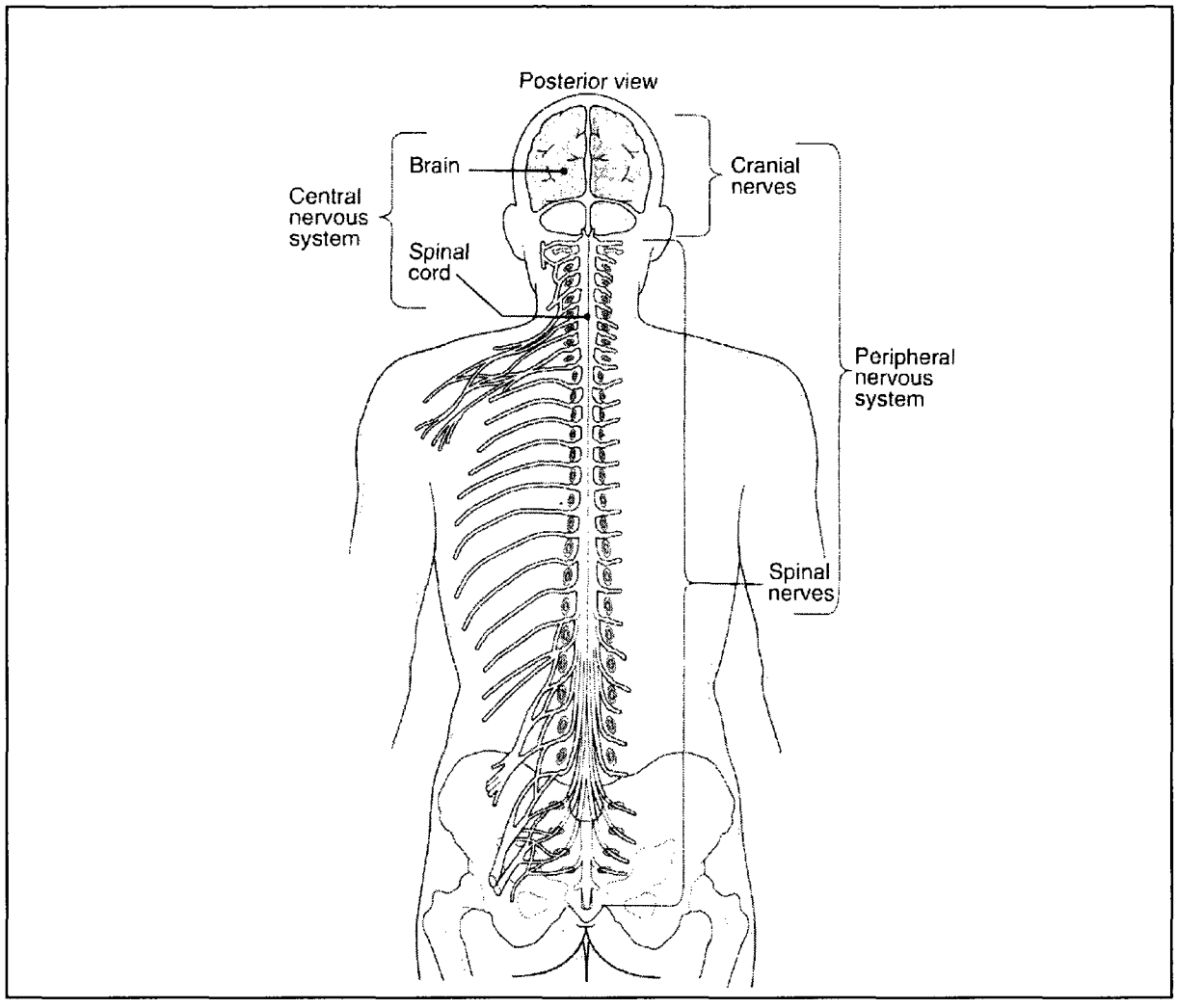

Figure 1.1 Anatomy of human body depicting central nervous system and peripheral nervous system. Figure adapted from Reference [13]

Within the nervous system, there exist mainly two types of cells: neurons and glial cells. Neurons are specialized excitable cells that receive and transmit electrical and chemical signals by conducting impulses, thus completing the circuitry functions within the nervous system. Neurons exist within both CNS and PNS and are the main building blocks of nervous system. Neurons are often distinguished by the presence of a cell body and a long process that is a threadlike extension of cytoplasm and is known as an axon as shown in Figure 1.2 [13]. An axon usually has one or more side branches called axon collaterals and one or more dendrites. The primary job of an axon is to transmit neural messages by conduction of nerve impulses from cell body to end of the neuron. On the other hand, dendrites and the cell body mainly act as the input zone that receives nerve stimulation and initiates nerve impulses in response [15].

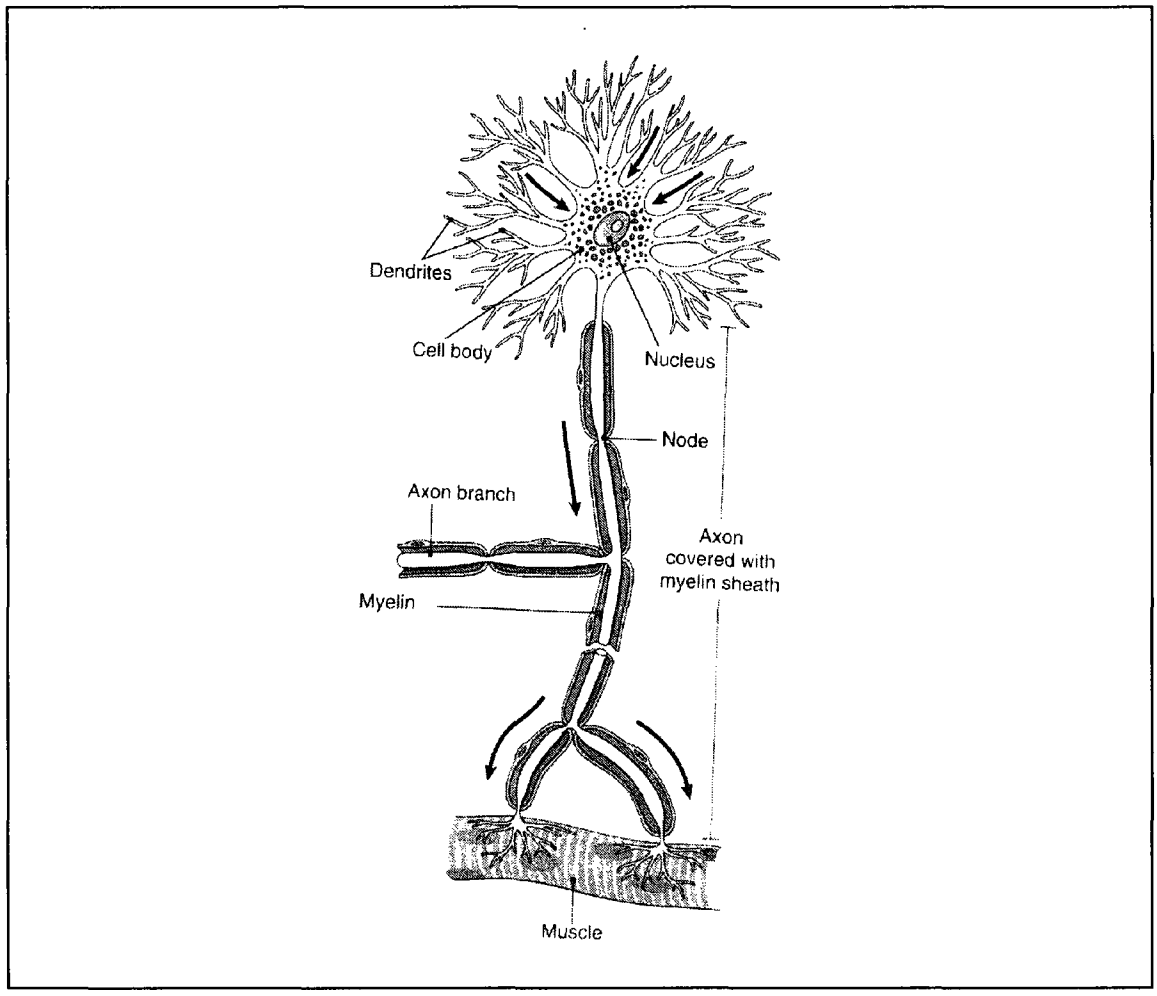

Figure 1.2 Structure of a neuron. Figure adapted from Reference [13]

Glial cells have always been understood to exist for supporting the function of neurons. But with turn of the century, glial cells are being much appreciated for their dynamic role in nervous system given their capability of carrying out major functions such as regulating the composition of extracellular fluid within the CNS [15]. Glial cells are also known for their ability to regenerate. Four types of glial cells that exist within CNS are astrocytes, microglia, ependymal cells and oligodendrocytes; within PNS there exists only a single type of glial cell namely the Schwann cells. The functions of different types of glial cells are briefly described below and their structures are shown in Figure 1.3:

i) Astrocytes: are the most numerous type of glia and are star-shaped. They have long delicate processes that extend through the brain tissue by attaching neurons to blood capillaries of the brain. They perform important functions such as feeding the neurons by converting glucose from blood and converting it into lactic acid for neurons. Their role in presence of the blood-brain barrier has already been described. Recent findings suggest that astrocytes influence growth of neurons and manners in which they form neural circuits [15].

ii) Microglia: are small sized, usually stationery cells in CNS. Upon damage to the brain or spinal cord tissue, they enlarge in size and act as macrophages thereby performing phagocytosis by engulfing and destroying microorganisms and cellular debris [15].

iii) Ependymal cells: resemble epithelial cells and form thin sheets that line the fluid-filled cavities in brain and spinal cord. Some of these cells also take part

in producing fluid that fills these spaces while others have cilia that keep the fluid circulating within the cavities [15].

iv) Oligodendrocytes: are smaller in size and have fewer processes as compared to astrocytes. They help in holding the nerve fibers together and their most important function is to produce myelin sheath around nerve fibers in the CNS that improves the conduction of electric impulses [15].

v) Schwann cells: exist only in the PNS, support functions of nerve fibers and also produce myelin sheaths in some cases. Schwann cells have the ability to wrap themselves around a single nerve fiber in layers and presence of myelin, a white fatty substance, in their cell membrane helps to ensheath these nerve fibers. Myelin sheath is important for transmission/conduction of electric impulses along nerve fibers and within a neuron, only axons have myelin sheath and not the dendrites. This function of ensheathing the nerve fibers, is performed by Schwann cells in PNS and oligodendrocytes in CNS [15].

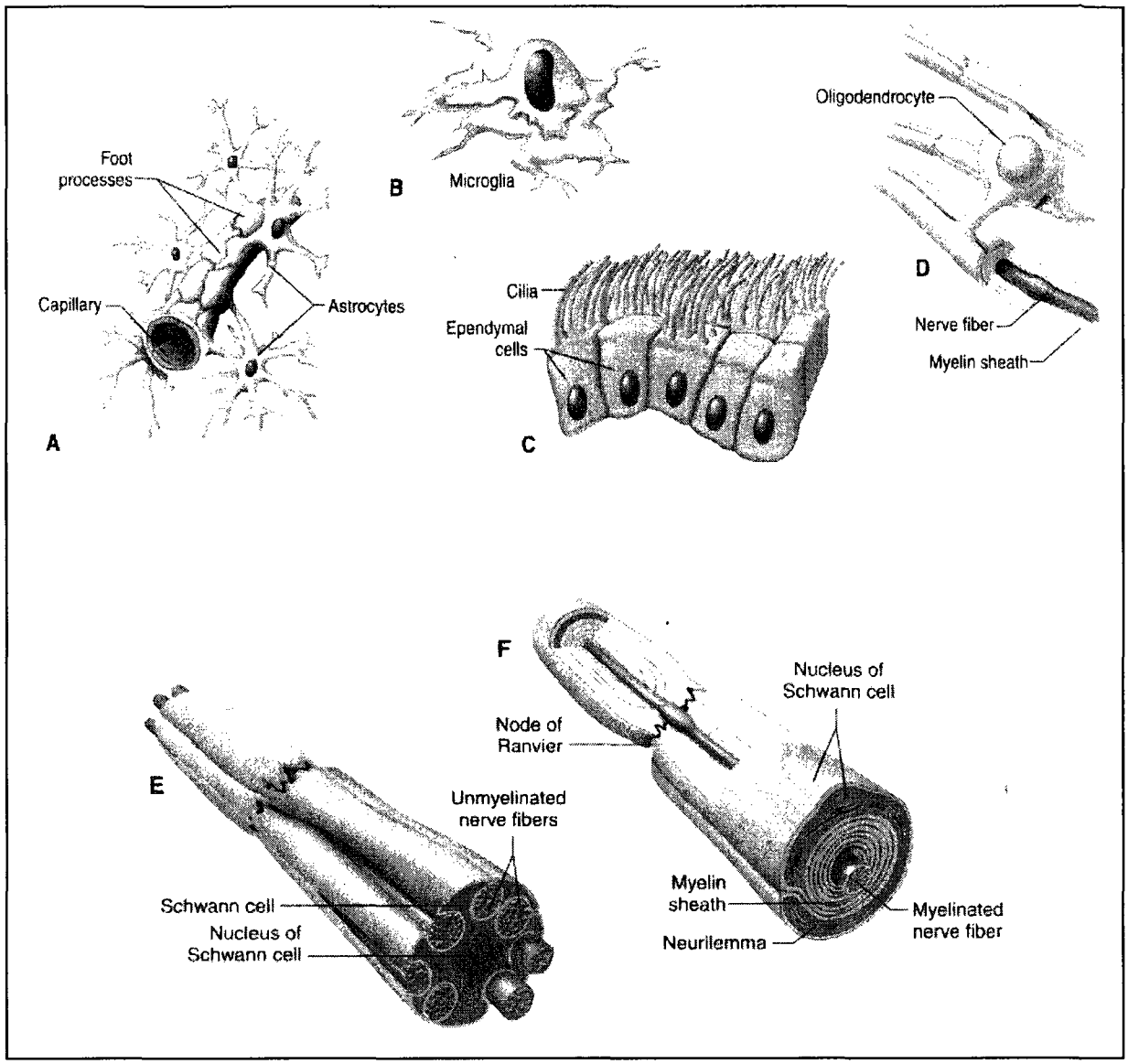

Figure 1.3 Different types of glial cells that exist in the nervous system (A) astrocytes (B) microglial cell (C) ependymal cell (D) oligodendrocytes (E) and (F) two types of schwann cells. Figure adapted from Reference [15]

1.2.1 Spinal Cord Injury and associated Physiological changes

Spinal cord injury can be classified as traumatic or non-traumatic. A sudden traumatic physical impact as a result of vehicular accidents, diving injuries, accidental falls or gunshot wounds can fracture the bony structure of spinal column that protects the spinal cord tissue and cause considerable damage to the spinal cord tissue. Non-traumatic injuries, on the other hand, occur due to medical conditions such as arthritis, cancer, inflammation or infections, or disk degeneration of the spine. Injuries to the spinal cord in any form, can lead to dislocation, compression known as contusion injury, or even create a wound that penetrates and cuts the spinal cord, known as transection injury [17].

In our research work we have focussed on transection model of spinal cord injury. It is decidedly the most challenging scenario, given the extent of lesion that completely destroys communication and basic functionality between the two ends, proximal and distal, of the injured spinal cord [5, 18], that upon transection are also known as rostral and the caudal ends.

SCI drastically affects the normal functioning of the spinal cord and leads to disconnect in the motor and sensory communication pathways, thus affecting functionality below the site of injury. Primary damage after SCI involves death of cells existing within spinal cord including neurons, oligodendrocytes, astrocytes & precursor cells, and formation of cysts & cavities that may interrupt the descending and ascending axonal tracts [4]. Given the non-proliferative characteristic of neurons, their death leads to loss of function, whereas death of axons causes disconnect in the communication pathways between the CNS and the PNS. After the initial injury, a secondary injury known as the glial scar arises that causes

additional structural damage and functional loss. Although the formation of glial scar is body's inherent mechanism to stabilize the fragile CNS tissue after injury and to help repair the blood-brain barrier and prevent an overwhelming inflammatory response to limit cellular degeneration [6], it has an extremely inhibitory effect on regeneration.

Glial scar is comprised of reactive astrocytes that form a tight boundary with their processes [19], transmembrane molecular inhibitors of axonal growth, macrophages and local microglia that perform phagocytosis [4]. All these factors combine to create an inhibitory environment within glial scar that present a physical barrier [20], and thus the lack of pathway, for regeneration of axons. Over time the glial scar develops to become rubbery, tenacious, growth-blocking membrane [6].

1.2.2 Injury and Regeneration mechanism in PNS

Although CNS and PNS constitute the two subsystems within nervous system, often a comparison is made between their respective regeneration mechanisms after injury. The reason for this is quite evident. Being entities of the same nervous system it has been observed that post injury, PNS possesses the ability to regenerate itself due to the permissive environment provided at site of injury, even though efficiency of regeneration is dependent on the gap of injury. CNS on the other hand, has a complex and inhibitory environment that does not encourage axonal regeneration by itself.

Injury to PNS causes damage to nerves leading to functional loss in the associated muscles and sensory organs. Literature indicates that this damage occurring in peripheral

nerves can be shown to be partially reversible since they have the capacity for self-regeneration [21]. Presence of Schwann cells in the PNS helps in guiding damaged axons, from the proximal to the distal stump of injured nerve fiber, and eventually establishes their communication once again. After the axons have been injured, cellular changes cause degradation of the distal nerve stump. Axons are then surrounded by Schwann cells at the distal stump that proliferate rapidly to form narrow tubes using their extensions, known as bands of Bünger. These bands of Bünger provide a mechanical support and guide the axonal migration. The debris from injury is cleared within a duration of approximately 7 months in cases of human beings and regeneration of axons begins from proximal end, towards the distal end [22]. Some other factors that contribute to regenerative mechanism are cell adhesion molecules and extracellular matrix [20].

The extent of regeneration of peripheral nerves is dependent on size of gap arising as a result of injury, age group of the individual etc. When the transected gap between nerve ends is greater than 2 cm, nerve autografts are recommended to obtain functional recovery after injury [23-25]. Though use of autografts is considered as the gold standard, some of the issues associated with it are morbidity at donor site, formation of neuromas, structural differences between donor and recipient grafts and limited availability of material for extensive repair [23]. These issues, as shown by extensive research, are being addressed by use of tubular conduits or nerve guides that are fabricated from biocompatible materials to aid in nerve regeneration over longer gaps [26-31].

Given the regenerative mechanism within PNS due to presence of a more permissive environment, it proves to be a good learning model that can assist in arriving at a suitable regenerative technique for spinal cord injuries [6].

1.3 Role of Tissue Engineering

Tissue engineering is an evolving area of research and can be defined as "the application of principles and methods of engineering and life sciences toward fundamental understanding of structure-function relationships in normal and pathological mammalian tissues and the development of biological substitutes to restore, maintain, or improve tissue function" [32]. Within the realm of tissue engineering, scaffolds can be utilized for developing new tissues or repairing and regenerating injured tissues. The scaffold can direct growth of cells, usually in presence of growth promoting factors and thereby aid in tissue development.

Based on their crucial application, the scaffolds must possess adequate physical properties such as mechanical strength and porous morphological structure. Mechanical strength of the scaffold plays an important role in helping maintain its *in vivo* efficacy given the presence of biomechanical forces at the site of implantation. Also the scaffold must be strong enough to support and stabilize the tissue that it is helping to regenerate. Porous structure of the scaffold helps in cellular growth of the tissue by providing a substrate to which cells can attach and grow. Also this morphology can be utilized to seed cells and thus aid in their proliferation, growth and differentiation. The scaffold must be biocompatible and not give rise to any adverse infections or inflammation *in vivo*, post implantation.

Depending on the application of the scaffolds, it may be desirable to have degradable material for the fabrication of the scaffold, especially if the tissue is expected to support further tissue growth and development. Absence of any synthetic remains once the tissue regeneration is well underway proves to be beneficial since the probability of infection and chronic inflammation are reduced. However the time of degradation of the scaffolds should match closely with the rate of tissue regeneration so that the developing tissue continues to have the support of the scaffold till needed [33].

Injuries to the spinal cord result in significant loss of original neural tissue that comprises the complex and well arranged architecture of cells and extracellular matrices. Utilization of concepts of tissue engineering can be attempted to help regenerate the damaged neural tissue, by implanting a scaffold at site of injury. The main aim of implantation of a scaffold after SCI is to achieve functional recovery and reversal some of the SCI effects.

1.4 Concept of Tubular Strategies

SCI leads to disconnect in axonal tracts that affects functionality below the site of injury. As has already been discussed, after injury a cascade of events known as secondary injury leads to formation of glial scar thereby creating an inhibitory environment resulting in inability of axonal regeneration.

To reverse the effects of SCI and lead to functional recovery, it is necessary that the severed axons be allowed to regenerate and reconnect. The conceptual design of a hollow

tubular implant, as proposed by others and us [18, 34-45], involves enclosing the rostral and caudal ends of the transected spinal cord within it. The tubular implant is intended to act as a structural bridge that prevents formation of scar tissue and serves as a protective casing to support axons in extending from inhibitory boundary of glial scar to a permissive environment of uninjured CNS [7]. A schematic representation is shown in Figure 1.4. It is necessary for this implant to possess adequate mechanical strength so that it can support the rostral and caudal ends of the injured spinal cord during the regeneration process. It is aimed that by providing such a conducive environment, the regeneration and reinnervation of axons beyond the glial scar can be encouraged. It is known from literature that axons do not lose their regenerative ability after injury [6, 46] due to the presence of 'growth cones' within the dystrophic endbulbs of transected axons that still have their viability maintained after injury. Therefore when provided with a growth permissive environment, it is possible for the axons to re-grow.

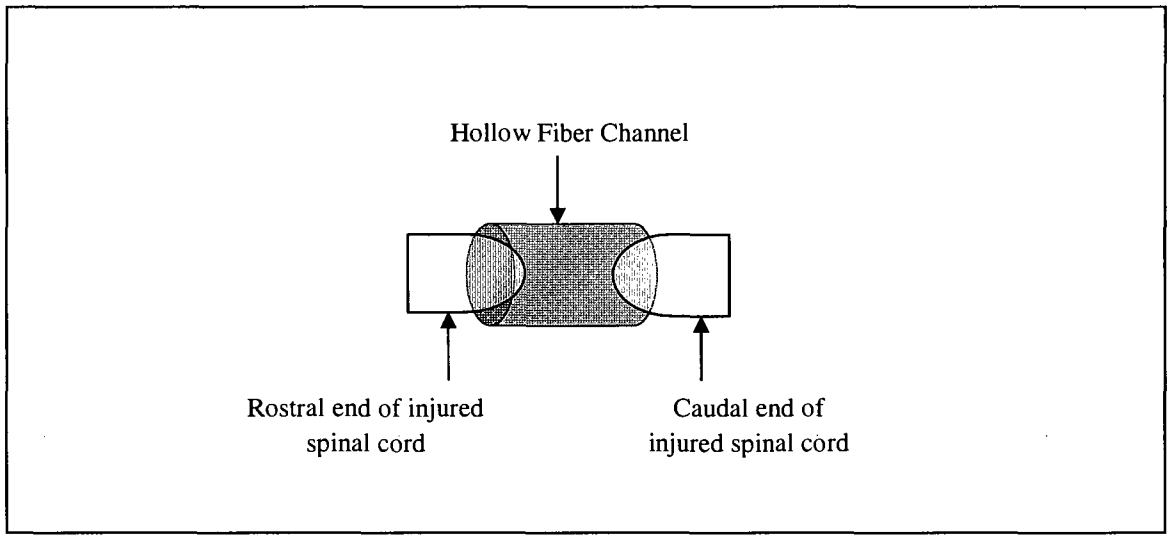

Figure 1.4 Schematic design of tubular strategy after SCI

The choice of material for fabrication of the tubular implant is an important criterion. Use of biodegradable biomaterials in this regard is advantageous since they are completely resorbed in the body, after having served their purpose [37-39, 47]. On the other hand, tubular implants fabricated from non-degradable biomaterials continue to be present in the body after their purpose has been served [18, 34-36, 41, 42, 45]. A secondary surgery performed for removal of these implants can be detrimental to the process of tissue regeneration at site of injury [33]. Use of non-degradable materials has been shown to lead to formation of a fibrous capsule on outer surface of tubular implant along with occurrence of calcification in some studies [18] and an inflammatory response characterized by presence of macrophages and foreign body giant cells, in other studies [34].

Implantation of a biodegradable tubular implant, can promote process of tissue regeneration, and upon complete degradation can be replaced by the newly developed tissue, without the presence of a foreign material over extended course of time. To successfully achieve this task, it is important to closely match the rates of tubular implant degradation & tissue development, for continued mechanical and structural support to the developing tissue [33].

One of the challenges associated with use of biodegradable materials for fabrication of tubular implants, is to provide the implants with suitable mechanical strength. Mechanical strength is a very important physical property of the tubular implant necessary for providing structural support and stability to injured spinal cord tissue *in vivo*. In different species, the entire spinal cord has an elastic modulus ranging between 230 to 600 kPa including the membranous pia mater [35]. Given the above, mechanical properties of the tubular implant

should be designed to closely match those of the spinal cord tissue. A weak tubular implant has been shown to collapse *in vivo*, due to thinning of the tubular wall brought about by combined action of compressive forces and phagocytosis leading to its collapse at site of injury [34]. Alternatively an excessively strong tubular implant can damage the surrounding tissue due to its undesirable rigidity. As shown by Nomura et al. [43] use of coil reinforced guidance channels, led to formation of syringomyelic cyst formation causing further deterioration to the tissue regeneration process. In both circumstances, the process of nerve regeneration was adversely affected, clearly due to mechanical strength mismatch.

While making an effort to design a tubular implant with enhanced mechanical properties, it is important to regulate its mass to avoid any further damage to the already injured tissue. The biodegradable implant with a higher mass will undesirably lead to an increased accumulation of acidic by-products upon its degradation whereas a tubular implant with low mass may not extend desirable mechanical properties. The solution to this problem lies in carefully regulating the mass of the tubular implant. A suitable model that presents itself in nature is that of human bone. Bone is renowned for its excellent load bearing capacity, being a tissue that achieves an accurate compromise between its mechanical strength and optimum weight [48]. Presence of a porosity gradient within the two layers of bone structure, inner layer being more porous than outer layer, gives the bone its unique capability. Figure 1.5 shows the cross section of the bone tissue. By mimicking the conceptual design of bone within the tubular implant, even with use of biodegradable materials, it may be possible to offer adequate mechanical strength along with an optimum weight.

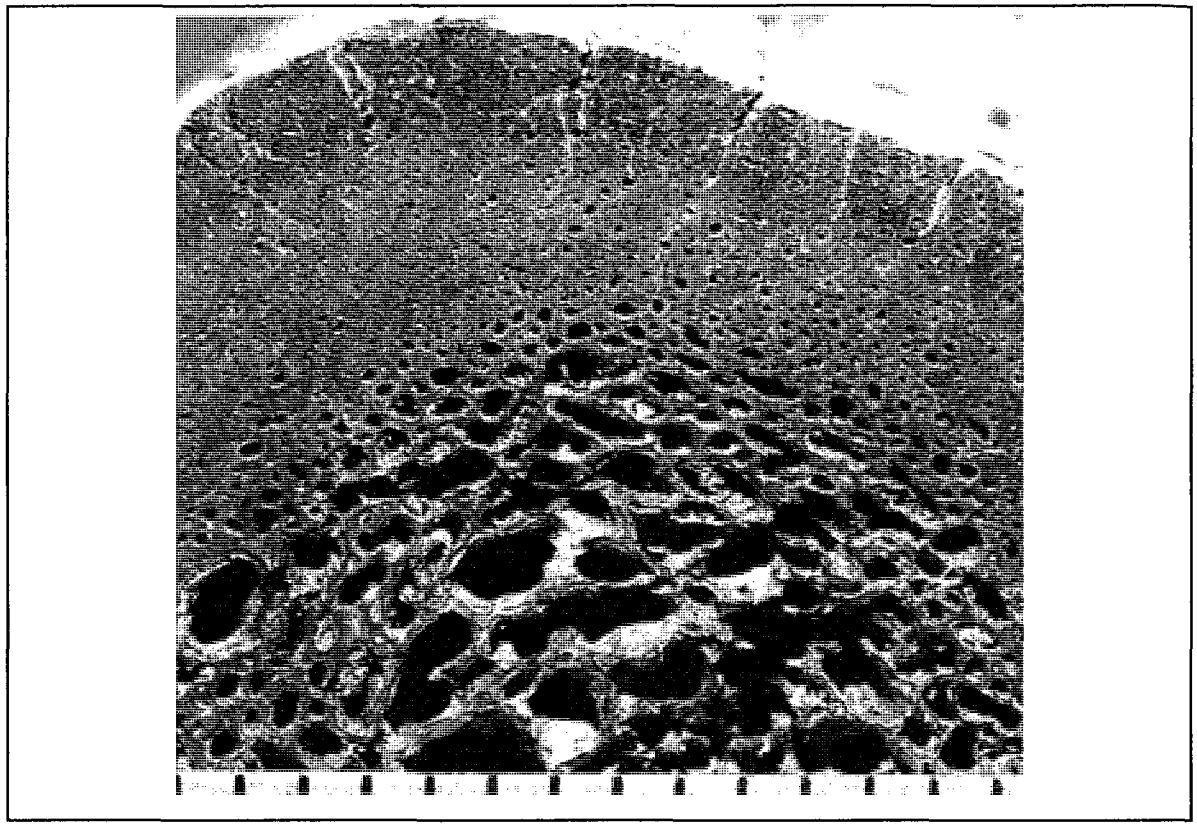

Figure 1.5 Cross section of bone tissue shows the porosity gradient between the outer and inner layers

Within the realm of tissue engineering, fabrication of scaffolds with gradient structures has been attempted in the past. However, the application of gradient structured scaffolds has so far, never been utilized for providing mechanical strength to tubular implants that are used for tissue regeneration after SCI. Harley et al. [49] fabricated porous tubular scaffolds with gradient in porosity and pore size, along the radius of the scaffold. The concept was to study the direction of growth of myofibroblasts after peripheral nervous injury, and this was achieved by making the inner wall of the tubular scaffold completely permeable to cell growth in contrast to cell-impermeable outer layer. Several other approaches, for repair or replacement of tissues or organs, using the concept of functionally graded scaffolds has also been researched [49-52]. Each layer of such functionally graded scaffolds is designed to perform a desired biological function based on the fact that different pore sizes encourage growth of different cell types. The presence of a porosity gradient within such scaffolds provides it the desired mechanical strength. Such conceptual designs of the scaffold, achieved by conventional and rapid prototyping techniques, mimic the structural arrangement of naturally occurring tissues or organs where each layer is designed to perform specific biological, mechanical and anatomical functions [50]. Interactions between different cell or tissues, growing within a single scaffold with different pore sizes were also studied by Oh et al. [51] who developed cylindrical scaffolds with porosity gradient along the longitudinal direction using a centrifugation method, to study such cellular interactions. In addition Zein et al. [52] used fused deposition modeling technique, equipped with an extruder that deposited semi-molten polymer material layer by layer to create tissue engineering scaffolds with a porosity gradient. Centrifugation, freeze drying,

conventional and rapid prototyping are some of the other techniques that have been attempted for creation of porosity gradient within the scaffolds [49-51].

Presence of a porous structure of the tubular implant from the perspective of tissue engineering can further help in the overall tissue regeneration process at the site of spinal cord injury. The pores within the implant can maximize cell attachment, proliferation & differentiation along with vascularisation and tissue growth [7, 47, 51].

In view of the above discussion, we propose a tubular structure known as the hollow fiber channel (HFC) to be used for implantation after spinal cord injury. The HFC has been proposed to be fabricated using biodegradable polymers and must be designed to possess adequate mechanical strength with an optimum mass and desirable porous morphology. The project goals listed below include design, development and fabrication of the HFC along with techniques to analyze and assess its physical properties such as mechanical strength, degradation behaviour *in vitro*.

1.5 Project Goals

The goals of this project have been listed as follows:

a) To fabricate degradable HFCs by dip-coating and sub-critical CO_2 process.

b) To characterize and compare different types of HFCs and test their mechanical properties *in vitro*.

c) To follow the degradation performances of the HFCs over time in vitro.

1.6 Hypotheses

A degradable HFC with layered porosity that mimics the porous bone structure will be mechanically strong for a given unit mass for potential applications in SCI repairs.

2. Literature Survey

This project establishes the fabrication technique of hollow fiber channel, a tubular implant that has been proposed by us for reversing the devastating effects of SCI, and analyzes its physical properties *in vitro*. For its efficacy, it is important for the HFC to possess adequate mechanical strength, porosity and suitable rate of degradation. In this literature survey we discuss a wide range of tissue engineering strategies, including scaffolds and tubular implants, proposed by other research groups for purpose of bringing functional recovery after SCI. We also discuss the different methodologies used to introduce porosity gradient within tubular implants and techniques to establish their mechanical strength.

2.1 Regenerative Strategies after SCI

From discussion in the previous chapter, it can be stated that regenerative response of adult mammalian spinal cord is not encouraging due to the inhibitive environment that exists after injury. A study performed by Ramon Cajal in 1928 was the starting point indicating towards the regenerative ability of damaged axons after SCI. With use of peripheral nerve implants at site of injury in the spinal cord, it was shown that axons exhibited regeneration having been provided a growth permissive environment. Interestingly in this case it was established that within peripheral nerve grafts presence of Schwann cells, also known for their regenerative role after PNS injury, helped in axonal regeneration [53]. Lately it has been shown that the damaged axons after SCI do not lose their regenerative ability after

injury [6, 46] and presence of 'growth cones' within their dystrophic end bulbs remains viable thus enabling their regeneration.

Having established that regeneration of axons is indeed possible, attempts have been made in providing a growth permissive environment by using principles of tissue engineering [11, 54]. To begin with, research in this area included the use of scaffolds and matrices that were meant to provide a structural support to the regenerating tissue, at site of implantation. The design of scaffolds was further developed and components, such as cells seeded within scaffold, growth factors, peptides, gels [12] were used in combination or alone, to provide therapeutic benefits to help reverse the effects of SCI. Recently, the concept of tubular strategy, a hollow cylindrical shaped scaffold, has emerged [7]. The tubular implant, also known as nerve guidance channel or nerve guide, is meant to enclose the caudal and rostral end of the injured spinal cord to provide them mechanical support and also directionally guide the regeneration axons. In the initial stages after SCI, the tubular implant limits formation of scar tissue by allowing accumulation of neurite growth promoting factors [55] and protects the injured stumps from surrounding inhibitory environment.

2.2 Tubular Implants as Regenerative Strategies

Concept of a tubular implant for use as regenerative strategy after SCI has gained considerable importance in the last decade. In PNS injury tubular implants have shown successful results in case of nerve lesions with a gap of less than 3 cm. In fact recently biodegradable nerve conduits for repair in PNS, have been approved for clinical use in

human subjects by US Food and Drug Administration (FDA) and Conformit Europe (CE) [56, 57]. In case of SCI tubular implants have not been able to provide results that indicate functional recovery; however their use seems promising since axonal regeneration to some extent has been observed [18, 45, 58, 59].

Given the complex pathophysiology of the SCI, use of a bioengineered approach that utilizes hollow cylindrical shape of the tubular implant along with a combination of any of these elements such as seeded cells within its structure, presence of matrix within its lumen, presence of neurotrophic factors may be capable of providing desired functional recovery [12]. Use of these techniques has potential to regenerate damaged axons across the injury gap, since the tubular implants provide a permissive environment through the inhibitory boundary of glial scar [60]. Purpose of using these elements within an unfilled tubular implant will render it capable of replacing lost neural tissue, provide protection to damaged ends of spinal cord from the inhibitory glial scar and enhance axonal regeneration and synaptic plasticity. These activities may prove helpful in reversing some or all effects of SCI. Some combination approaches have shown regeneration of axons with help of seeding cells within the tubular implant. A few examples of cells used for this purpose are neural stem cells, Schwann cells, olfactory ensheathing glia [8, 9, 55, 61, 62].

It is important to experiment the proposed regenerative strategies by use of an appropriate animal model. Rat models are a common choice in area of SCI research since they are easy to care for, inexpensive, have less surgical infections and the techniques for their functional analysis are well established. For experimenting the performance of a tubular device, partial or complete transection rat model is usually recommended [5]. The

partial model refers to hemisection or severing one half of spinal cord (along its length), while the other half remains intact, whereas transection model refers to complete severance of spinal cord. Even though probability of occurrence of a partial injury in real life is higher, main issue with use of this model is the difficulty in establishing whether regeneration observed in axons is due to the implanted tubular strategy or due to axons that were spared during the injury [5, 18].

In partial injury model, polymer tubular implant fabricated from PLGA 50:50 and poly(lysine) and seeded with neural stem cells (NSCs) post injury, exhibited coordinated and weight-bearing hindlimb stepping in the adult rats after 70 days [9]. Implantation of the scaffold with NSCs was shown to improve functional recovery and reduce scar tissue. Another study involving the use of Schwann cells seeded within tubular implants made from poly(β-hydroxybutyrate) (PHB) exhibited neuronal survival and regeneration after SCI in rats [60, 61]. Addition of extracellular molecules fibronectin, laminin and collagen were further seen to improve cell survival to help bridge the spinal trauma zone and promote axonal regeneration across the implant. Regenerating axons were seen to enter tubular graft from both ends and extended across its entire length. Unfilled collagen tubular implants guided axonal regeneration and contributed to innervation and hence improvement in motion, of hindlimbs of adult rats affected by SCI. The axons from rostral end of spinal cord were observed to grow into caudal end through the collagen tube [63]. The regeneration and myelination of axons was attributed to unexpected presence of Schwann cells that had migrated into collagen tube after its implantation at site of injury. The direct contact of growth cones of rostral injured axons with ventral roots led to their reconnection causing

accumulation of neurotrophic factors that helped in migration of Schwann cells into the tube.

To eliminate the uncertainty that arises in case of partial injury model and ascertain regenerative ability of injured axons with tubular strategies, some complete transection SCI models that were researched will be discussed below. Due to retraction of spinal cord after transection, a gap arises and for functional recovery the descending axons involved in locomotor functions must regenerate and myelinate across this gap and into the caudal end to form synaptic connections with target neurons. The implant at site of injury is expected to help with this traversal of injured axons. The benefit associated with use of transection model is a relative measure of stabilization in pathological changes and subsequent neurological outcomes that allows a clear assessment of biocompatibility and effectiveness of tubular strategy.

Unfilled poly(2-hydroxy-ethyl methacrylate-co-methyl methacrylate) (PHEMA-MMA) hydrogel channels implanted after transection injury, exhibited regeneration of only brainstem motor nuclei [18]. However when different matrices such as collagen, fibrin, Matrigel™, methylcellulose, were combined with growth factors, such as fibroblast growth factor-1 (FGF-1) and neurotrophin-3 (NT-3), within the lumen of similar hydrogel channels, regeneration of a variety of neurons was observed [45]. The specificity of matrix and growth factor combination towards a particular type of axons was highlighted. This confirms the advantages that a combination approach may bring to the tubular strategy. Another study showing a similar example was conducted by Patist et al. [64]. Tubular implants containing longitudinally oriented macropores connected to each other by a network of micropores

were fabricated using poly (D, L- lactic acid) and loaded with brain-derived neurotrophic factor (BDNF). Upon implantation after SCI, they exhibited a neuroprotective effect on neurons in rostral end and substantial improvement of hind limb function was observed, even though a low number of axons were observed to be myelinated. Use of Schwann cells either seeded within lumen of the tubular implant or used as a nerve graft to bridge the injured ends of the spinal cord, constituted another regenerative strategy. Tubular implants fabricated from poly(L-lactic acid) were seeded with Schwann cells. When implanted after a complete transection injury, they exhibited enhanced formation of myelinated axons and blood vessels, signifying angiogenesis [55]. In addition, a combinatory approach involving Schwann cell graft, with presence of chondroitinase ABC for reducing inhibition in the glial scar and olfactory ensheathing glia, was implanted in adult rats [65]. Significant improvements in hindlimb and forelimb coupling of animals were observed along with an increase in number of myelinated axons. However prominent descending tracts did not successfully regenerate. Regeneration of axons has been shown to be limited within the Schwann cell graft only and does not venture beyond the implant boundaries.

2.3 Biomaterials for Tubular Implants

While the importance of a combinatorial approach as a regenerative strategy has been discussed at length, biomaterial used for fabrication of tubular implants also play a very important role in determining their efficacy. The biomaterial used for tubular implant fabrication must be noncytotoxic, noncarcinogenic, nonimmunogenic, nonmutagenic, and cause no irritation and allergic response either at local or systemic level *in vivo*. The chosen

biomaterial must possess the ability to be modified into a desired shape, should be easy to handle and transplant, have porous morphology to allow for cellular adhesion and growth that promotes tissue regeneration & vascularisation [10, 27].

A wide variety of biomaterials, especially polymers both natural and synthetic, have been used for fabrication of tubular implants [12, 66]. The benefit of natural biomaterial lies in their low cost and easy availability, besides increased biocompatibility. Among them are naturally derived molecules such as agarose, collagen, chitin. On the other hand, synthetic materials are attractive alternative options since their properties such as mechanical strength, rate of degradation, morphology etc. can be optimized as needed. Some examples are poly(α-hydroxyacids), poly(ethylene glycol) (PEG), poly(β-hydroxybutirate) and hydrogels such as poly(2-hydroxyethyl methacrylate) (PHEMA), poly(2-hydroxy-ethyl methacrylate-co-methyl methacrylate) (PHEMA-MMA).

For ease of classification, polymeric biomaterials are classified based on their degradation properties as degradable and non-degradable.

2.3.1 Degradable Materials

As the name suggests, these biomaterials degrade in the body leaving behind no foreign material after a given period of time. From the perspective of tubular implants used for SCI, presence of a non-degradable implant has been shown to be harmful leading to constriction of regenerating spinal cord ends or foreign body reactions that develop over long term [64, 67, 68]. A secondary surgery performed for retrieval of implant can further

damage the injury area. Some benefits associated with tubular implants fabricated from synthetic degradable biomaterials include: ability to control degradation kinetics and mechanical strength [39] of the implant, release of non toxic by-products after degradation that can be excreted by metabolic pathways *in vivo*, and the benefit of use of implant as a drug delivery device that can be designed for sustained-release of therapeutic agents through diffusion [10, 69, 70] over a desirable duration of time. Given the degradable nature of the tubular implant, its mechanical strength will decrease complemented by increasing strength of the regenerating injured tissue that it is supporting [33].

a) Collagen

Collagen has been tested as a potential material for spinal cord repair, given its biocompatibility, elasticity, structural flexibility that allow it to be easily fabricated in various shapes and abundance in nature [71]. Collagen tubular implant after SCI has been shown to reduce scar tissue invasion, orient axonal regeneration and lead to formation of well-vascularized tissue cable connecting rostral and caudal spinal cord stumps [8]. The implantation of collagen filaments in young rats has also led to regeneration of axons directed along the collagen filament implant [62]. In spite of these developments, no functional recovery of limb function has been shown since due to lack of significant axonal regeneration of injured spinal tracts. Even though collagen is a biodegradable polymer the resorption period of the collagen tube has been observed to be up to 3.5 years in some cases [8]. Since a shorter resorption period is desired for SCI applications, this aspect will need to be adjusted during fabrication. One needs to be cautious about using collagen in SCI repairs

however, since there is also the possibility of collagen being a component of the inhibiting glial scar [7, 39]. This ambiguity often casts a doubt on potential use of collagen as biomaterial after SCI.

b) Agarose

Agarose is a hydrogel, a linear polysaccharide that is obtained from sea weed [72]. It has soft, flexible and tissue like properties and is therefore considered a good candidate for use for SCI repairs. Agarose has been used as a three dimensional scaffold *in vivo* and served as a carrier of trophic factors such as BDNF with the purpose of encouraging neurite growth at site of injury [70]. Agarose scaffolds were also fabricated with uniaxial linear pores, using the freeze drying technique, with the purpose of physically aligning regenerating axons [72]. These scaffolds exhibited controlled rate of degradation *in vitro* and also had the potential to be used as a drug delivery vehicle. Stokols et al. [73] fabricated agarose scaffolds with multiple channels extending throughout the length of scaffold. The uniaxial channels with precise dimensions helped in linear organization of regenerating axons and increased their penetration when BDNF was incorporated within the scaffold. Compared to random growth, organized and linear growth of axons as described above, can increase number of regenerating axons beyond lesion site and thus help in completing synaptic circuits for leading to functional recovery.

c) Chitosan/Chitin

Chitin is known as the most abundant polysaccharide in nature and due to its properties of biocompatibility, biodegradability, low toxicity and cost it has found use in some biomedical applications such as membranes for deep burns, ulcer conditions and orthopaedic injuries [74, 75]. Chitosan is prepared from deacetylation of chitin and has a lower rate of degradation when compared to chitin and is therefore preferred for fabrication of scaffolds to be used after SCI [12, 76]. Chitosan can be developed into porous membranes with help of supercritical CO_2 using phase inversion technique [77] and have been shown to be capable of sustaining cell adhesion & proliferation, thus possessing the potential to be used as a drug delivery vehicle. Main issues with use of chitosan scaffolds is difficulty in controlling its physical properties such as pore size and mechanical strength since the biomaterial is known to swell when hydrated [26, 75]. In terms of obtaining functional recovery, tubular implants of chitosan were filled with collagen and used in a partial SCI model in rats. Axonal regeneration of nerve fibers that traversed across the area of injury and into the caudal end [59] were observed. Even though these results were encouraging, to establish efficacy of the strategy a complete transection injury model must be able to show similar results.

d) Poly-β-hydroxybutirate

Poly(β-hydroxybutirate) (PHB) belongs to the family of poly(hydroxy-alkanoates) (PHA) and exists in microorganisms in the form of energy storage granules. It is known to degrade *in vivo* into the non-toxic form of β-hydroxybutyric acid [60]. This thermoplastic

polyester is known for its biocompatibility and mechanical properties comparable to that of polylactides. The only drawback is its high brittleness [78]. PHB patches have been studied for development of dura substitute material [79]. For a partial injury model of SCI, unfilled tubular scaffolds fabricated from PHB, exhibited axonal growth on the outside of the implant and not inside. When coated with alginate hydrogel containing fibronectin, these implants exhibited only neuroprotection for the injured spinal cord [61] but in combination with Schwann cells, regenerating axons were observed to enter graft from both ends, extending across its entire length and bridge the spinal trauma zone [60].

e) Poly(α-hydroxy acids)

This group of synthetic biodegradable polymers also known as aliphatic polyesters consist of poly(lactic acid) (PLA), poly(glycolic acid) (PGA), poly(lactic-co-glycolic acid) (PLGA), poly(ε-caprolactone) (PCL) and some of their copolymers. PLA and PGA have been commonly used for the last few decades in clinical setting as absorbable sutures and orthopedic fixation devices and have been recently approved by US Food and Drug Administration (FDA) and Conformit Europe (CE) for use as absorbable nerve conduits for clinical repair of peripheral and cranial nerves [57].

Research studies related with SCI have shown that aliphatic polyesters adapt easily and have biocompatibility within CNS environment [2, 10, 26, 28-31, 37-39, 55, 58, 64, 80-86]. Various techniques are used, such as electrospinning [84], solvent casting & particulate leaching [80, 81], phase inversion [31, 85], microbraiding [2, 26], and gas foaming [87], to fabricate tubular implants with a porous morphology which is helpful for tissue engineering

as has already been discussed before. The degradation kinetics of aliphatic polyesters and its copolymers can be controlled depending on their composition. A prime example of this is PLGA which is a copolymer of PLA and PGA. Varying the ratio of glycolic and lactic acid monomers (GA and LA), PLGA can exhibit different rates of degradation [12, 88, 89]. The mechanical strength of tubular implants fabricated from aliphatic polyesters can also be controlled based on their composition and method of fabrication [90-93]. The only drawback associated with the use of these biomaterials is that during degradation release of acidic by-products leads to a drop in pH value at the site of implantation [33, 85]. Also the tubular implants have been shown to loose flexibility and become stiff after some time post implantation [57] and break up into polymer pieces that can harm the regenerating tissue [72].

2.3.2 Non-Degradable Materials

Non-degradable biomaterials that have been used for fabrication of scaffolds and matrices for implantation after SCI include poly[N-(2-hydroxypropyl)methacrylamide] (PHPMA), NeuroGel, poly(hydroxyethyl-methacrylate) (pHEMA), blend of hyaluronan & methylcellulose (HAMC) and xyloglucan hydrogel [94-98]. Synthetic non-degradable biomaterials include poly(2-hydroxyethyl methacrylate-co-methyl methacrylate) (PHEMA), poly(2-hydroxyethyl methacrylate-co-methyl methacrylate) P(HEMA-co-MMA), poly(acrylonitrile-co-vinylchloride) (PAN/PVC), and silicone. Given the structural stability and ability to closely match the mechanical properties of the spinal cord tissue, the non-degradable biomaterials have been suggested for fabrication of tubular implants [12, 35].

The non-degradable hydrogels have been known to offer ease of fabrication, lower protein absorption [42], and potential to be used as drug delivery vehicles [94] or be seeded with cells [96], but their main drawback is their non-degradability. These biomaterials continue to reside in body as foreign materials, after tissue restoration and may present a risk causing delayed immune response or rejection [33, 39].

a) PHEMA/P(HEMA-co-MMA)

These non-degradable synthetic hydrogels are known for their biocompatibility and non-toxicity have recently been researched in greater depth for fabrication of tubular implants after SCI [18, 34-36, 41-45, 99]. The attractive features for their use are soft texture and mechanical properties that closely match with spinal cord tissue. Tubular implants of PHEMA/P(HEMA-co-MMA) were fabricated to match the modulus of elasticity of spinal cord tissue [36, 42]. These implants, when used for implantation after complete transection SCI, resulted in regeneration of a few types of axons [18]. This growth was improved with regeneration of axons from different neurons on incorporating different types of matrices and growth factors within the lumen of the implant. In spite of these measures, functional recovery remained elusive [45]. To further improve upon this axonal regeneration, a longer implantation period of P(HEMA-co-MMA) channels was observed, during which the channels collapsed due to lack of sufficient mechanical strength [34]. To strengthen them, coil reinforced tubular implants were fabricated from the same biomaterial [41], but their implantation resulted in development of syringomyelic cyst [43]. Syringomyelic cyst developed in the rostral stump of the injured spinal cord as a result of obstruction of

cerebrospinal fluid (CSF) due to swelling of the injured spinal cord. This physiological condition prevented axonal regeneration, led to caudal migration of the rostral stump thereby causing further damage to the already injured area of the spinal cord.

Use of PHEMA/P(HEMA-co-MMA) hydrogels have not been successful in showing functional recovery after SCI although advances in axonal regeneration have been successful. Even though they are biocompatible in nature, use of tubular implants fabricated from PHEMA/P(HEMA-co-MMA) have been associated with *in vivo* development of fibrous tissue capsule and the presence of giant foreign body type cells and calcification around the implant.

b) PAN/PVC

Tubular implants fabricated from PAN/PVC have often been studied in combinatorial approaches for SCI regeneration [67, 68, 100, 101]. PAN/PVC channels filled with suspension of Schwann cells facilitated regeneration of myelinated and unmyelinated axons when implanted into a transected model of SCI in rat [67]. However this permissive environment was unable to lead the axonal regeneration into the caudal end of the spinal cord. Interestingly similar channels and presence of Schwann cells, in a partial injury model of SCI, [68] axonal re-growth of specific neuronal pathways could be observed with regeneration of axons from different regions. Regenerated axons were also able to enter the host cord environment without presence of neurotrophic growth factors.

Fabrication of PAN/PVC tubular implants requires organic solvents during synthesis which can be harmful for *in vivo* environment [12] and semi-permeability exhibited by tubular implants may interfere with its axonal regeneration response [55]. Finally the results that have been shown with use of PAN/PVC are limited to partial injury model and can be attributed to the presence of Schwann cells, since therapeutic ability of PAN/PVC has not been specifically established [39, 55].

2.4 Fabrication Techniques for Tubular Implants

There are many different methods by which tubular implants can be fabricated. Concept of any fabrication technique is to develop a tubular implant with appropriate structural, morphological and mechanical properties to help improve its *in vivo* efficacy and achieve functional recovery after SCI. Specific fabrication techniques can be used to enhance mechanical strength, porosity and pore size during fabrication. For example gas foaming technique helps in achieving desirable porosity and pore size, electrospinning helps in providing extra cellular matrix (ECM) structural properties that aid in cell growth and attachment and freeze drying technique provides conducive fabrication environment thereby maintaining the efficacy of drug loaded tubular implants. In the following text, techniques to prepare HFCs will be reviewed.

2.4.1 Solvent Casting

The solvent casting technique involves dissolving polymer in a solvent and casting it in the desired shape of a tubular implant [102]. In some cases a porogen, such as sodium chloride (NaCl) is added to polymer solution, to be leached out in water-based media after the solvent has completely evaporated for obtaining a porous morphology of the implant [81, 86].

This commonly used technique often involves variations in the method by which polymer is shaped. Widmer et al. [86] used an extruder equipped with a piston extrusion tool mounted on a hydraulic press as shown in Figure 2.1. The tool was filled with dried wafers of polymer solution dissolved with NaCl crystals as porogen. Upon heating, the extrusion

tool converted polymer wafers to semi-liquid state to be easily extruded with the piston in a tubular shape. The tubular implants were then washed in water to leach out NaCl crystals. Figure 2.1 provides a better insight into the design of the extrusion tool.

Li et al. [28] used a different approach to solvent casting technique. The polymer sheets were cast and before drying, were patterned using physical imprinting and embossing methods employing a master pattern and a secondary template. These imprinted sheets were assembled as tubular implants using rolling-fusing method. As a result of imprinting and embossing, the tubular implant possessed multiple intralumenal walls with precise topography along longitudinal axis. This technique increased surface area of the tubular implant by eight times as compared to regular tubular implants. Presence of patterning inside the lumen was designed to help in cellular infiltration, proliferation and axonal guidance, thereby further promoting tissue regeneration. However, more studies are needed to establish their efficacy.

Multi-lumen tubular implants were developed by Moore et al. [103] using solvent casting technique, with PLGA dissolved in methylene chloride as a polymer solution, injected into a tube shaped mold. Steel wires were inserted in the mold to create lumens within the final implant, and moulds were dried for over 24 hours in an airtight chamber attached to a high-vacuum pump. This multi-lumen tubular implants exhibited greater permeability than single lumen implants due to the presence of interconnected pores [37]. Wong et al. [81] fabricated multi-lumen tubular implants with PCL dissolved in acetone and used NaCl crystals as porogen. Tubular implants with a variety of designs for the inner lumen, such as single lumen, multi-lumen, open path with and without core, were fabricated

by injecting the polymer solution in the appropriately shaped moulds. While the concepts are interesting, results from these designs show that the open path designs of the tubular lumen, both with and without cores, when implanted *in vivo* helped in axonal regeneration with lesser connective and fibrous tissue.

Advantages of solvent casting technique are its simple approach and use of inexpensive equipment. The mechanism of salt leaching helps in providing desired level of porosity within both inner lumen and outer surface of the tubular implant [37]. The main drawback associated with this technique is the use of organic solvents such as methylene chloride, acetone to create polymer solutions. Since the residual solvent in the implant is hard to completely remove, the resulting implants prepared using solvent casting may have negative effects on biocompatibility and physical properties of the implant [102].

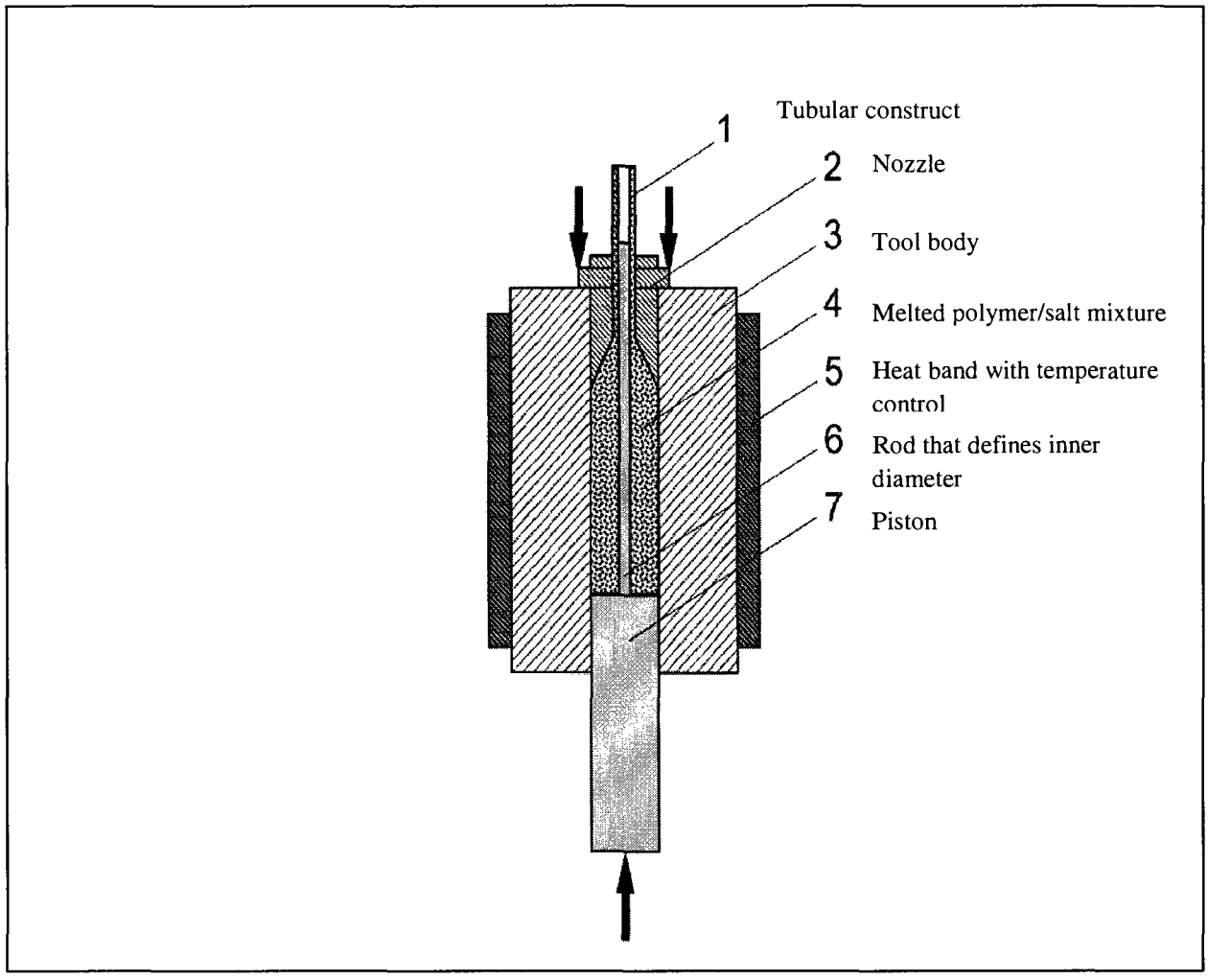

Figure 2.1 Piston Extrusion Tool for Solvent Casting. Figure adapted from Reference [86]

2.4.2 Phase separation

a) Thermally Induced Phase Separation

Changes in thermal energy to induce separation of two phases such as homogenous polymer-solvent or polymer-solvent-non-solvent within the polymer solution by either solid-solid demixing or liquid-liquid phase separation, is the principle applied in the case of thermally induced phase separation (TIPS) [104]. Polymer solution cast on the surface first undergoes liquid phase separation and then sublimation during which solvent rich phase is removed.

He et al. [82] fabricated multi-lumen tubular implants by injecting PLGA solution in either acetic acid or dioxane, with granular ammonium bicarbonate as porogen in a stainless steel injection mould that was fixed with wires acting as mandrels. The schematic representation of the mould is shown in Figure 2.2. The polymer solution was injected at a temperature of -40°C and mould was further maintained at low temperatures for 4 hours. After removal from the mould, the tubular implants were further lyophilized for 5 days before immersing in water for 2 days for leaching of porogen. Use of different solvents within TIPS technique can lead to different porosities in tubular implants. For example glacial acetic acid exhibited poor interconnected lamellar-like structures and dioxane led to formation of open pore morphology. Interestingly dimethylsulphoxide (DMSO) resulted in radial structure due to its dendritic crystallization within the implants [104].

Sundback et al. [105] fabricated porous biodegradable conduits from poly (DL-lactide-co-glycolide) (DL-PLGA) dissolved in acetic acid by using combined injection molding and TIPS technique. The tubular implants contained longitudinal channels that were

axially aligned, numbers of which could be easily varied, within its structure to guide regenerating axons and provide support for adherence of Schwann cells. The TIPS technique was modified such that polymer solution was injected under low pressure into the cold mould at room temperature. An outer skin layer, semi permeable in nature, on the fabricated implant was observed due to rapid quenching of polymer solution as soon as it initially contacts the cold mould surface.

Advantage of using TIPS technique is well-defined microporous structure that can be manipulated by using different types of solvents for instance use of dioxane instead of acetic acid as a solvent provides more porous morphology. Some of the disadvantages associated with this technique are formation of non-porous lamellae low porosity on the outer surface of the implant, compact bulk macrostructure and a difference in pore size between inner lumen of the tubular implant and the outer layer.

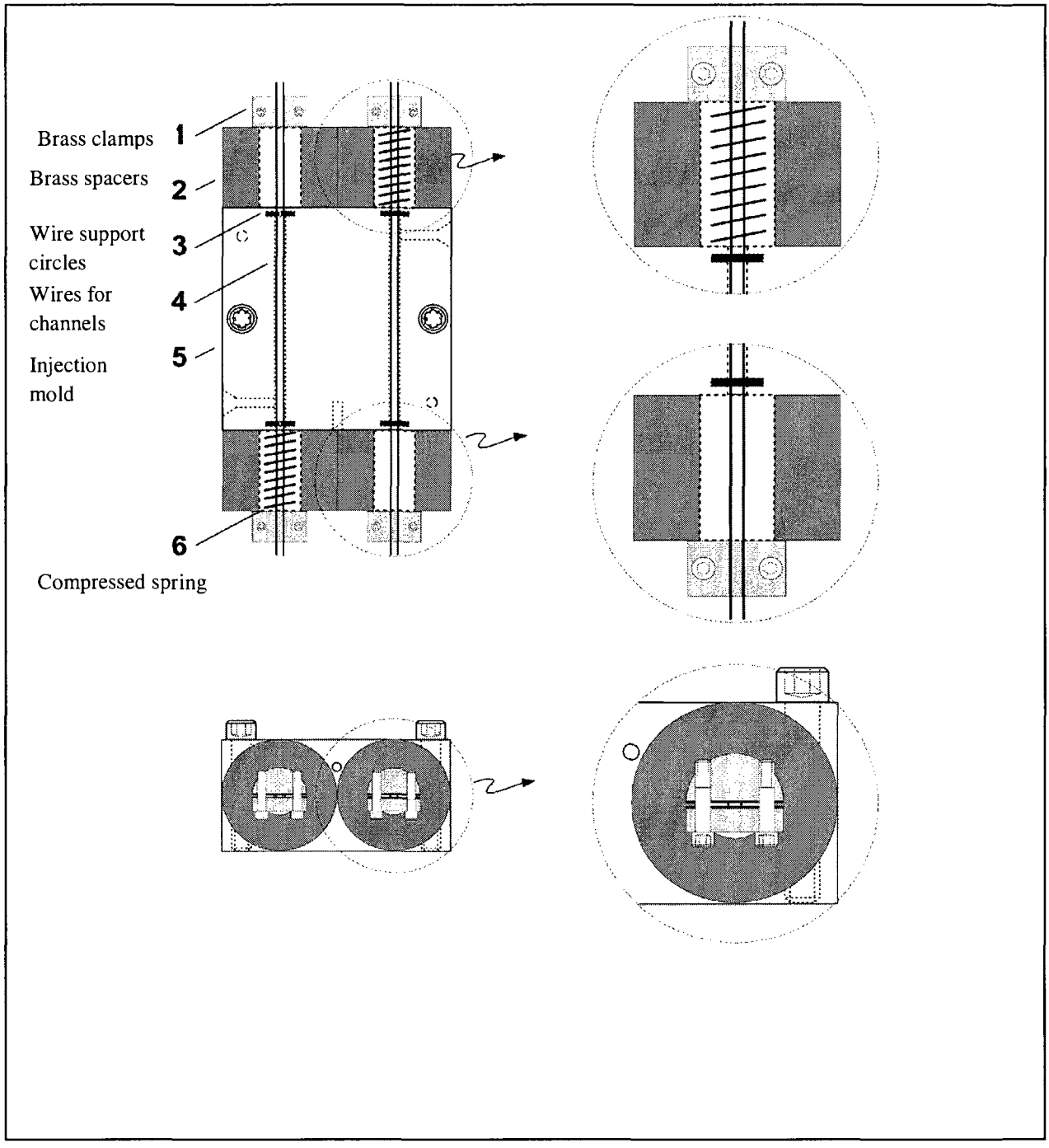

Figure 2.2 Injection molding tool used for fabrication of tubular implants using the thermally induced phase separation technique. Figure adapted from Reference [105]

b) Liquid-Liquid Centrifugal Casting

The method of liquid-liquid centrifugal casting has been mostly used to create tubular implants from biomaterials such as hydrogels that cannot be dissolved in solvents. The phase separation occurs during rotation of the solution at high speed and when propagating polymer radical becomes insoluble in solvent [42]. Phase separation within the polymer is induced by filling polymer in a cylindrical mould and rotating it at high speed. Dalton et al. [36] created tubular implants of PHEMA by polymerizing 2-hydroxy ethyl methacrylate (HEMA) in a cylindrical mould by application of centrifugal force at 5000 rpm for 5 hours, that pushes PHEMA to the edge forming a thin tubular structure. Figure 2.3 depicts the schematic of this process. Increasing the rotational speed led to fabrication of thinner walled tubes and increase of concentration of monomer led to thicker walled tubes. Luo et al. [42] added monomer methyl methacrylate (MMA) to enhance phase separation over gelation in the above configuration. The copolymerization led to faster separation of PHEMA-MMA phase, due to the hydrophobicity of MMA, as compared to PHEMA phase separation. The tubular implants achieved higher mechanical strength with increased concentration of MMA and had microporous gel morphology on the outside of the implant without use of porogens and an inner sponge phase. This design of a bilayered tubular implant, achieved as a result of centrifugal casting, was thought useful for delivery of proteins and other drug release mechanisms in a controlled manner. With slight change in chemistry, P(HEMA-co-MMA) tubular implants fabricated by the same method, with an outer gel-like layer and an interconnected macroporous inner layer, possessed appropriate mechanical strength lying within recommended range for SCI tubular implants [35]. This was made possible by ensuring that phase separation occurs before gelation process.

So far the liquid-liquid centrifugal technique had been used for fabrication of tubular implants using non-degradable hydrogels. Goraltchouk et al. [40] synthesized biodegradable tubular implants consisting of L-lactide (LLA) and polyethylene glycol (PEG), terminated by methacrylate (MA) groups. The polymerizing mixture of MA-LLA-PEG in a solution with water, was centrifuged at 2500 rpm for 6 hours. The degradation and mechanical properties of the polymer could be adjusted by varying the ratio of LLA and PEG. In MA-LLA-PEG tubes crystallinity and hydrophobicity increased with LLA content and amorphous content and hydrophilicity increased with PEG molar mass and content.

The main advantages associated with this technique are lack of skin layer formation on outer surface of tubular implant and flexibility to vary porosity and mechanical of the tubular implant by varying parameters such as monomer combinations, speed of rotation and solubility of monomers [40].

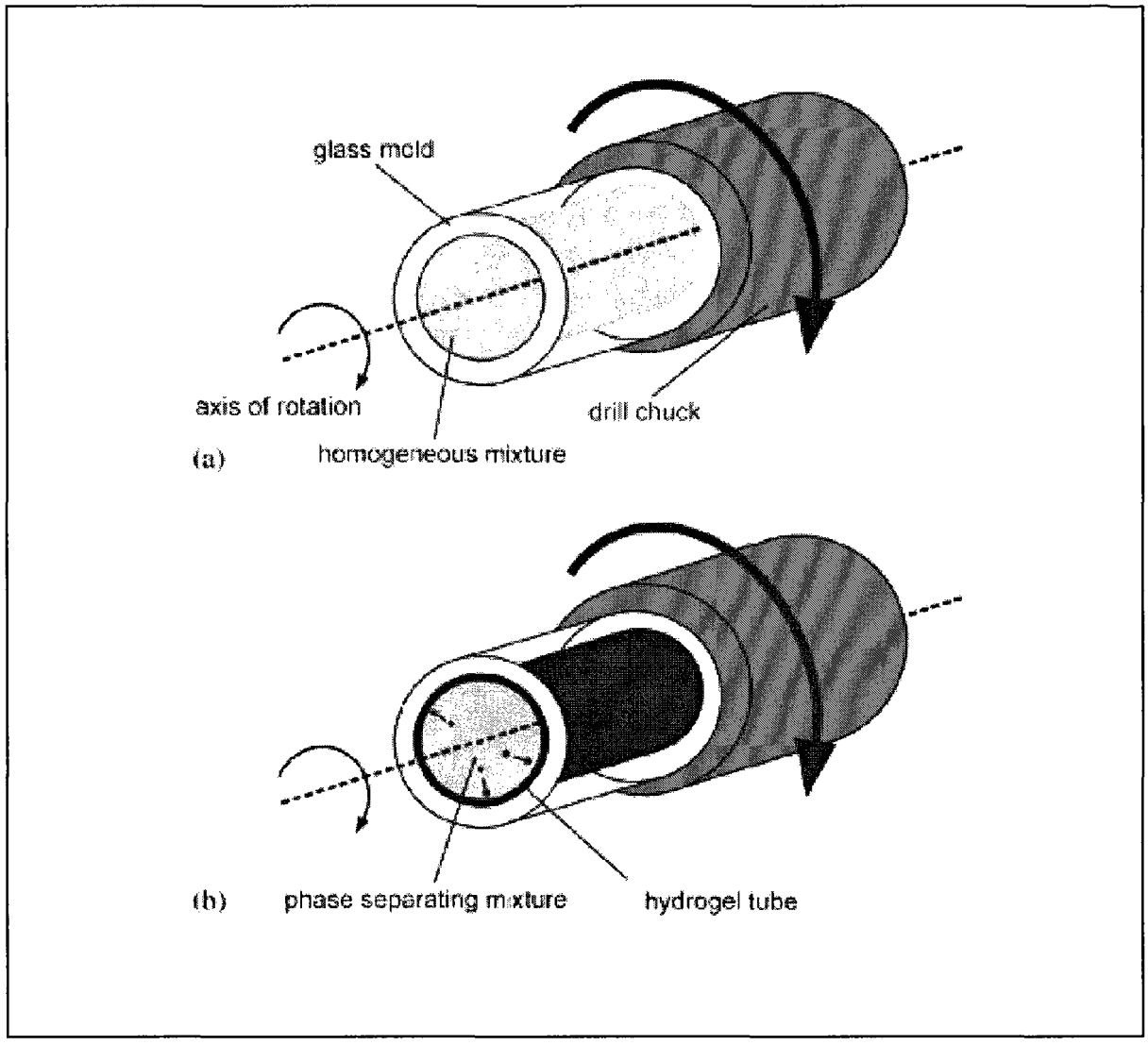

Figure 2.3 Fabrication of tubular implants using liquid–liquid phase separation technique. Figure adapted from Reference [35]

2.4.3 Wet Phase Inversion

The technique of wet phase inversion (WPI) fabricates semi permeable tubular implants, also known as hollow fiber membranes (HFM), from polymer solution using an annular spinneret with a bore liquid precipitant of deionized water. The polymer solution was pumped at a rate lower than the deionized water to allow the polymer to precipitate into the shape of tubular implant [85]. It was necessary to manipulate these rates to obtain an appropriate texture of the HFM [31]. A schematic diagram of this technique is shown in Figure 2.4.

Wen et al. [85] fabricated tubular implants using wet phase inversion technique using polymer solution with different solvents. By varying parameters such as spinneret size, pairing of solvent & non-solvent used and concentration of polymer solution, polymer implants could be obtained with variable sizes, surface morphologies and porosities. To increase the guidance role and promote nerve regeneration after SCI, semi permeable HFMs were designed and fabricated with aligned grooves inside their inner lumen [31]. HFMs could be fabricated with dimensionally controlled grooves within inner lumen, desirable groove width, inner and outer diameters. These requirements were sensitive to concentration of polymer solution & its flow rate and choice of non-solvent and its flow rate. HFMs exhibited homogeneous surface and bulk degradation which could prove to be helpful for axonal regeneration after SCI [85].

The WPI technique allows for fine-tuning of physical properties such as permeability, inner and outer surface morphologies and size of the tubular implant. Besides these, it provides highly aligned structures with inner lumen of the tubular implant to offer

guidance cues to regenerating axons [85]. The fabrication of aligned grooves within the tubular implant can help guiding axons immediately close to inner wall; however axons in the centre may need further guidance to avoid aberrant growth behaviour [29].

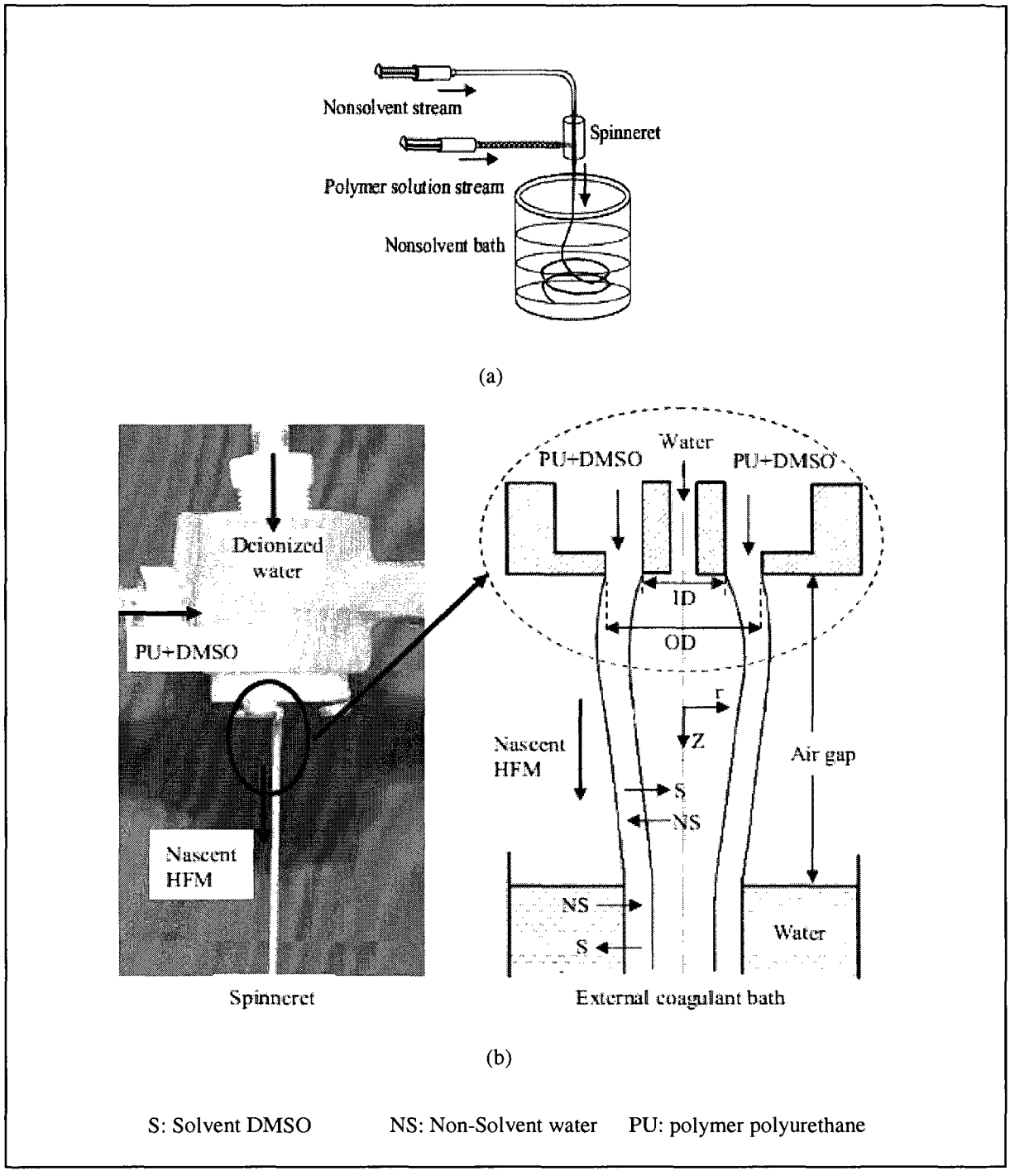

Figure 2.4 Wet Phase Inversion technique for fabrication of tubular implants (a) schematic of phase-inversion technique and (b) design of the spinneret. Figure adapted from Reference [29]

2.4.4 Dip-coating

As the name suggests this technique involves the first step of immersion of a mandrel to dip-coat it and adhere layer of polymer on its surface. Second step involves precipitation or deposition of polymer on mandrel by using a non-solvent. The non-solvent creates a phase separation effect within polymer solution that leads to solidifications of polymer and capturing of its microporous structure [106]. The final thickness of the tubular implant can be controlled by number of dip-coatings.

Bender et al. [80] fabricated longitudinally aligned multiple channel tubular implants, by dip-coating PVA mandrels in a solution of poly(caprolactone) (PCL) and tetrahydrofuran (THF) and using water as non-solvent for precipitation after the initial immersion/dip-coating technique. Nerve guides with multiple channel geometry were fabricated to provide larger surface area for extending axons in order to improve and enhance axonal elongation.

Wan et al. [106] fabricated tubular implants using polyphosphoester solution for dip-coating and, water, methanol or mixture of water-methanol were experimented as different non-solvents for precipitation. After precipitation the tubular implants were air dried by rotation and then dried either in vacuum environment or freeze dried before removing them from the mandrels. It was established that viscosity of polymer solution should neither be too high to cause irregularities on implant surface nor too low to require many dip coatings, and speed of rotating mandrel should be optimum to allow uniform drying. Mechanical strength of tubular implant could be maintained with minimum three dip-coatings and porosity of tubular implants could be controlled by ratio of methanol & water in non-solvent bath and method of drying by either vacuum or freeze drying.

The advantages of dip-coating technique are ease of fabrication, generation of porous structure with use of non-solvent bath and the ability to incorporate different porosities at a layer by layer level of the tubular implant [106]. The drawbacks associated are use of organic solvent for creating polymer solutions since residual amount of solvent after fabrication cannot be determined. Sometimes formation of air bubbles due to insufficient drying time can cause aberrations on the surface of tubular implant.

2.4.5 Freeze-Drying

This technique involves preparation of an emulsion, dissolving a polymer in a solvent or hydrogel with a non-solvent, which is then frozen before phase separation. In this case, formation of ice crystals act as a porogen, the size of which can be controlled by varying freezing temperature and concentration of polymer solution [107]. Concentration of polymer solution, solvents and freezing temperature, play an important role in this technique.

Stokols et al. [72] fabricated linearly oriented nerve guidance tubular implants from agarose by using freeze drying technique. These implants had uniaxial linear pores, with dimensions within range of 100-200 μm, extending full length of scaffold. These linear pores were designed to help in guidance of regenerating axons by physically aligning and restricting their direction of growth in an effort to increase probability of achieving functional recovery after SCI. The pores obtained were polygonal in shape with an arranged honeycomb like structure, large enough to allow vascularisation and infiltration of cells supporting regeneration.

Huang et al. [75] fabricated longitudinally oriented tubular implants combining techniques of lyophilizing (freeze drying) and wire heating. The polymer solutions of PLGA and chitosan were freeze dried and filled in rubber moulds with Ni-Cr wires as mandrels. Electric current was passed through the mandrels to create longitudinal channels within the two types of tubular implants. These channels were designed to increase surface area of the tubular implant to provide support and guidance to regenerating axons. Tubular implants fabricated from chitosan were observed to be more permeable than PLGA implants but it was found difficult to control pore size in chitosan implants.

The advantages associated with freeze drying technique are use of conducive operating conditions during fabrication of tubular implants since low temperatures do not compromise the efficacy of implants as compared to other harsh techniques such as melting casting. Also a separate porogen is not required to introduce porosity since ice crystals can provide a desirable microarchitecture [72].

2.4.6 Microbraiding

Microbraiding involves a similar approach as used in making of yarns from fibers. Bini et al. [26] fabricated microbraided tubular implants using PLGA and chitosan fibers. Polymer fibers were initially wound on a number of spindles that were then used to braid a tubular structure on a teflon mandrel. A schematic of this process is shown in Figure 2.5. These tubular implants have been shown to be flexible *in vivo* as compared to other synthetic implants, even when same biomaterials were used in both cases. *In vitro* degradation study showed that outer surface of PLGA tubular implant was flexible,

permeable and displayed no swelling whereas in chitosan implants 60% swelling was observed. In addition *in vivo* studies showed no inflammatory response [23] and good viability for cells was shown in both cases. Tanaka et al. [2] fabricated microbraided channels using PGA whose inner lumen and outer surface were coated with collagen solution. Different number of collagen layers was coated on tubular implants and higher number of layers helped in increasing mechanical strength of the implant as shown by *in vitro* and *in vivo* studies.

The advantage of microbraiding technique is that tubular implant of any desired length can be fabricated and its diameter can be adjusted by controlling the diameter of mandrel. Porosity of the implant is obtained as a result of various braiding parameters such as number of polymer fibers in a spindle, number of monofilaments in a fiber, number of spindles and braiding angle of spindles used during the technique. The disadvantages are lack of ability to control permeability of tubular implant and secondly the inner lumen of the tubular conduit lacks a comparatively smooth surface that is important to help in axonal outgrowth [85].

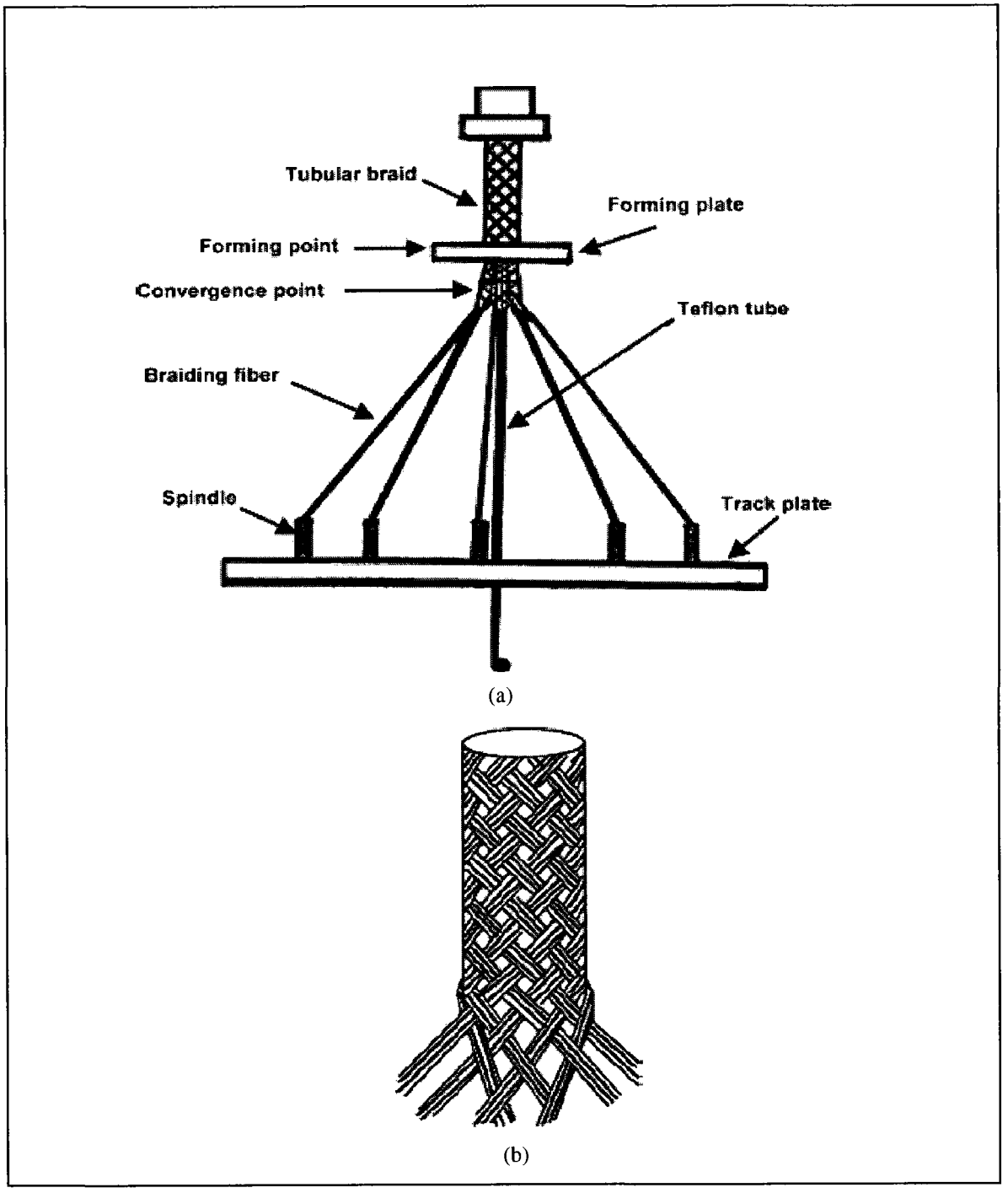

Figure 2.5 Depiction of microbraiding technique for fabrication of tubular implants (a) schematic of microbraiding process and (b) sample of microbraided tubular construct. Figure adapted from Reference [26]

2.4.7 Electrospinning

Electrospinning technique has increasingly gained wide importance in field of tissue engineering. The electrospun fibers have been used for fabrication of scaffolds and are now finding use for fabrication of tubular implants. This technique has found application as skin replacement, fabrication of vascular grafts, prosthetic heart valves in soft tissue engineering [108]. Electrospinning uses electrostatic force to produce polymer fibers ranging in diameter from few microns to nanometres. Polymer solution when ejected in a jet from the end of a syringe, due to the presence of a high electric field, produces nano sized polymeric fibers that can be collected on a spool that has been electrically grounded [107]. Morphology of the tubular implant fabricated from this technique has a connected porous geometry [109]. A schematic diagram to better explain the electrospinning technique has been depicted in Figure 2.6.

Valmikinathan et al. [84] first created sheets of sintered PLGA microspheres that were cut into strips on which PLGA fibers were electrospun, before being rolled to form spiral tubular implants. These implants possessed nanofibrous morphology besides having adequate mechanical strength being fabricated from microsphere sintered sheets.

Advantages associated with use of electrospun fibers are increase in surface area and presence of surface texture mimicking extracellular matrix that encourages cell attachment and proliferation. Electrospun fibers offer better control over orientation of fibers within the tubular implant thus providing the benefit of axonal guidance. The low mechanical strength is the main drawback associated with fabrication of tubular implants from electrospinning [84].

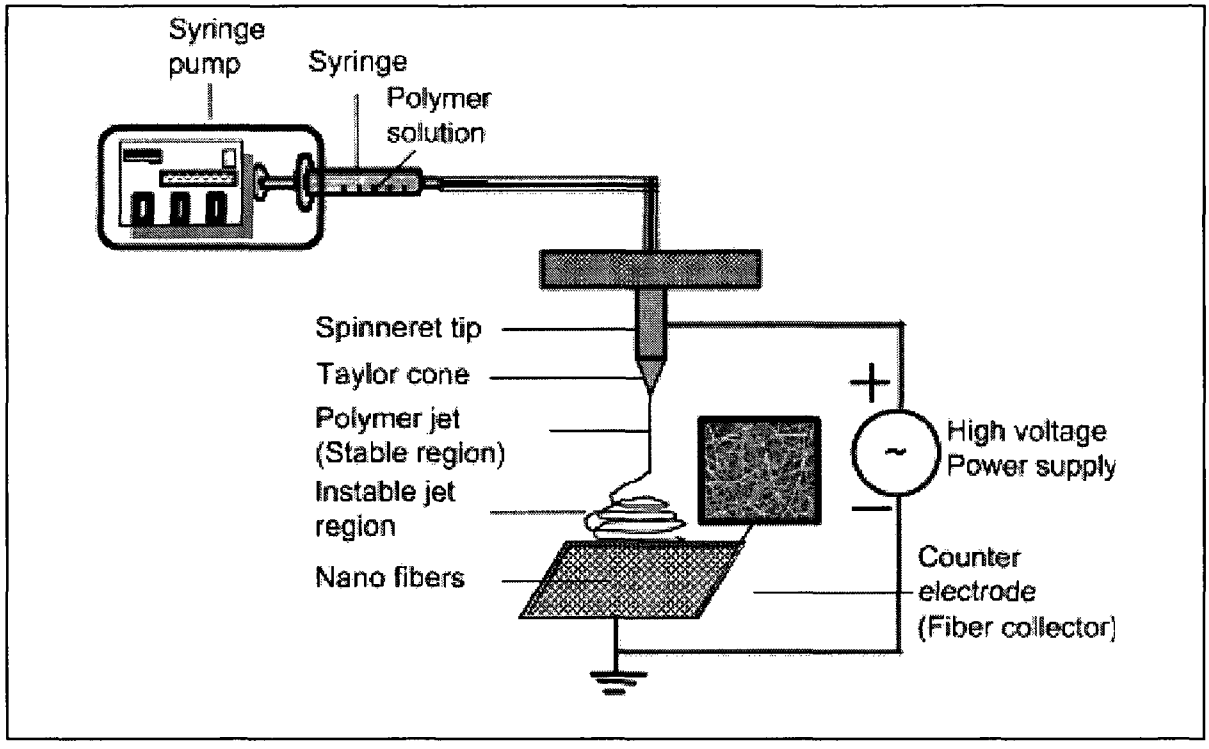

Figure 2.6 Schematic of electrospinning process for fabrication for fabrication of tubular implants. Figure adapted from Reference [109]

2.4.8 CO_2 Gas foaming

Gas foaming technique using supercritical CO_2, has found increased use for fabrication of porous scaffolds used for tissue engineering. In its compressed state, supercritical CO_2 ($scCO_2$) (31.1 °C and 7.38 MPa respectively [110]) has the unique ability to plasticize a wide range of polymers. Complete saturation of $scCO_2$ followed by its depressurization creates a foamed morphology within the polymer matrix wherein pore size, distribution and density can be controlled by factors such as temperature and saturation pressure of foaming process and rate of pressure drop during depressurization [87, 111, 112]. Even use of CO_2 at sub-critical temperatures and pressures been shown to be effective in generation of porous structures [113].

Temtem et al. [77] fabricated tubular implants from chitosan using $scCO_2$ gas foaming technology. Chitosan was dissolved in acetic acid and then placed in a high pressure chamber under the effect of $scCO_2$. They were able to show that the tubular implants did not have any effect of cytotoxicity and this was attributed to the complete removal of acetic acid due to action of supercritical CO_2. Yang et al. [10] developed single and multi-lumen tubular implants using gas foaming technique. Growth factor loaded microspheres were mixed with a porogen, NaCl particles, and deionized water to obtain a mixture that was loaded into stainless steel moulds and foamed under effect of sub-supercritical CO_2 at 800 psi. After leaching, the final tubular implants exhibited to have a well controlled porosity that could be controlled by adjusting the porogen to polymer ratio. Encapsulation of the growth factor within the microsphere, after foaming, provided a more sustained release. Also the ability to control porosity was related to modulate mechanical strength of the tubular implants.

Advantages associated with CO_2 gas foaming technique are its non-toxicity, ease of availability, low cost and no residue. It has been shown that a controlled morphology can be obtained based on pressure and temperature conditions, rate of depressurization and soaking time of the polymer within the $scCO_2$ environment [77]. The supercritical $scCO_2$ used as a processing solvent has replaced other organic solvents [114]. Also use of $scCO_2$ has been effectively known to remove organic solvents and possess sterilization effects. Koegler et al. [115] established that scaffolds fabricated from a PLGA and chloroform solution exhibited a reduction in residual chloroform to a safer limit of 50 ppm after being fabricated using $scCO_2$. Although no guidelines have been set by U.S. Department of Health and Human Services and the FDA for the amount of chloroform in implantable devices, but the chloroform in oral medication has been limited to 60 ppm [116]. The sterilization effects of $scCO_2$ were shown by Dillow et al. [117]. The disadvantage of using the CO_2 foaming technique is the presence of a non-porous skin layer formed on surface of the tubular implants that can pose to be a barrier for the cell nutrients and waste products of cell metabolism. Also the pore network has a relatively closed morphology [87].

2.5 Different designs for tubular implants

The concept and applications of single lumen tubular implant have already been discussed in detail. Even though different biomaterials and combination of cellular therapies and growth factors have exhibited axonal regeneration after SCI, so far functional recovery has remained elusive. It has been theorized that within single lumen tubular implant, the innervations targeted by regenerating axons may not be accurate thus leading to their

misdirection and subsequently polyinnervation of axonal branches originating from the same motor neuron [38]. In order to avoid this, since accuracy is important to help find the axons their original or related end organ to subsequently obtain functional recovery after SCI, multi-lumen tubular implants have been proposed [10, 37, 38, 80, 81, 118].

Each lumen within the multiple-lumen tubular implant, is expected to behave as an individual guidance channel thereby providing segregated functional pathways for regeneration of different type of axons [10]. Thus multiple lumens within the tubular implant can be made to mimic micro-architectural layout of the spinal cord tracts. This method may enhance targeting specific group of regenerating axons and can also allow for delivery of a specific therapeutic approach conducive [39]. Organization and reconnection of different tracts in the spinal cord are important for functional recovery [81]. Figure 2.7 shows the schematic design and picture of a fabricated tubular implant.

Besides obtaining accuracy in innervations, the multi-lumen tubular implants have been designed to have increased surface area for cell attachment and enhanced axonal elongation [37, 80]. This design for multi-lumen tubular implants has also been shown to alter the physical properties of the implant. As compared to single lumen, the multi-lumen tubular implants have been shown to possess higher flexibility towards compressive loads, greater resistance to deformation and increased porosity. Due to higher swelling when implanted, increased rate of degradation has also been reported [37]. When single and multi-lumen tubular implants were implanted after complete transection SCI in rat model, no significant statistical difference was observed in accuracy of axonal regeneration [38].

Use of multi-lumen tubular implants has also been described as an advanced step towards sustained delivery of therapeutic agents [5] as was shown by step wise release of nerve growth factor (NGF) from single and multi-lumen tubular implants [10]. The implants continued to possess their original dimensions after 13 days of subcutaneous implantation and exhibited tissue infiltration.

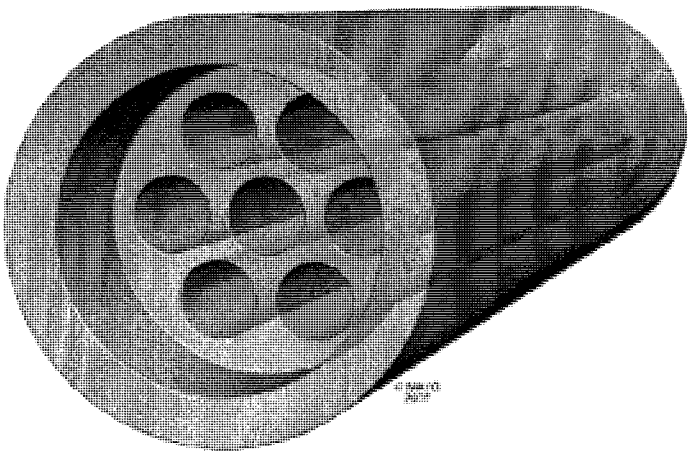

(a)

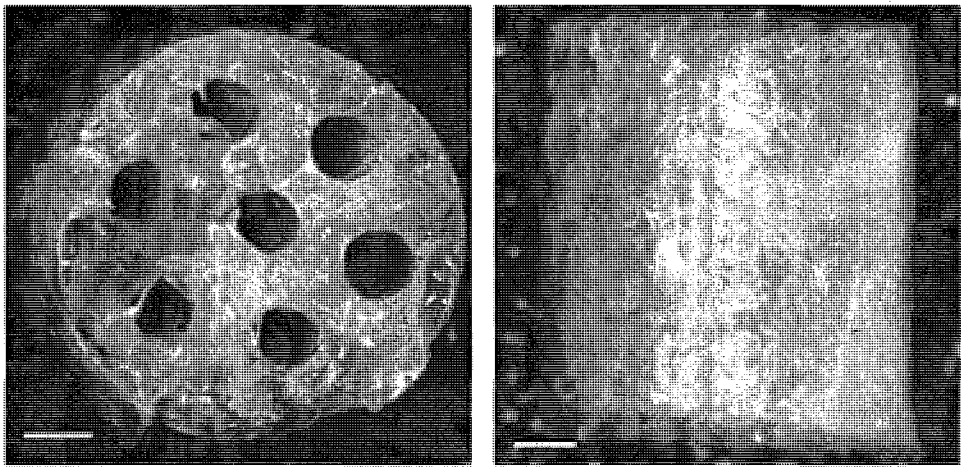

(b)

Figure 2.7 Design of multi-lumen tubular implants (a) Schematic layout of the implant with seven channels and (b) PLGA tubular implants fabricated from parallel wire moulds. Figure adapted from References [38, 103]

2.6 Porosity Gradient in Tubular Implants

Porosity gradient within scaffolds for tissue engineering has been studied mainly with aim to encourage regeneration of damaged organs or tissues. Different sized pores present within each scaffold layer can encourage growth of a variety of cell types thereby creating each layer of scaffold to perform a desired biological function. Such conceptual designs of the scaffold, have been achieved by conventional and rapid prototyping techniques [50]. For tissue regeneration after SCI, the concept of porosity gradient within a tubular implant has been designed for providing adequate mechanical support [35, 42], therapeutic measures such as controlled drug delivery [69, 118], protecting infiltration of glial scar at site of injury and promoting regeneration within inner lumen of the implant [29, 31, 85]. Different techniques have been used for creation of tubular implant with porosity gradient such as centrifugation, freeze drying, conventional and rapid prototyping [49-52].

Bi-layered chitosan tubes were fabricated by Wang et al. [118] with an outer layer of chitosan film fabricated by dip-coating/immersion precipitation technique and an inner layer of nano/micro fibres coated with peptide, fabricated by electrospinning process. The inner layer had interconnected pores and high surface area for attachment & growth of cells to facilitate angiogenesis. The purpose of the chitosan layer was to protect the physical integrity of the inner fibrous layer. The mechanical property of the bilayered tube was observed to improve with the presence of the outer layer and also its biocompatibility was maintained. Goraltchouk et al. [69] created a bilayered tubular implant with a porosity gradient designed for used as a drug-delivery system. The inner layer of chitosan and outer layer of chitin had microspheres trapped between them that were loaded with two model

proteins, bovine serum albumin (BSA) and recombinant human epidermal growth factor (rhEGF). Harley et al. [49] fabricated porous tubular implants with gradient in pore size, along the radius, using freeze-drying technique by co-precipitation of glycosaminoglycans in a suspension of collagen and acetic acid. This implant was designed with purpose of nerve regeneration after nervous system injuries. Inner wall of the tubular implant was designed as permeable, with open-cell foam morphology and radially aligned pore channels to enhance cellular growth and proliferation. On the other hand, outer wall had a non-oriented amorphous pore structure, closed-cell foam morphology and high relative density to encourage protein permeability but no cellular infiltration. Oh et al. [51] fabricated a tubular implant of PCL with a porosity gradient, using centrifugation rotation method at a high speed of 3000 rpm. Within the tubular implant, pore size was within a range of ~88 to ~405μm increasing gradually along its length and porosity was within a range of ~80% to ~94%. The study concluded that cells and tissues require different pore sizes for their growth such as 380-405 μm for chondrocytes and osteoblast growth, 186-200 μm for fibroblast growth and 290-310 μm for new bone formation thereby proving the tubular implant as a good tool for systematic cellular studies.

2.7 Techniques for establishing Mechanical Properties of Tubular Implants

As already established in literature [35], the elastic modulus of the entire spinal cord in different species of animals, lies within the range of 230-600 kPa. Accordingly, for the tubular implant to be successful *in vivo*, its mechanical properties such as Modulus of Elasticity/Young's Modulus should match that of surrounding spinal cord tissue. Therefore

attempts have been made to design the tubular implants to possess mechanical properties that lie within this range.

Quite a few studies have been undertaken for establishing mechanical properties of tubular implants intended for axonal regeneration after SCI. There is no single testing approach that has been standardized to calculate mechanical properties of a given tubular implant and the techniques differ from each other mainly in two respects: type of force being applied and direction of force being applied. Some studies have tested tubular implants by applying tensile type of force [18, 34, 35, 42, 45, 80, 84, 86, 118] whereas other studies have applied compressive type of force either in transverse direction [41, 74, 82] or in longitudinal direction [2, 10, 119] with respect to orientation of the tubular implant.

Mechanical testing poses to be a challenge due to the differences between the *in vivo* and *in vitro* conditions experienced by the tubular implant. While performing mechanical testing of the implant *in vitro* biomechanical loads along with temperature, pH and osmolality should be closely mimicked as they exist *in vivo*. Also *in vitro* conditions use application of a uniaxial load with ends of the tubular implant being open during testing whereas *in vivo* the tubular implant is either sutured or fit properly to injured stumps of spinal cord and the biomechanical loads are likely to be applied constantly from multiple angles [34].

Luo et al. [42] established Young's modulus of PHEMA-MMA tubular implants by applying tensile force using a micromechanical tester and the similar approach was used by Dalton et al. [35] for mechanically testing the PHEMA tubular implants. Results indicated that mechanical properties of these tubular implants were within the range of mechanical strength of the entire spinal cord, as discussed above. Given their mechanical properties,

these implants were able to exhibit axonal regeneration upon implantation in a SCI rat model [18, 45]. However, in order to obtain sufficient axonal regeneration to provide functional recovery, increased mechanical strength was required [34]. Efforts to this effect resulted in excessively strong implants [41] that resulted in further injury in form of syringomyelic cavity after SCI [43].

Other studies established mechanical properties of tubular implants fabricated from aliphatic polyesters by applying force in tensile direction using a mechanical tester [80, 84, 86]. The modulus of elasticity was calculated based on tensile force required to pull apart two ends of tubular implant till it failed. Use of tensile force for calculating mechanical properties may only provide material properties of the tubular implant and does not mimic *in vivo* biomechanical forces that are expected to be experienced by it.

Compressive force was applied to calculate Modulus of Elasticity of chitosan tubular implants by Ferier et al. [74] in transverse direction and of PLGA implants by He et al. [82] in longitudinal direction. In both cases the compressive force was applied and the mechanical behaviour of the tubular implants was analyzed.

A different type of mechanical testing was performed by Tanaka et al. [2] and Kawaguchi et al. [119] to analyze mechanical behaviour of bioabsorbable polyglycolic acid-collagen (PGA-collagen) tubular implants. Compressive force was applied perpendicular to the longitudinal axis (transverse direction) or along the radius of the tubular implant. The force applied and displacement obtained was plotted and mechanical strength of the tubular implants was analyzed by application of Timoshenko's theory of elastic stability that had been modified accordingly [3]. They observed an estimate of mechanical properties of tubular implants based on their hollow cylindrical shape with a narrow lumen. An effort was

made to provide an estimate regarding *in vivo* biomechanical conditions as they would exist after implantation of the tubular implant.

Some other approaches that were used included use of three-point bending test by de Ruiter et al. [37] to establish mechanical properties of multi-lumen tubular implants. When mechanical strength of single and multi-lumen tubular implants was compared, the multi-lumen implants exhibited increased flexibility. However no value for modulus of elasticity was quoted for any of the tubular implants. Wang et al. [118] reported mechanical testing of bilayered chitosan tubular implants, by application of point load in the compressive direction using a mechanical tester. This method does not reflect the strength of the tubular implant since the biomechanical load being applied on the implant may not be concentrated at a specific point and may be spread over its entire length.

Finally it can be assimilated from the above discussion that mechanical strength of the tubular implant, to be used for tissue regeneration after SCI, plays a crucial role towards its *in vivo* efficacy. While establishing the mechanical strength of the tubular implant, it is quite essential to account both for its shape and morphological structure. This criteria can be met by performing the mechanical testing by application of force along the longitudinal direction of the tubular implant and calculating the value of Modulus of Elasticity. Also to analyze the mechanical behaviour of the tubular implant after implantation, mechanical testing by application of transverse direction force or force along the radial direction of the tubular implant can be performed. Such a direction application of force helps to mimic the biomechanical forces as are expected to be experienced by the tubular implant after implantation. However, this technique can only be used to compare between tubular

implants of a similar type and cannot be used as a standardized measurement technique for all tubular implants.

3. Experimental

3.1 Materials

Polymers, poly (DL lactide-co-glycolide) with 50:50 monomer ratio (PLGA 50:50) at an inherent viscosity range (I.V. range) of 0.76 – 0.94 dL/g (M_w = 81,600 g/mol), poly (ε-caprolactone) (PCL) with I.V. of 1.08 dl/g (M_w = 123,000 g/mol), and poly (lactide-co- ε-caprolactone) (PLCL) (80:20) with an I.V. of 1.26 dl/g (M_w = 175,000 g/mol) were purchased from Durect Corporation (Pelham, AL). Deionized distilled water was obtained from ZenoPure Quatra 90 LC setup (Zenon Environmental Inc., Burlington, ON) and used at 18 MΩ.cm resistance. Chloroform was purchased from VWR International. Bone-dry CO_2 was supplied by BOC (Ottawa, ON) and glass rods with outer diameter of 3mm were purchased from Pegasus Industrial Specialties Inc (Cambridge, ON). All chemicals were used as received unless otherwise indicated.

The polymer molecular structures are listed below:

Poly (DL lactide-co-glycolide) (PLGA 50:50)

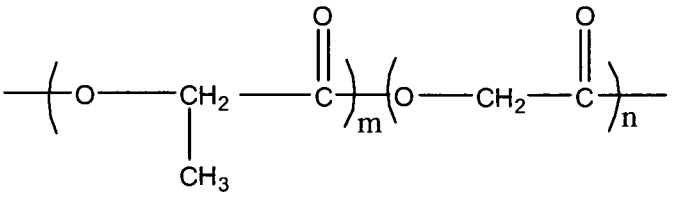

m: n = 50:50

Poly (ε-caprolactone) (PCL)

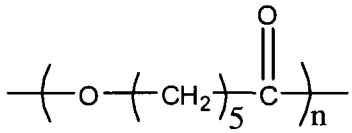

Poly (lactide-co- ε-caprolactone) (PLCL 80:20)

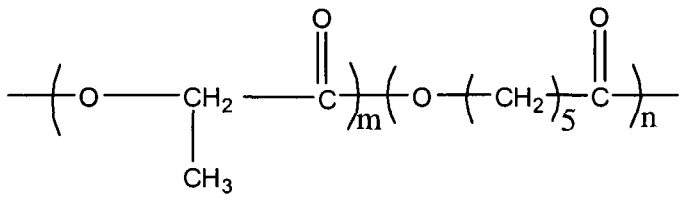

m: n = 80:20

Chemical and physical properties of the polymers used were provided by the manufacturer and are listed in Table 3.1 and 3.2.

Table 3.1 Chemical Properties of the Polymers [120]

Polymer	Inherent Viscosity (dL/g)	Melting Point (°C)	Glass Transition Temperature (°C)	Approximate Resorption (months)
PLGA 50:50	0.76 – 0.94	Amorphous	45-50	1-2
PCL	1.08	58-63	(-65) – (-60)	>24
PLCL 80:20	1.26	Amorphous	17-23	16

Table 3.2 Physical Properties of the Polymers [120]

Polymer	Density (g/mL)	Tensile Strength (MPa)	Elongation (%)	Modulus (MPa)
PLGA 50:50	1.34	41.37 – 55.16	3 - 10	$1.38 \times 10^3 - 2.76 \times 10^3$
PCL	1.11	20.68 – 34.47	300 - 500	$2.07 \times 10^2 - 3.45 \times 10^2$
PLCL 80:20	1.22	~5.17	~150	$4.13 \times 10^2 - 13.78 \times 10^2$

3.2 Fabrication of Hollow Fiber Channels (HFCs)

3.2.1 Dip-Coating Technique

Polymers were dissolved in chloroform to obtain 15% (w/v) solutions. The HFCs were prepared using a dip-coating technique by dipping a 3mm glass mandrel in polymer solution, which was then dried horizontally using a BDC 2002 digital stirrer (Caframo Limited, Wiarton, ON) at speed of 250 rpm. The glass mandrel with the polymer layer was dried for two hours to avoid formation of bubbles, before another layer was coated on top. This process was repeated till a final diameter of 4mm was achieved. Figure 3.1 shows a schematic of the dip-coating technique. After dip-coating, the polymer tubes were dried for 10 days in a vacuum chamber, at gauge pressure of - 24 kPa and room temperature.

Single layered HFCs were obtained by dip-coating 11 layers of PLGA solution and double layered HFCs were obtained by first dip-coating 7 layers of PLGA solution followed by 6 layers of PLCL/PCL_3/1 (w/w) blend solution.

Some HFCs were also fabricated with a reversed layout of porosity gradient and characterized as reverse porosity HFCs. This typical structure was achieved by dip coating 7 layers of PLGA solution followed by 7 layers of PLCL/PCL_9/1 (w/w) blend solution. By altering the ratio of the PLCL/PCL blend, a different morphology was achieved.

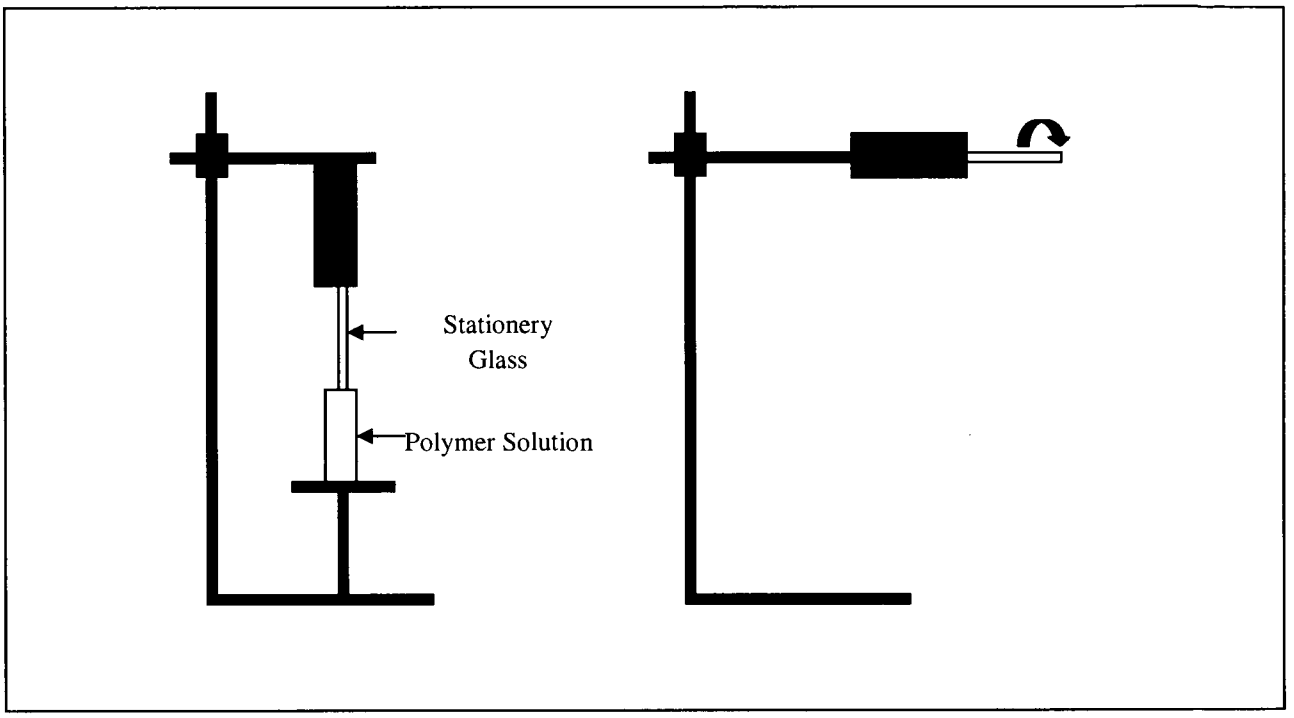

Figure 3.1 Schematic of HFC Fabrication by Dip-coating technique

3.2.2 Sub-critical CO_2 foaming

To obtain the desirable foamed morphology of HFC, the single and double layered polymer tubes, were saturated with sub-critical CO_2 at a pressure of 5.86 MPa at room temperature (~25°C) for 5.5 hours. Before soaking in sub-critical CO_2 environment, the polymer tube was encased in a hollow cylindrically shaped teflon mould and capped at both ends, to ensure that the final HFC that was produced had accurate dimensions. The mould and its caps at the two ends were designed with holes for exposure to sub-critical CO_2. A schematic of the stainless steel foaming chamber is shown in Figure 3.2.

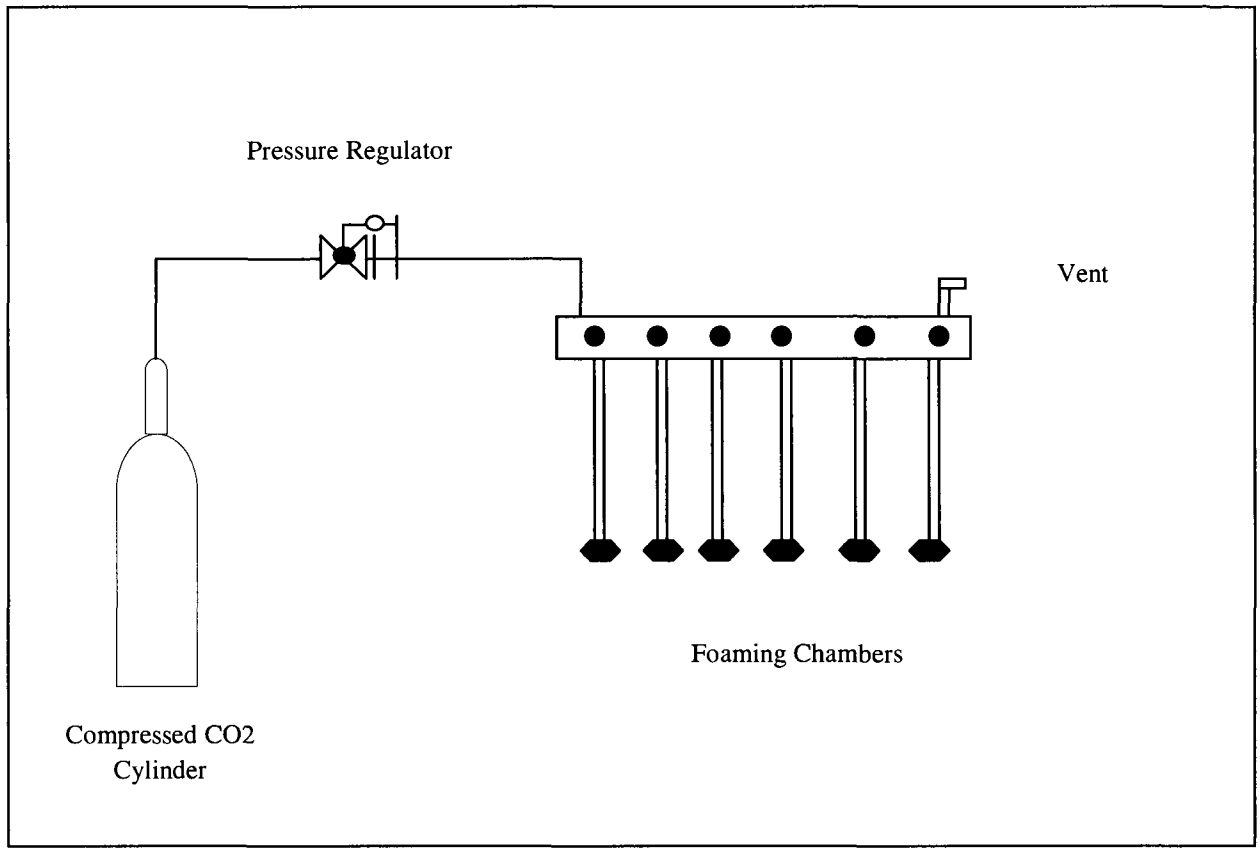

Figure 3.2 Schematic of the sub-critical CO_2 foaming process

3.3 Mechanical Testing of HFCs

Mechanical testing of single and double layered HFCs was done using Instron Mechanical Tester floor model 4482 (Norwood, MA). More than 3 samples of each single and double layered HFC, with an inner and outer diameter of 3mm and 5mm, respectively were tested. The HFCs were tested, based on ASTM standards (D 618 00, E6-03, E9-89a, E111-97) with minor modifications. The uniaxial compressive force was applied at speed of 0.1mm/sec to avoid damage to HFC structure during testing and to obtain wide range of data for necessary calculations. Each HFC was compressed up to 3.5 mm to analyze the behaviour exhibited by the foamed structure of the HFC.

3.3.1 Longitudinal direction

Longitudinal direction mechanical testing was performed for single and double layered HFCs by application of compressive force along the longitudinal axis of the HFC at a speed of 0.1 mm/min, using a 100 N load cell thereby compressing the HFC by 3.5 mm. A schematic of direction of force application is shown in Figure 3.3. The mechanical testing was done at room temperature. The modulus of elasticity was calculated from the slope of the stress-strain curve by using the following relationship [41]:

$$Modulus\ of\ Elasticity = \frac{Stress\,(\sigma)}{Strain\ (\varepsilon)}$$

where:

$$\sigma = \frac{F}{\pi/4\left(d_o^2 - d_{ii}^2\right)} \qquad (1)$$

$$\varepsilon = \frac{l_f - l_i}{l_i} \qquad (2)$$

F denotes the force applied, d_o, d_{ii}, denote the outside and inside diameter of the HFC respectively and l_i, l_f denote the initial length and final length after application of force of the HFC respectively.

For the mechanical testing of all the HFCs, a single factor ANOVA test was used (with significance level of $\alpha = 0.05$) to compare the average values of all the samples.

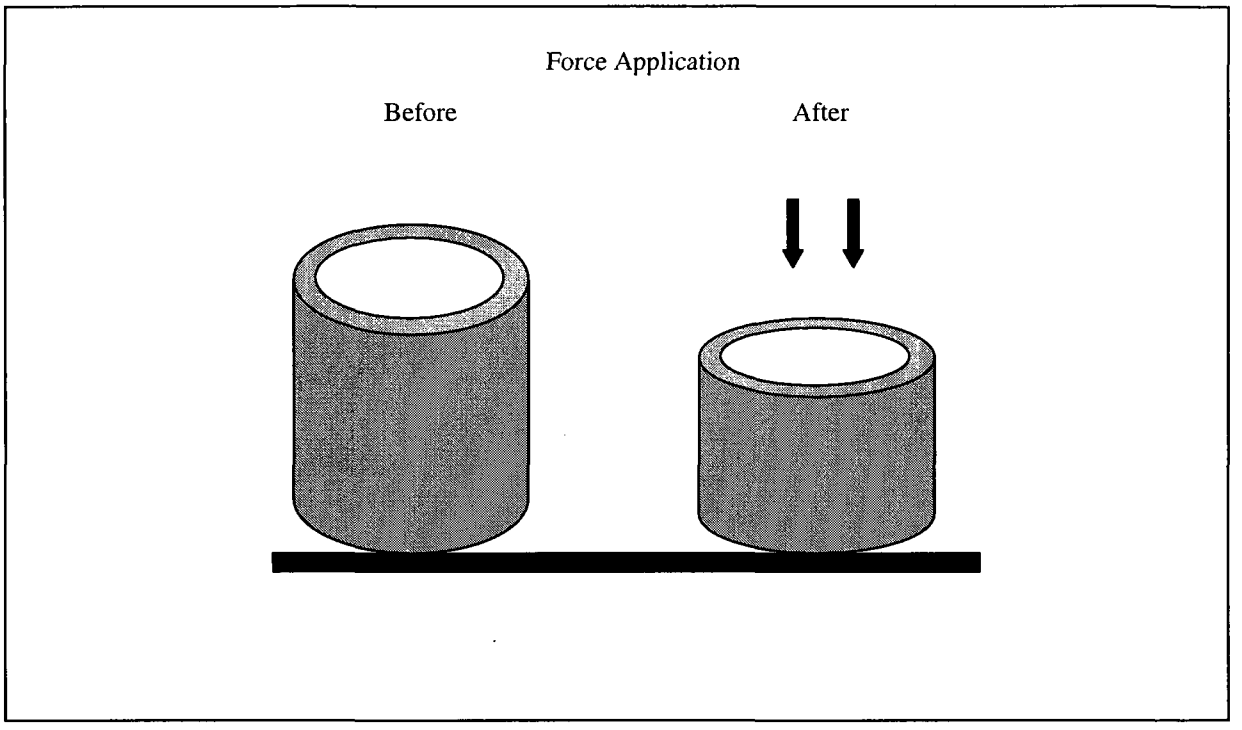

Figure 3.3 Schematic of mechanical testing in longitudinal direction

3.3.2 Transverse direction

Transverse direction mechanical testing of single and double layered HFCs was performed by application of compressive force perpendicular to the longitudinal axis of the HFC or application of force along its radial direction, at a speed of 0.1 mm/min, using a 100 N load cell thereby compressing the HFC by 3.5 mm. The mechanical testing was done at room temperature. A schematic of direction of force application is shown in Figure 3.4.

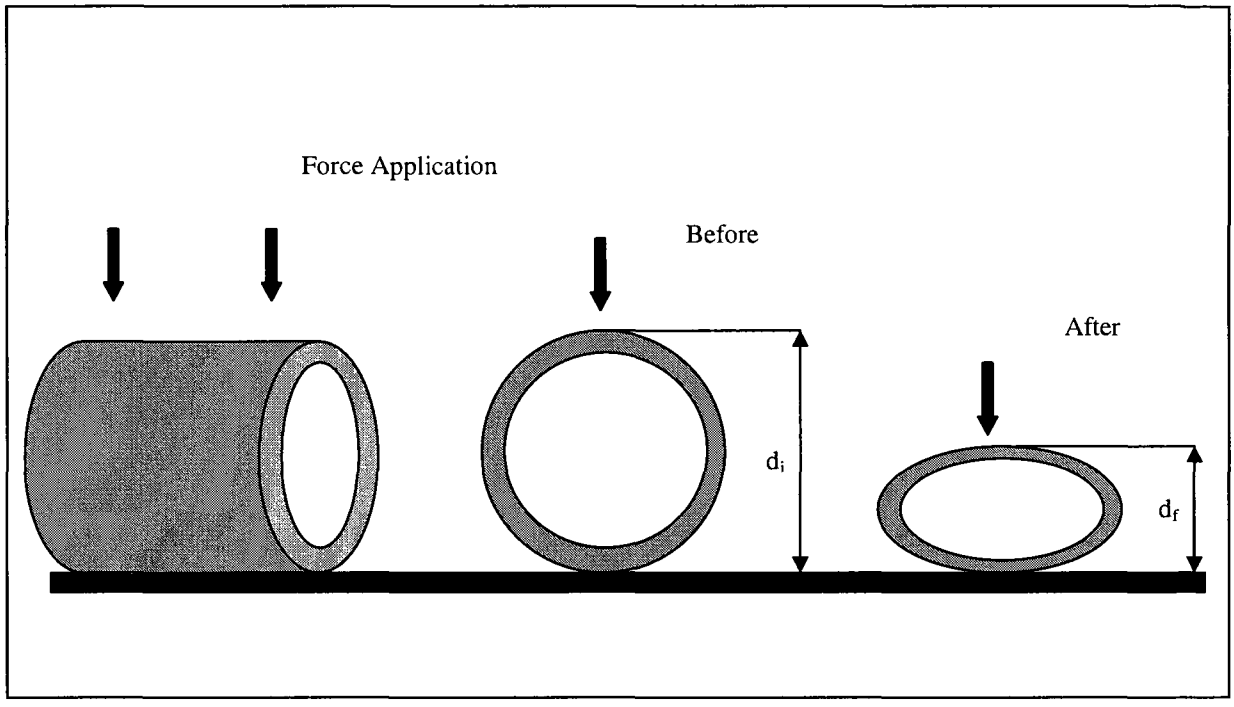

Figure 3.4 Schematic of mechanical testing in transverse direction

The data from the mechanical testing of each HFC was collected in the form of 'Force applied versus deformation obtained'. The strain (ε) was calculated as [2]:

$$\varepsilon = \frac{d_i - d_f}{d_i} \qquad (3)$$

where d_i and d_f are the initial diameter and final diameter after application of force, of the HFC respectively. Due to varying lengths of the HFCs, within a range of 8-11 mm, the force applied was normalized against length.

For each HFC tested a curve was plotted between 'Force per unit length (F) versus the subsequent strain (ε)'. This curve helped in establishing a comparison of mechanical strength between single and double layered HFCs.

Also a curve was plotted between 'Force per unit length and weight (F/w) versus strain (ε)', to analyze the mechanical strength offered by both single and double layered HFCs for a unit mass.

For the mechanical testing of all the HFCs, a single factor ANOVA test was used (with significance level of $\alpha = 0.05$) to compare the average values of all the samples.

3.4 Scanning Electron Microscope

The HFC samples were stored at room temperature for 2 days before they were fractured in liquid nitrogen. The HFCs were mounted on aluminum studs using Pelco conductive graphite paint (Redding, CA) and then sputter coated with gold-palladium coating of 7 μm thickness. The porous structures of the surfaces were observed under SEM (Tescan Vega-II XMU Variable Pressure SEM).

3.5 Characterization of HFCs

3.5.1 Image Analysis

For characterization of HFCs, the dimensions of individual cells were calculated using the Image Pro 3D Analyzer 6.0 software (Media Cybernetics, Inc., Bethesda, MD). The cell edge length, cell wall thickness and cell face thickness were measured. An average value was calculated from 10 measurements made from the sample group and standard deviation was also calculated.

3.5.2 Density & Porosity

To calculate the density 'ρ' of the HFC, its mass and volume were calculated and the following relationship was used [121]:

$$\rho = \frac{mass}{Volume} \qquad (4)$$

The volume of the HFC is given by:

$$Volume = \pi\left(r_o^2 - r_i^2\right)\ell \qquad (5)$$

where r_o, r_i and l are the outer diameter, inner diameter and the length of the HFC.

The porosity of the HFC was calculated by using the following relationship [121]:

$$Porosity = 1 - \frac{\rho^*}{\rho_s} \qquad (6)$$

where ρ^* and ρ_s are the densities of the foamed and unfoamed HFC.

3.6 Degradation Study

3.6.1 Study Layout

This study was carried out to investigate the *in vitro* degradation behaviour of single and double layered HFCs. The study was carried out over duration of 10 weeks, with each type of HFC batch, Single layered (Batch 1) and Double layered (Batch 2), having 40 samples each.

Before beginning the study, each HFC was weighed, using the Sartorius CPA225D analytical balance (Sartorius AG, Germany) and its weight was recorded at Week 0. After this each HFC was enclosed in a fine cotton mesh bag, thereby creating a small tea bag like structure, which was then suspended in a glass bottle containing 20 ml of PBS (physiological media) with 1% sodium azide dissolved in it to avoid growth of any bacteria in the HFC.

Starting Week 1 of the study, all the glass bottles containing the HFCs were placed at a temperature of 37°C. All the procedures of the degradation study were followed as per the guidelines in the ASTM F 1635-04 standard.

Throughout the degradation study, pH of the samples was monitored every two days and changed appropriately when observed to be lower than the physiological range. The samples were shaken twice daily to ensure that PBS infiltrated evenly throughout the HFC.

A set of 4 samples from each batch were retrieved at the same time point in each week. These samples were washed three times in dionized distilled water, frozen overnight at -20°C and then freeze dried for 48 hours with Labconco Freeze Dry System (Kansas City, MO) to ensure that there was no left over moisture within the HFCs.

After vacuum freeze drying, all HFCs were weighed within the cotton mesh bags and the mass loss was calculated fusing the following relationship:

$$mass\,loss = \frac{M_0 - M_t}{M_i} \qquad (7)$$

where M_0 and M_t are the mass of the HFC enclosed in the bag at Week 0 and 't' refers to the time point (Week 1, 2, 3 ... 10) during degradation respectively, and M_i is the initial mass of the HFC without the bag at Week 0.

3.6.2 Characterization of Samples (Mechanical Testing, SEM pictures, Image Analysis)

All samples retrieved each week were weighed and their dimensions (length, outer diameter and inner diameter) were measured using electronic digital vernier caliper (VWR, Mississauga, ON). For characterization purposes, their volume, density and porosity was calculated as described in Section 3.5.2.

Three samples from each batch, Batch1 and Batch2, were tested for their mechanical strength along the longitudinal direction as per the method in Section 3.3.1.

Also one sample from each batch was viewed under SEM for Image Analysis as described in Section 3.5.1.

4. Results

4.1 Morphology of HFC

During fabrication of single and double layered HFCs it was essential to ensure that each layer being dip coated was created uniformly and smoothly without air bubbles. To achieve this, after dip coating the polymer tubes were dried for 2 hours till the desirable number of layers had been dip-coated. Then, before foaming the polymer tubes were dried for 10 days in a vacuum chamber that helped evaporate most of the solvent and thus led to HFCs being fabricated reproducibly and without any air bubbles.

All fabricated HFCs, single and double layered, had an inner diameter of 3.04 ± 0.03 mm and outer diameter of 5.24 ± 0.11 mm. Given our fabrication technique the length of HFCs varied slightly and the average value was 9.77 ± 1.92 mm.

4.1.1 Single layered HFC

Morphology of single layered HFC is shown in Figure 4.1. As shown in the cross sectional view, the single layered HFC is fabricated only from one material PLGA 50:50 and has uniform porosity throughout the structure.

Characterization of foamed structure of HFC helped to establish that average pore size was 63.67 ± 15.73 μm. The porosity of single layered HFCs was calculated to be 77%. This value compares well with porosities obtained in scaffolds fabricated using such biodegradable materials [50].

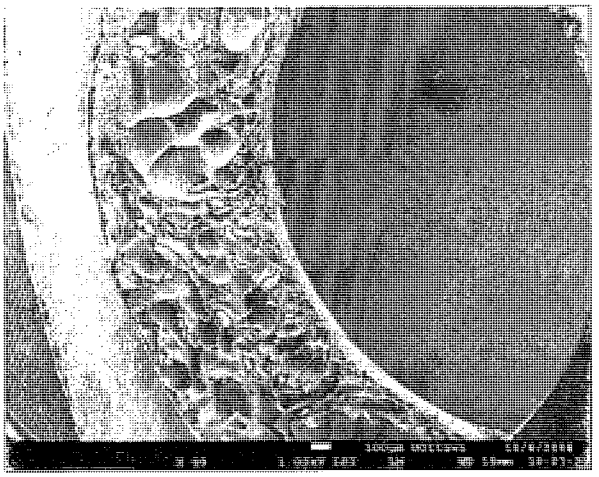

Cross Section view

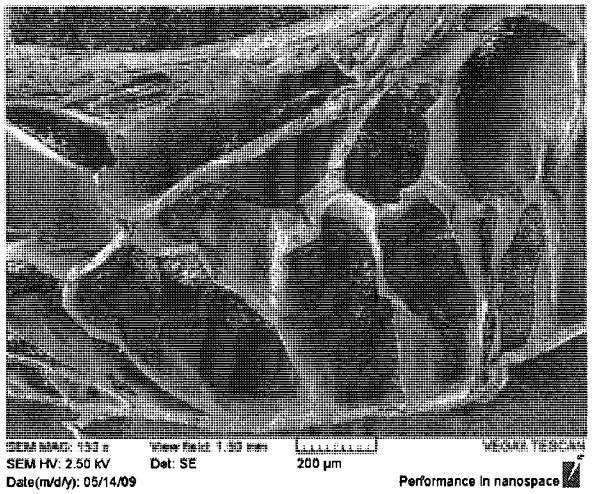

Cross Section view at higher magnification

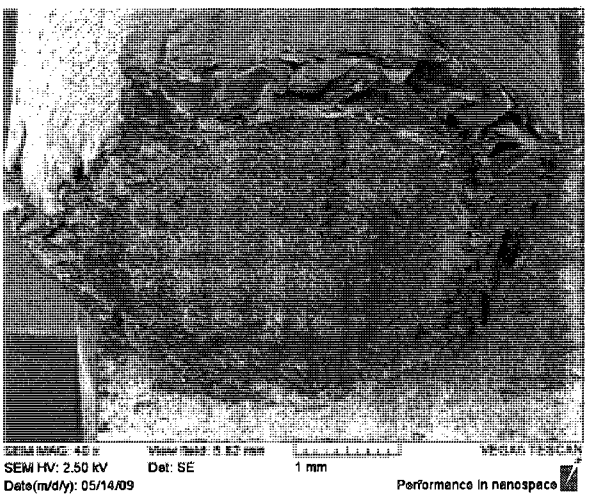

View of Inner Lumen and Outer surface

Figure 4.1 Morphology of Single layered HFC

4.1.2 Double layered HFC

Within the double layered HFC, the inner layer fabricated from PLGA 50:50 has larger pores as compared to the outer layer composed of PLCL/PCL_3/1 blend with smaller pores as shown in Figure 4.2. The gradient of porosity is distinctly visible within the cross section view of the double layered HFC, as the pore size of inner layer becomes smaller while moving radially outwards, from the inner lumen towards the outer layer.

Upon characterization of foamed structure of HFC, it was observed that average pore size of inner layer was 54.04 ± 5.04 μm and that for outer layer was 5.03 ± 1.05 μm.

The porosity of double layered HFCs has been calculated as 54%. This value compares well with porosities obtained in scaffolds fabricated using such biodegradable materials [50].

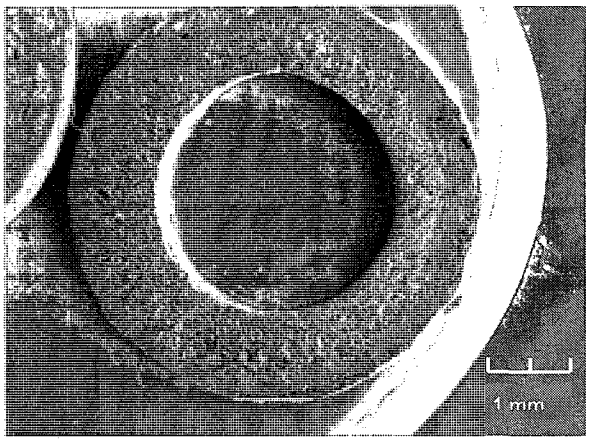

Cross Section view

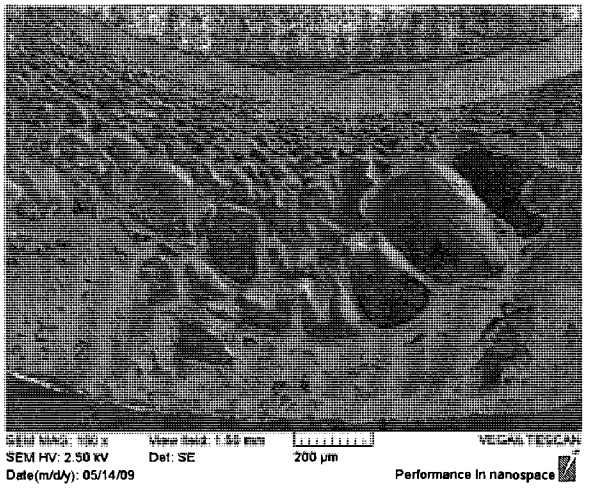

Cross Section view at higher magnification

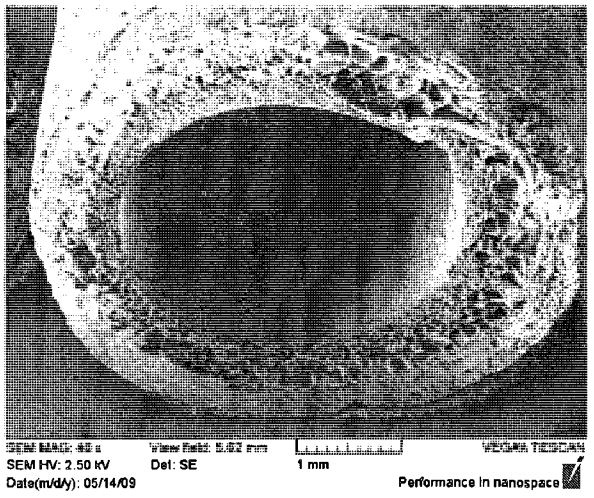

View of Inner Lumen and Outer surface

Figure 4.2 Morphology of Double layered HFC

4.2 Mechanical Testing

To establish the mechanical strength of the single and double layered HFCs, mechanical testing was performed by application of compressive force along the longitudinal axis of the HFC and this has been referred to as 'Longitudinal Direction' testing. This approach has been undertaken by some studies [34, 41] to establish mechanical properties of a tubular implant and helps in comparing the mechanical strength of single and double layered HFCs with other tubular implants that have been used for a similar purpose in this field of research. Also this technique is useful in establishing the mechanical strength of the HFC while accounting both for its cylindrical shape and foamed morphological structure.

'Transverse Direction' testing refers to applying compressive force perpendicular to the longitudinal axis of a tubular implant or along its radial direction. Due to very small annular dimensions of the HFC, this method was chosen solely to compare and analyze the difference in mechanical properties of single layered and double layered HFCs [3] fabricated in our laboratory. We feel that this technique helps in providing an estimate of *in vivo* biomechanical forces that are expected to be experienced by the HFC post implantation.

4.2.1 Mechanical Testing in Longitudinal Direction

'Longitudinal Direction' mechanical testing was done on both single and double layered HFCs. As discussed in Section 3.3.1, the modulus of elasticity was obtained from the slope of the 'Stress vs Strain' curve. This slope was obtained from the indicated region of the curve as shown in Figure 4.3.

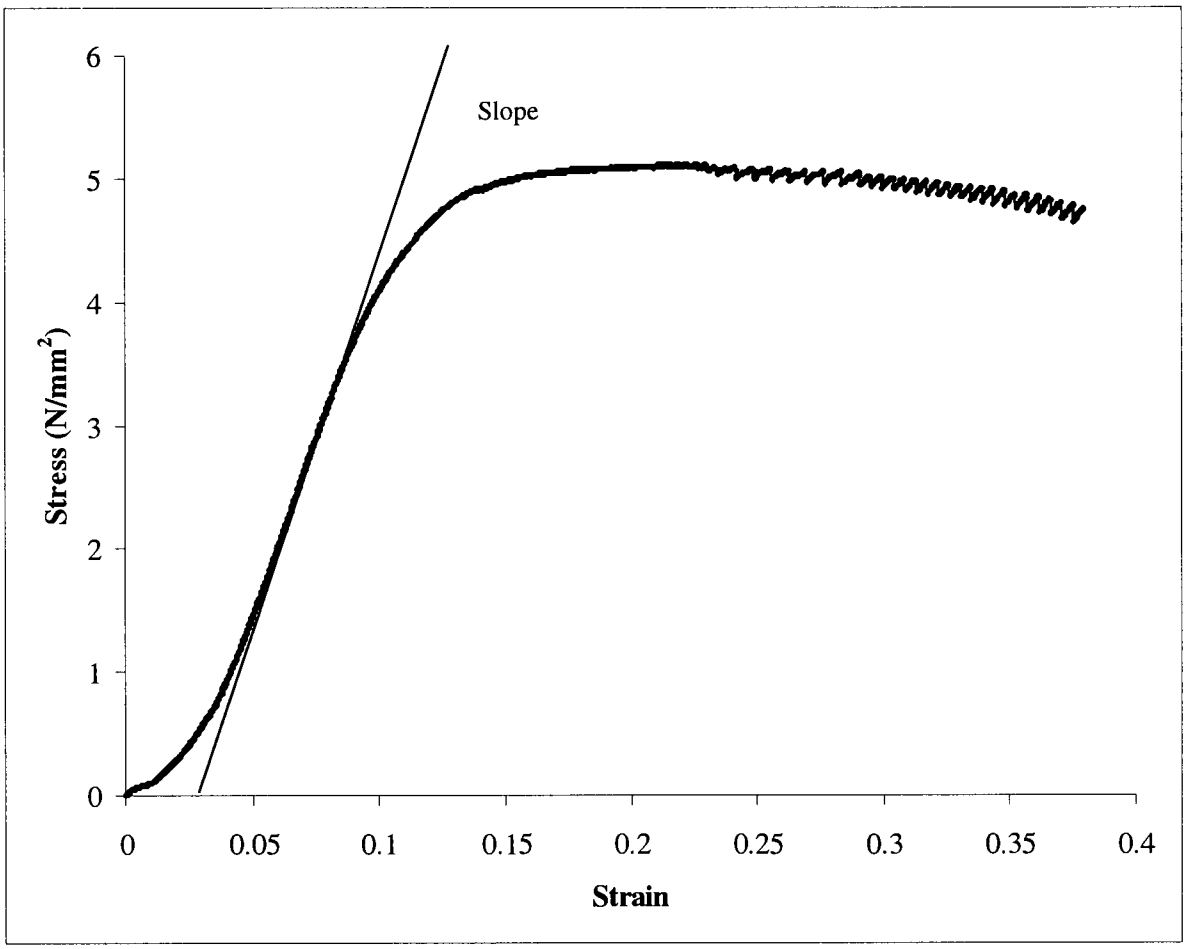

Figure 4.3 Curve obtained from 'Longitudinal Direction' testing

4.2.2 Longitudinal Direction: Mechanical Strength of HFCs

The modulus of elasticity obtained by 'Longitudinal Direction' testing was 60.27 ± 8.85 MPa for double layered HFCs and 36.65 ± 6.20 MPa for single layered HFCs. The double layered HFCs were more than 1.5 times stronger than single layered HFCs, a comparison of which is shown in Figure 4.4.

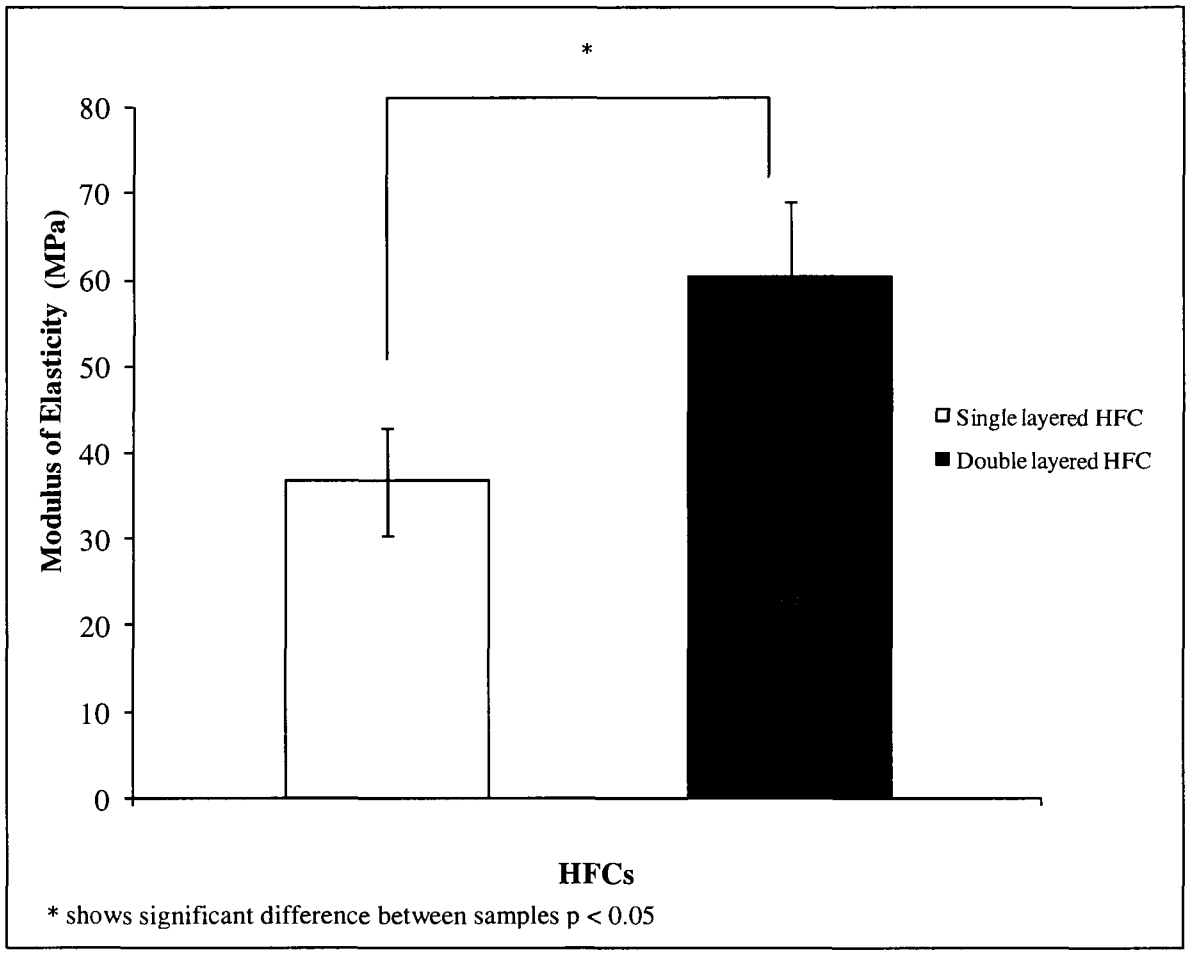

Figure 4.4 Comparison between modulus of elasticity for single and double layered HFCs by 'Longitudinal Direction' testing

4.2.3 Mechanical Testing in Transverse Direction

During the transverse direction testing, mechanical strength was analyzed for each of the HFCs, by normalizing the force applied with the length of the HFC. Figure 4.5 shows the typical shape of the curve achieved after transverse direction testing.

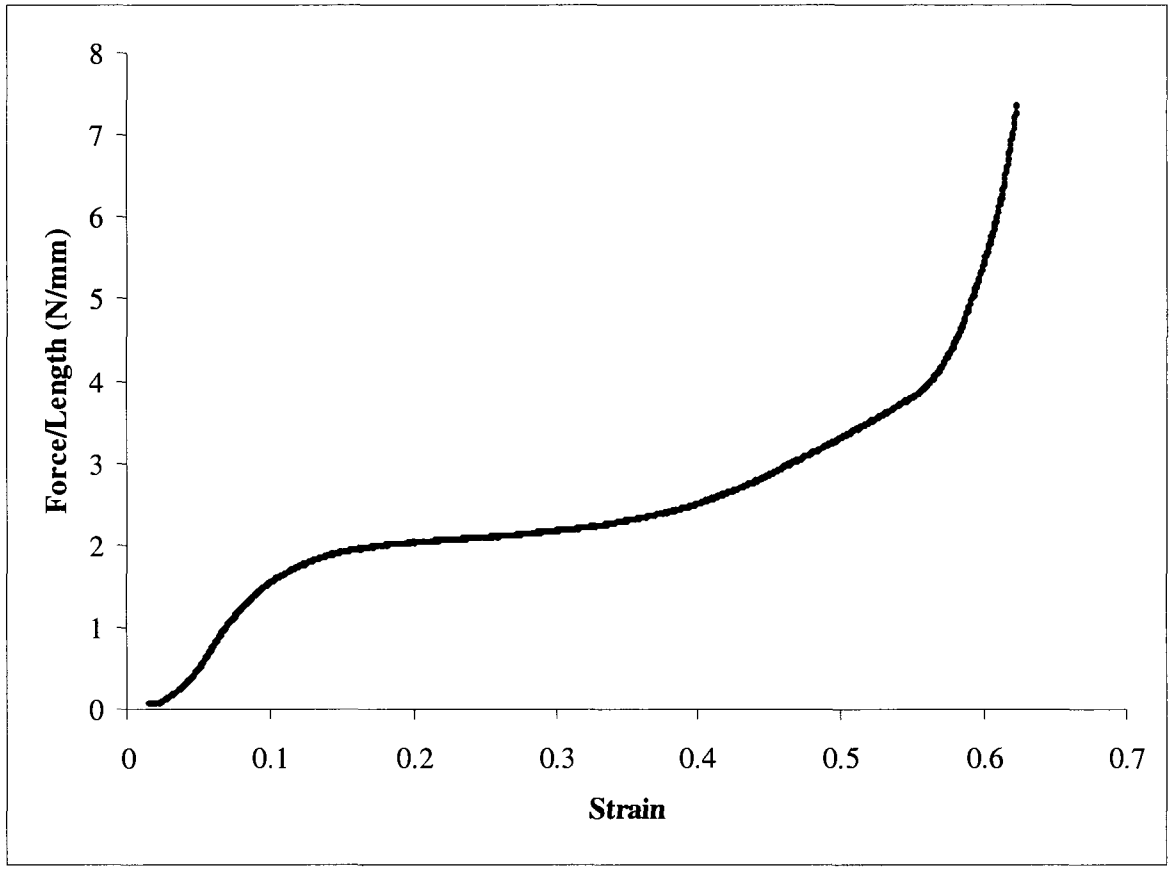

Figure 4.5 Curve from 'Transverse Direction' testing

4.2.4 Transverse Direction: Mechanical Strength normalized with length

The mechanical strength normalized with length for single and double layered HFC was analyzed by using the initial part of the slope, <10%, from the 'Force per unit length (F) versus the subsequent strain (ε)' curve[¶].

The unit mechanical strength, normalized with length, for double layered HFC was 390.09 ± 10.63 kPa and for single layered HFC was 181.91 ± 7.55 kPa. As shown in Figure 4.6, these values indicate that double layered HFC is twice as strong as single layered HFC.

[¶] For further details on this concept and derivation of units please refer Ref [2, 3]

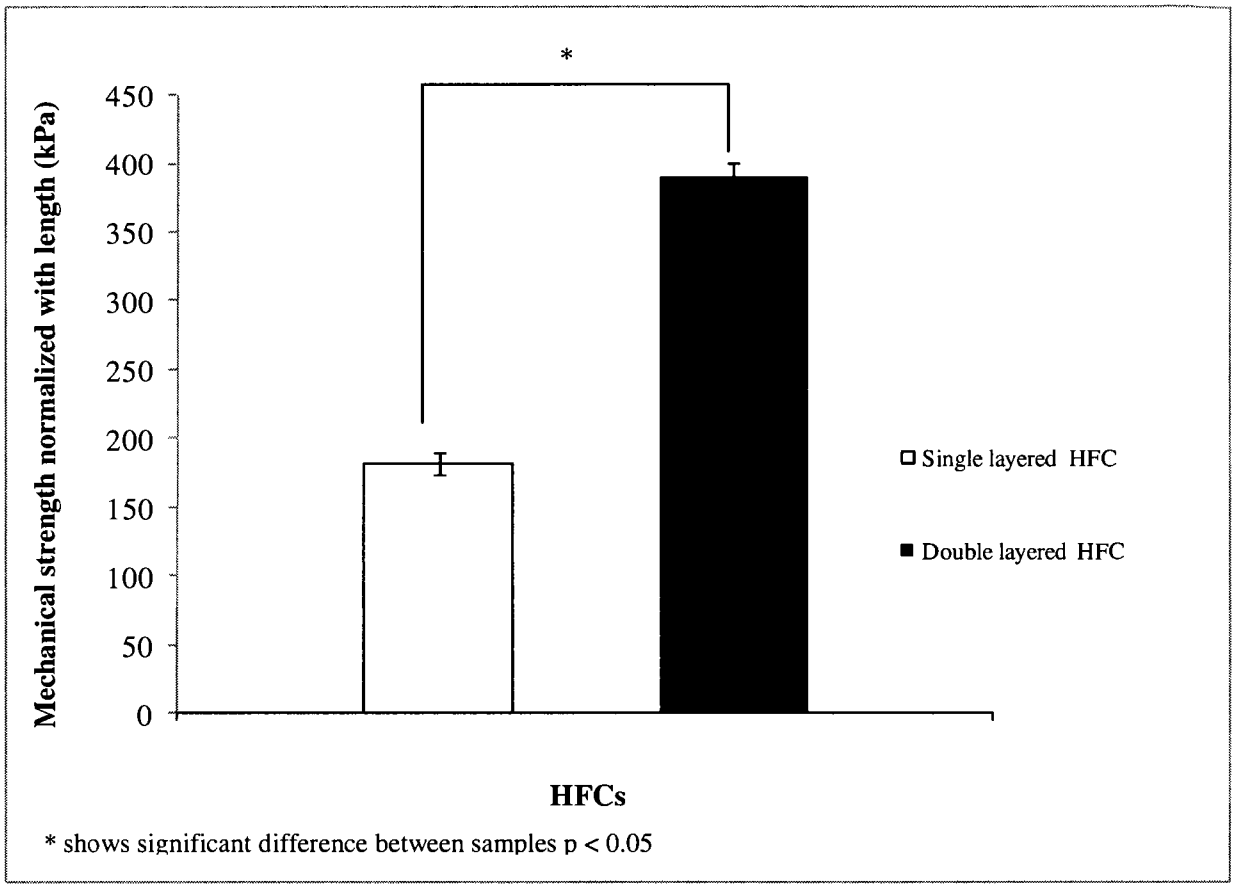

Figure 4.6 Comparison between mechanical strength normalized with length, for single and double layered HFCs

4.2.5 Transverse Direction: Mechanical strength normalized with length and weight

The mechanical strength normalized with length and weight was analyzed to establish the mechanical strength being offered by each type of HFC, single or double layered, for a given mass. This was done by using the initial part of the slope, <10%, from the curve plotted between 'Force per unit length and weight (F/w) versus strain (ε)'[¶].

Mechanical strength, normalized with length and weight, for double layered HFC was 5207.07 ± 420.30 kPa and for single layered HFC was 3370.70 ± 374.12 kPa. Figure 4.7 clearly indicates that the mechanical strength normalized with length and weight for double layered HFC was 1.5 times higher than the value obtained for single layered HFC. It is evident from this result that the double layered HFC provides higher strength for a given mass of HFC when compared to a single layered HFC.

This important result helps to bring us closer to our goal of being able to fabricate a HFC that possesses adequate mechanical strength for a given mass, thereby providing a structure that mimics the structure of bone.

[¶] For further details on this concept and derivation of units please refer Ref [2, 3]

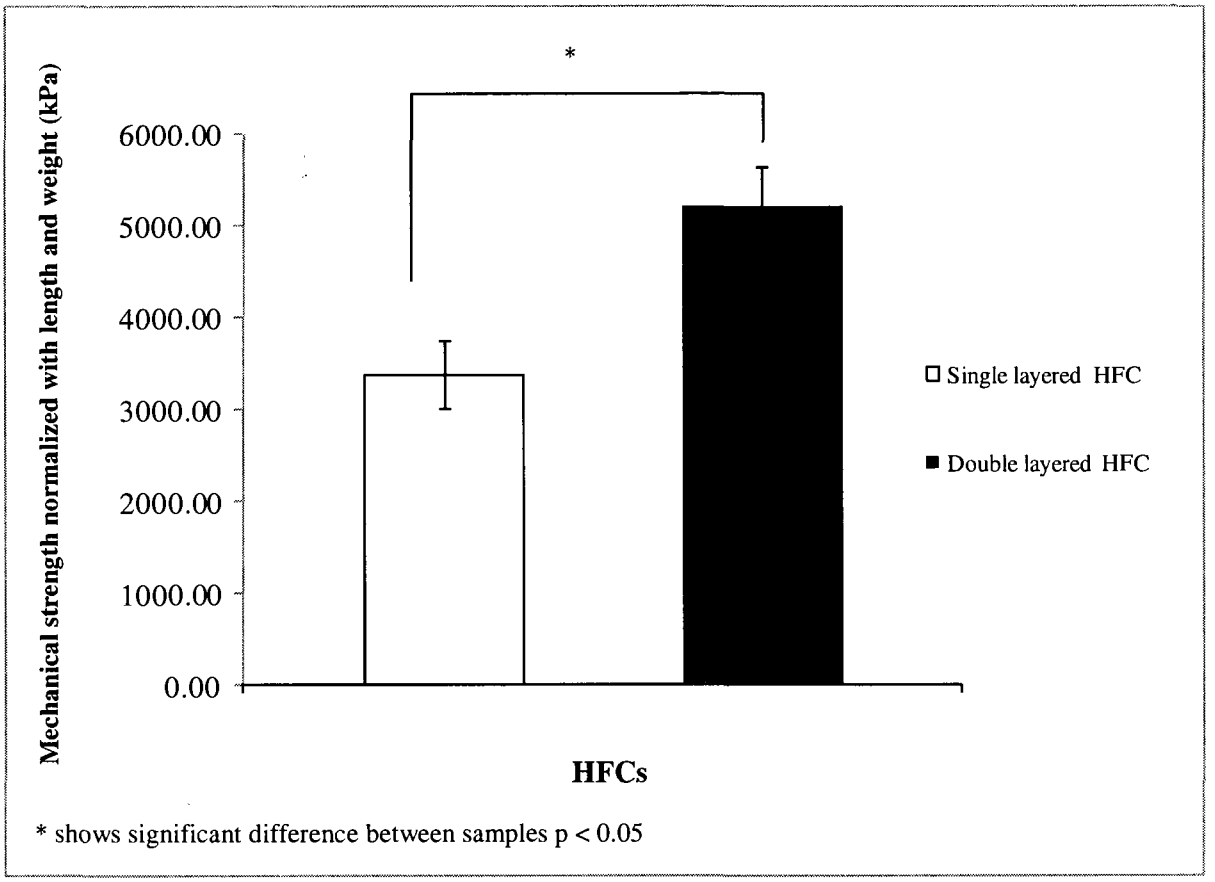

Figure 4.7 Comparison between mechanical strength normalized with length and weight, for single and double layered HFCs

4.3 Degradation Study

The main focus of this study was to understand and analyze the respective changes in mechanical strength of both single and double layered HFCs upon *in vitro* degradation. To better analyze the degradation behaviour of the HFCs, behaviour displayed due to mass loss, changes in volume & porosity were monitored. The general observation during the degradation study was that by Week 4, the single layered HFCs collapsed completely, breaking in pieces and losing their cylindrical shape. In double layered HFCs, this similar behaviour was seen by Week 8. As a result, after collapse of the HFCs only mass loss could be studied, since other properties such as volume loss, porosity and mechanical strength were structure dependant.

4.3.1 Mass Loss for single and double layered HFCs

As shown in Figure 4.8, during the first three weeks of degradation study, rate of mass loss was low and within 10%, for both single layered and double layered HFCs even though the rate of mass loss was greater for single layered than double layered HFCs. After Week 3, the rate of mass loss increased for both types of HFCs. For double layered HFCs, the increase in mass loss assumed a gradual slope, being 2% at Week 3 and going up to 73.5% at Week 10. However for single layered HFCs, mass loss at Week 3 was recorded at 4.5% and it jumped dramatically to reach 91% by Week 10. The rapid increase in mass loss for both single and double layered HFCs correlates with the time point when they lost their cylindrical shape, Week 4 and Week 8 respectively (as shown in SEM micrographs in Section 4.3.5).

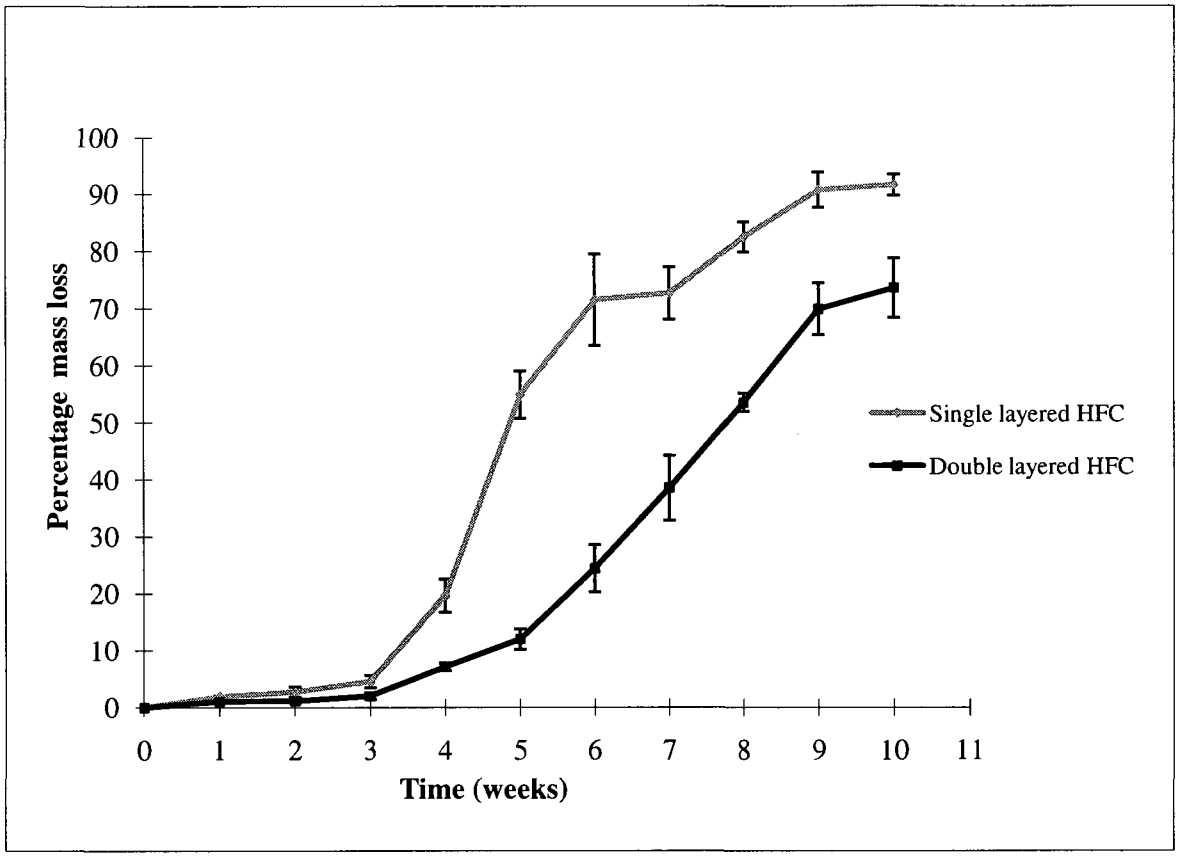

Figure 4.8 Percentage mass loss for single and double Layered HFCs

4.3.2 Mass Loss of two layers of double layered HFC

As discussed above, the rate of mass loss for single and double layered HFCs could be established during the degradation study but it was difficult to establish the rate of mass loss separately for inner and outer layer of the double layered HFC. However it was known that the inner layer was fabricated from the same biomaterial as the entire single layered HFC i.e. PLGA 50:50, albeit with different number of layers. Thus an attempt was made to mathematically calculate the individual rate of mass loss for the inner and outer layers of a double layered HFC, as discussed below. It was assumed that the rate of degradation of single layered HFC and the inner layer of double layered HFC was same, since they were fabricated from the same biomaterial.

The double layered HFCs were always fabricated by 6 times dip coating in PLGA 50:50 to constitute the inner layer and 7 times dip coating in PLCL/PCL_3/1 blend to constitute the outer layer. The following relationships were used:

$$\rho_{PLGA} = \frac{m_{PLGA}}{V_{PLGA}} \qquad (8)$$

where ρ_{PLGA}, m_{PLGA}, V_{PLGA} refer to the density, mass and volume of single layered HFC respectively. From the above, density of single layered HFC was obtained.

For double layered HFC:

Thickness of each layer dip coated (EL) = Total thickness of HFC / 13

This assumption was made based on the fact that during dip-coating of each layer, parameters such as duration of dip-coating and viscosity of polymer solution used were constant.

If r_o, ri denote the outer and inner radii of the double layered HFC and r_6 denotes the radii of the entire inner layer of PLGA 50:50 (since there are 6 dip coats), then:

$r_1 = r_i + EL;$ $r_2 = r_1 + EL;$ $r_3 = r_2 + EL;$

$r_4 = r_3 + EL;$ $r_5 = r_4 + EL;$ $r_6 = r_5 + EL;$

For the hollow cylindrical structure of double layered HFC:

$V_{InnerLayer}$, $m_{InnerLayer}$ is volume and mass respectively of inner layer of PLGA 50:50

$V_{OuterLayer}$, $m_{OuterLayer}$ is volume and mass respectively of outer layer of PLCL/PCL_3/1 blend

$m_{DoubleLayered}$ is the mass of the entire double layered HFC

$l_{DoubleLayered}$ is the length of the entire double layered HFC

$V_{InnerLayer} = \pi * l_{DoubleLayered} * (r_6^2 - r_i^2)$

$m_{InnerLayer} = \rho_{PLGA} * V_{InnerLayer}$

$m_{OuterLayer} = m_{DoubleLayered\ HFC} - m_{InnerLayer}$

Based on the above calculations the rate of mass loss of the outer layer was calculated. The individual rates of mass loss of inner and outer layer of a double layered HFC are plotted in comparison with its overall mass loss rate in Figure 4.9.

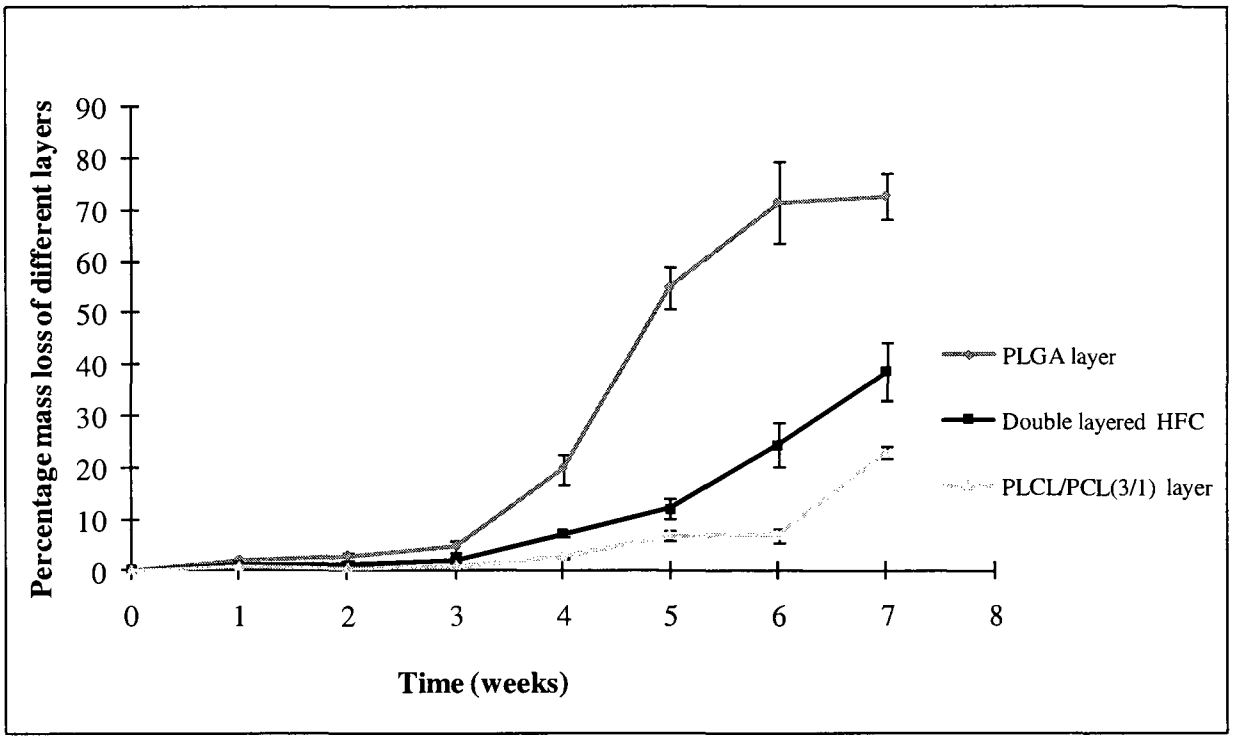

Figure 4.9 Percentage mass loss for the two layers of double layered HFC

4.3.3 Change in Volume and Porosity for single and double layered HFCs

For calculating the changes in volume, parameters of length (l), outer (d_o) and inner (d_i) diameter of the HFC samples were measured, recorded and volume calculated, after they were retrieved each week at the same time point.

As shown in Figure 4.10, the rate of volume loss was observed to be greater for single layered HFCs as compared to double layered HFCs. Data for single layered HFCs could not be collected after week 3, since their cylindrical shape had ruptured.

However, for double layered HFCs, the rate of volume loss was observed to stabilize after Week 3. At Week 6, the inner layer of the double layered HFC, fabricated from PLGA 50:50, collapsed completely thereby closing the lumen of the HFC. This behaviour was observed in all the double layered HFC samples at this time point. As a result, due to lack of a dimension of the inner lumen, during measurement and calculation, the volume is indicative of a closed cylindrical structure. This unexpected behaviour of the inner layer of the double layered HFC, is the reason behind the abnormal 'increase in volume' observed at Week 6 in Figure 4.10.

After Week 6, the inner layer of the double layered HFC continued to degrade and the debris from within the lumen cleared by Week 7. As a result the dimension for the inner lumen showed an increase and the rate of volume loss was recorded at 50.3% as compared to 22% at Week 5. The data from Week 6 is considered as an aberration in this case. After Week 7 the structure of double layered HFC collapsed and further volume related measurements could not be taken.

As shown in Figure 4.11, the porosity for single layered HFCs decreased considerably during the first 3 weeks, starting from its initial value of 77% and reaching a

low value of 40% at Week 3. Since the measurement of porosity was based on volume, after Week 3 the porosity for single layered HFC could not be calculated.

For double layered HFCs, reduction of porosity was observed at Week 1. Then onwards the trend exhibits little change in value of porosity and is recorded at 58% during Week 5. The only exception to this behaviour was value of porosity at Week 6, which was at an abnormally low value of 48.7 % due to unexpected changes in volume as a result of blockage of inner lumen of the HFC, as has already been discussed above. No porosity calculations could be made at Week 8, due to rupture of the cylindrical shape of the double layered HFC. For the double layered HFCs, after the initial drop in porosity, the value continued to increase throughout the degradation study.

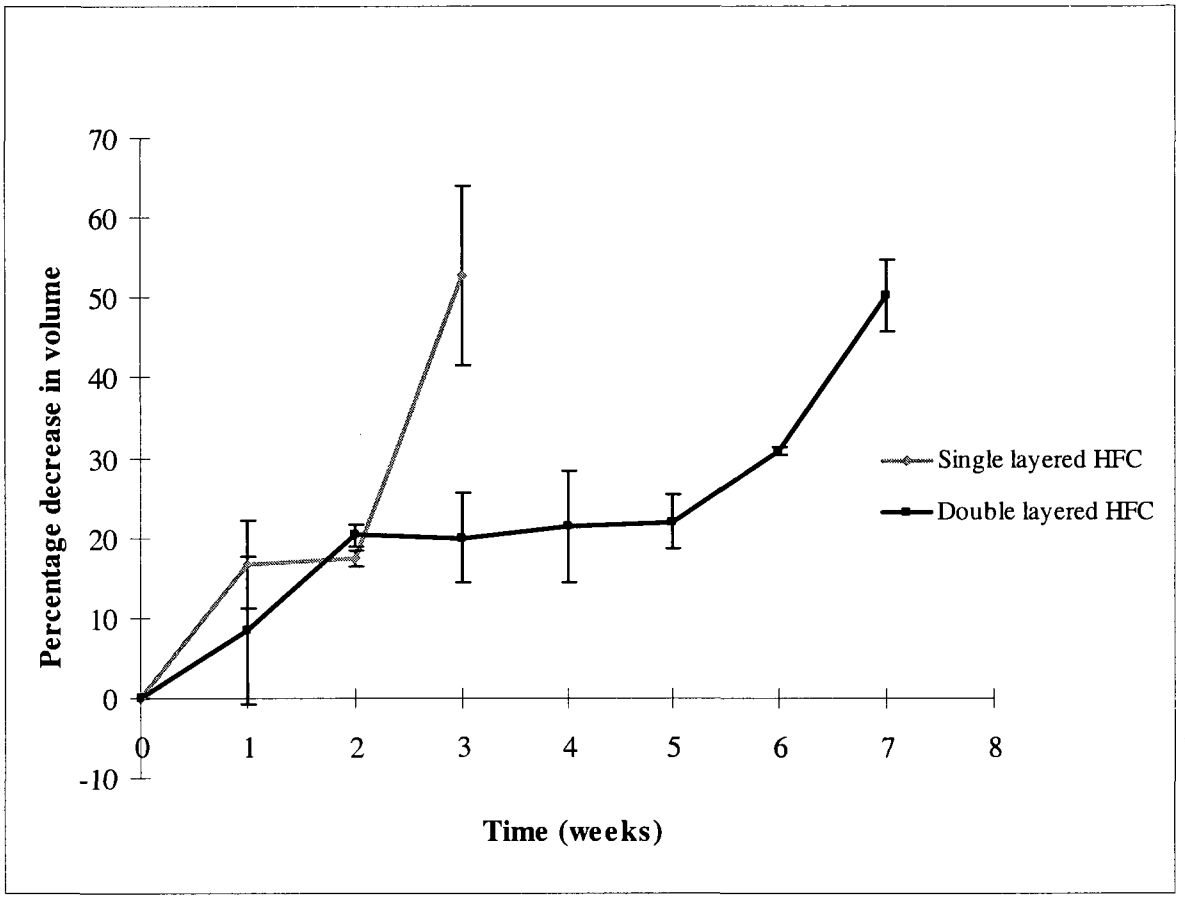

Figure 4.10 Percentage volume loss for single and double Layered HFCs

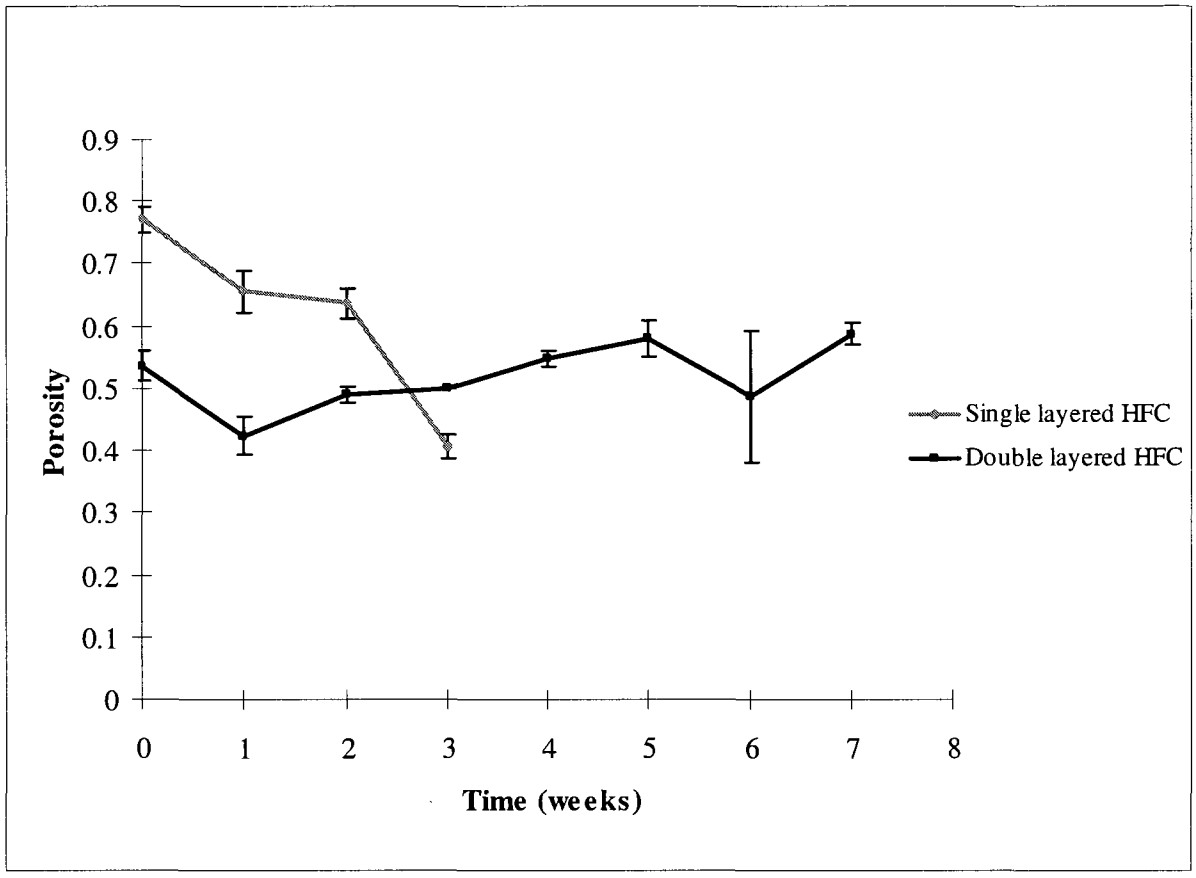

Figure 4.11 Change in Porosity for single and double layered HFCs

4.3.4 Change in Mechanical Strength of single and double layered HFCs

During the degradation study mechanical strength of single and double layered HFCs was clearly impacted. As was to be expected, the degradation of the biomaterials from which the HFC was fabricated, reduced its mechanical strength over the duration of 10 weeks.

4.3.4.1 Mechanical strength normalized with length

During the degradation study the difference in mechanical behaviour of single and double layered HFCs was compared by performing testing by the 'Transverse direction' method. As shown in Figure 4.12 the mechanical strength normalized with length increased twofold at Week 1 as compared to its value at Week 0 for both single and double layered HFCs. However, at Week 2 the mechanical strength began to decrease rapidly. For single layered HFCs the mechanical behaviour normalized with length, could not be analyzed at Week 4 because their structure collapsed.

For double layered HFCs the mechanical strength, normalized with length, continued to decrease and acquired a very low value, approximately 6 kPa at Week 7 after which the HFCs could not be mechanically tested due to their collapse.

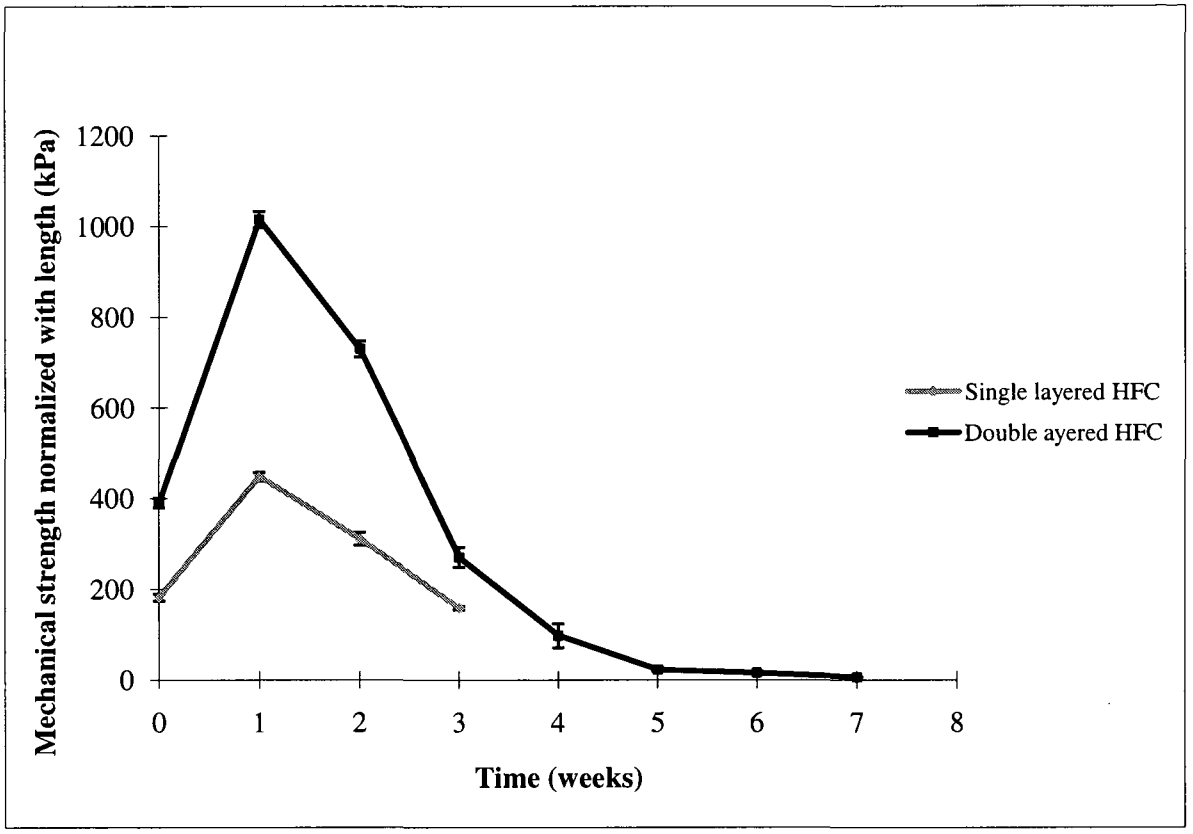

Figure 4.12 Change in mechanical strength normalized with length for single and double layered HFCs

4.3.4.2 Mechanical strength normalized with length and weight

For both single and double layered HFCs, mechanical strength normalized with length and weight showed a similar trend as shown for mechanical strength normalized with length.

As shown in Figure 4.13, a threefold increase was observed for both types of HFCs during Week 1 of degradation study, as compared to their values at Week 0. At Week 2 the mechanical strength began to decrease rapidly. Mechanical behaviour normalized with length and weight, could not be measured at Week 4 due to the collapse of single layered HFCs.

For double layered HFCs the mechanical strength (normalized with length and weight) continued to decrease and acquired a very low value of approximately 128 kPa at Week 7 after which the HFCs could not be mechanically tested due to their collapse.

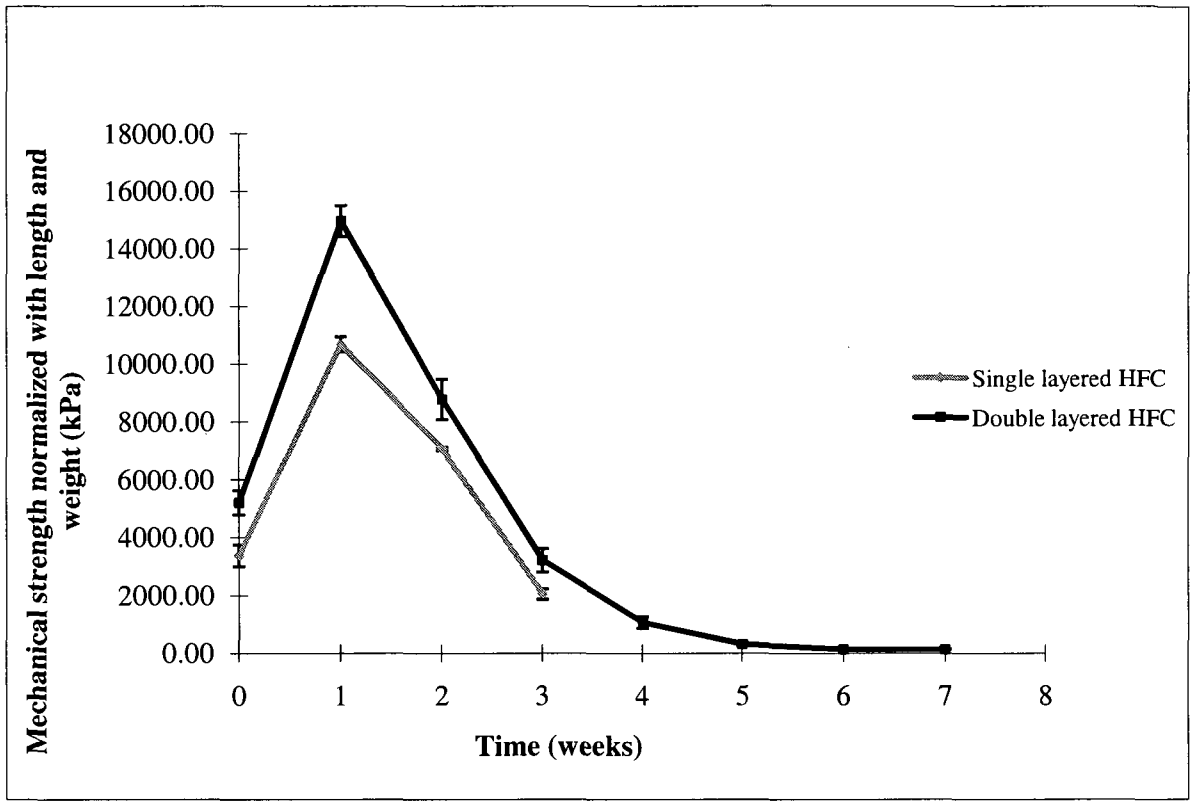

Figure 4.13 Change in mechanical strength normalized with length and weight for single and double layered HFCs

4.3.5 Change in Morphology for single and double layered HFCs

Subtle changes were noticed in the morphology of single and double layered HFCs during the degradation study.

For the single layered HFCs the degradation started after Week 1 and as shown in Figure 4.14, by Week 2 the inner wall started to break into small pieces in all the HFCs. By Week 3, very fine cracks could be noticed within the porous structure of the single layered HFC and Week 4 saw the collapse of the cylindrical structure of the HFC.

The double layered HFCs exhibited more sturdy structures, due to the presence of the outer layer of PLCL/PCL_3/ blend as shown in Figure 4.15. The HFCs were not much affected into Week 1 of degradation; however by Week 2 the inner layer of PLGA 50:50 began to degrade. By Week 3 very fine cracks appeared in the porous structure of the inner layer. At Week 4, the inner layer had begun to crumble and the outer layer started to show slight degradation as small cracks appeared on its surface but the cylindrical structure of the HFC was maintained. At Week 5 the inner lumen began to narrow down due to collection of debris of the degrading inner layer. At Week 6 this inner lumen was observed to be completely closed, thus giving the look of a 'solid cylindrical structure' to the degrading HFC. At Week 7, the degraded remains of the inner layer flowed out of its lumen thus clearing it up. With most of the inner layer seemingly to have degraded, the inner lumen of the cylindrical structure became larger as was shown by its dimensions. Now with only the outer layer remaining the cylindrical shape was still maintained but the HFC became quite fragile to handle. At Week 8, this cylindrical structure too collapsed thereby completely breaking up the double layered HFCs.

The observation of the collapse of cylindrical shape of the single layered HFC at Week 4 was confirmed by the similar observations made with the inner layer of the double layered HFC. At Week 4, the double layered HFC also showed crumbling of the inner layer which instead of breaking out from the structure, given the narrow lumen and lack of a circulation pathway, begins to collect in the lumen of the double layered HFC. Thus from this observation it can be concluded that indeed the PLGA 50:50 layer degrades sufficiently to lose its shape by Week 4.

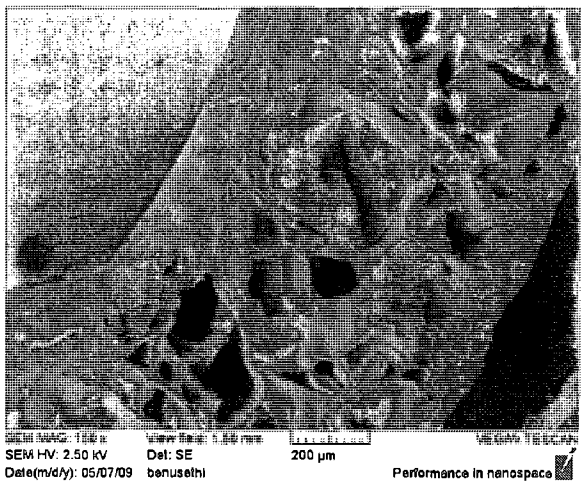

Week 0

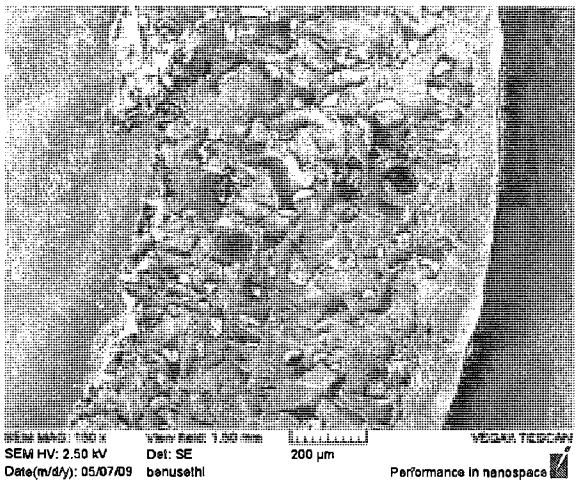

Week1

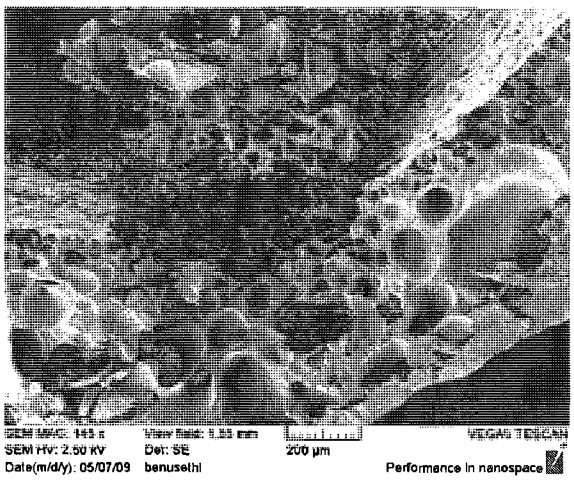

Week2

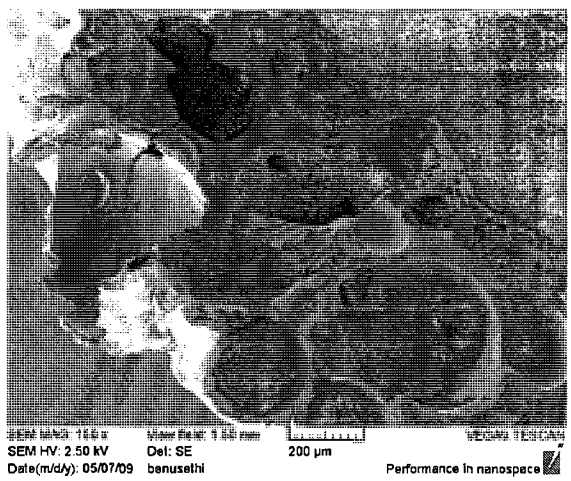

Week3

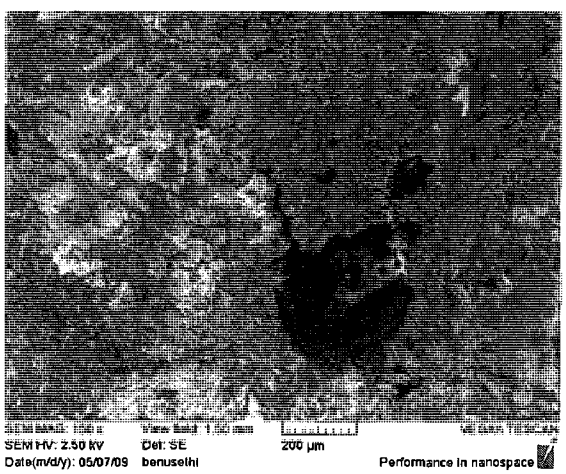

Week4

Figure 4.14 Change in morphology for single layered HFCs

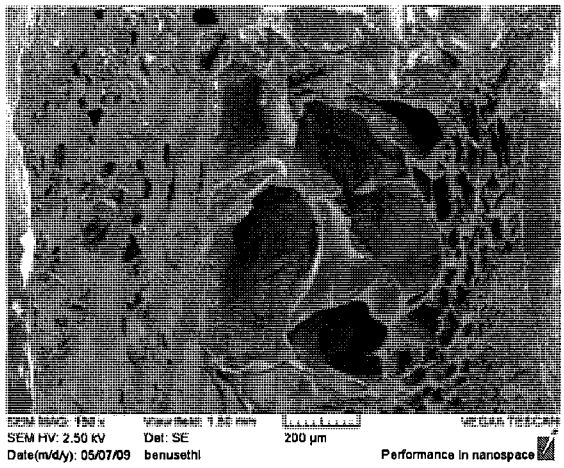

Week 0

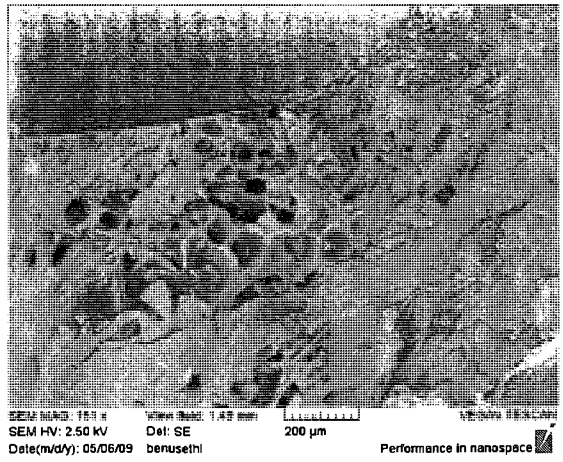

Week 1

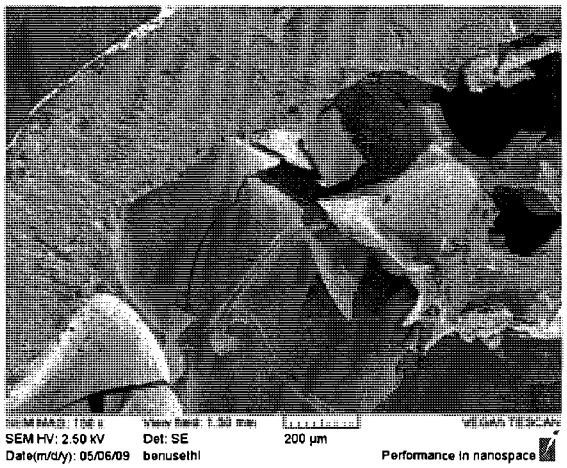

Week 2

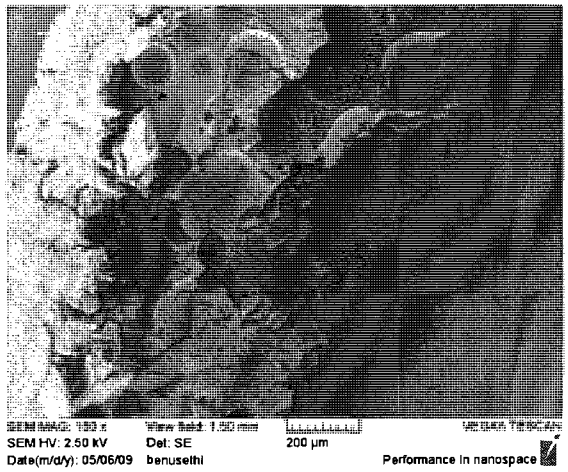

Week 3

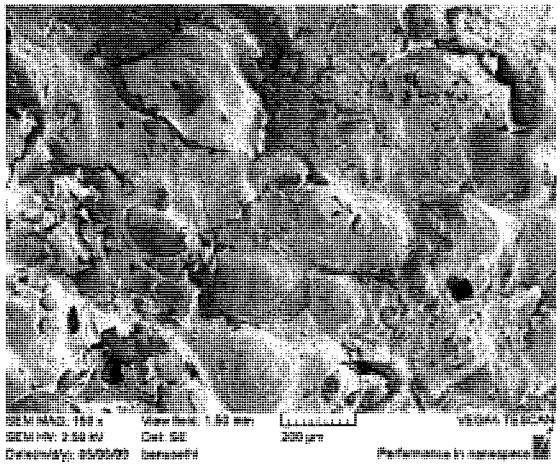

Week 4

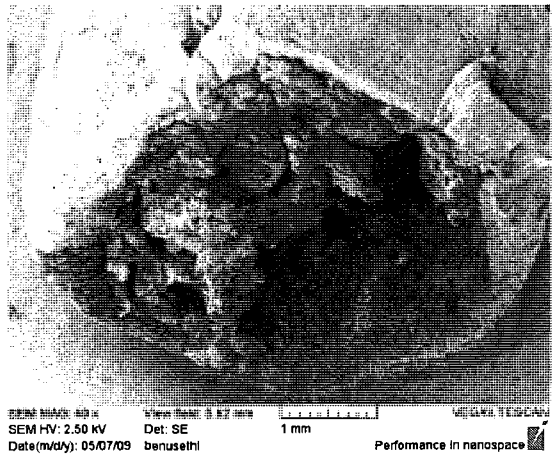

Week 4

Figure 4.15 Change in morphology for double layered HFCs

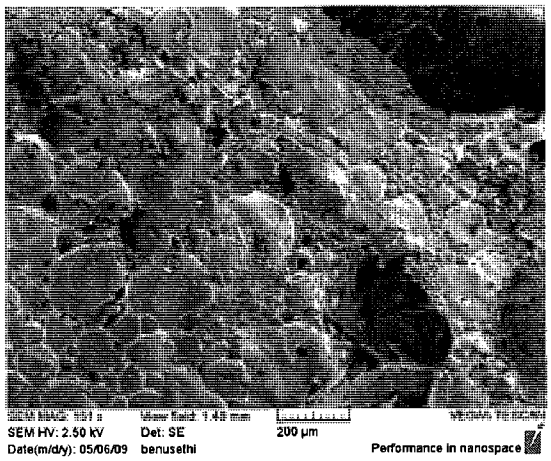

Week 5

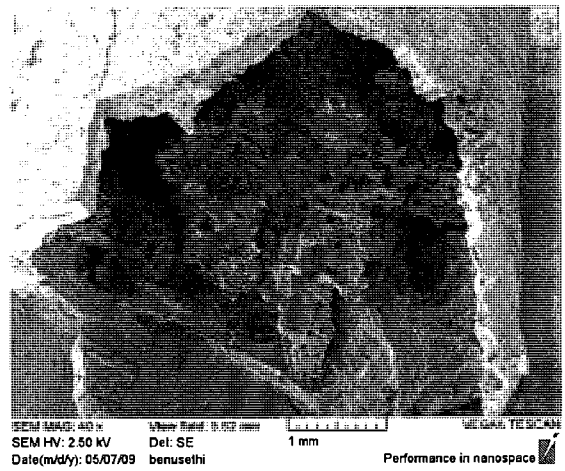

Week 5

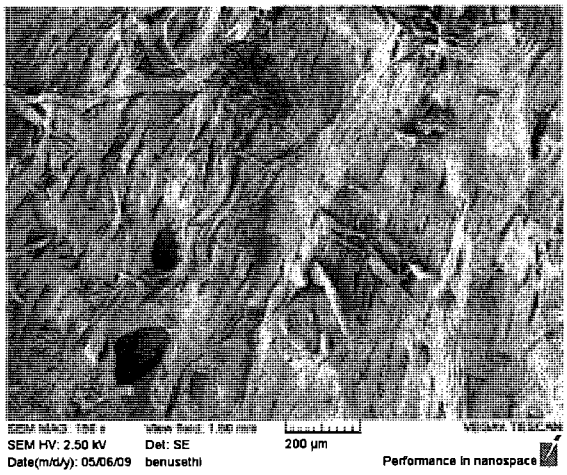

Week 6

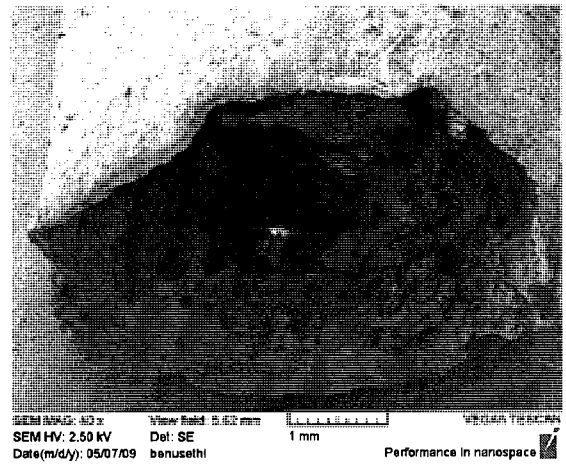

Week 6

Figure 4.15 Change in morphology for double layered HFCs (continued)

4.4 Reverse Porosity

The morphology achieved for the reverse porosity HFCs was exactly the reverse layout of porosity gradient as had been observed in case of double layered HFCs. The inner layer has small pores as compared to the outer layer with larger pores as shown in cross section view of Figure 4.16.

Upon characterization of foamed structure of HFC, it was observed that average pore size of inner layer was 4 μm and that for outer layer was 70 μm.

The porosity of these HFCs has been calculated at 67%.

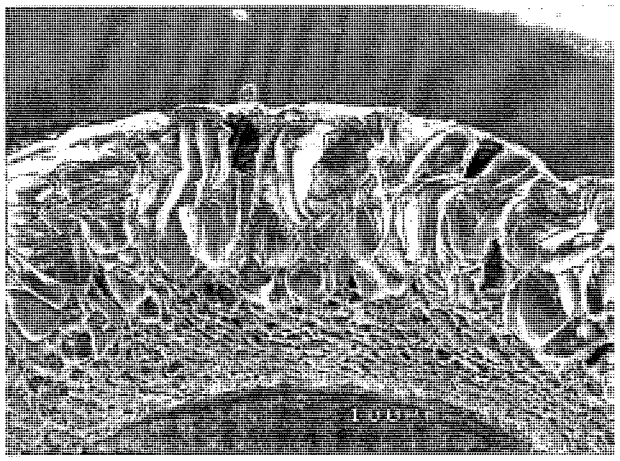

Figure 4.16 Morphology of reverse porosity HFC

4.4.1 Mechanical Testing

Mechanical testing of reverse porosity HFCs, performed using 'Transverse Direction' technique, established that they were less strong mechanically than double layered HFCs. Mechanical strength normalized with length when compared to single and double layered HFCs appeared to be the weakest as shown in Figure 4.17.

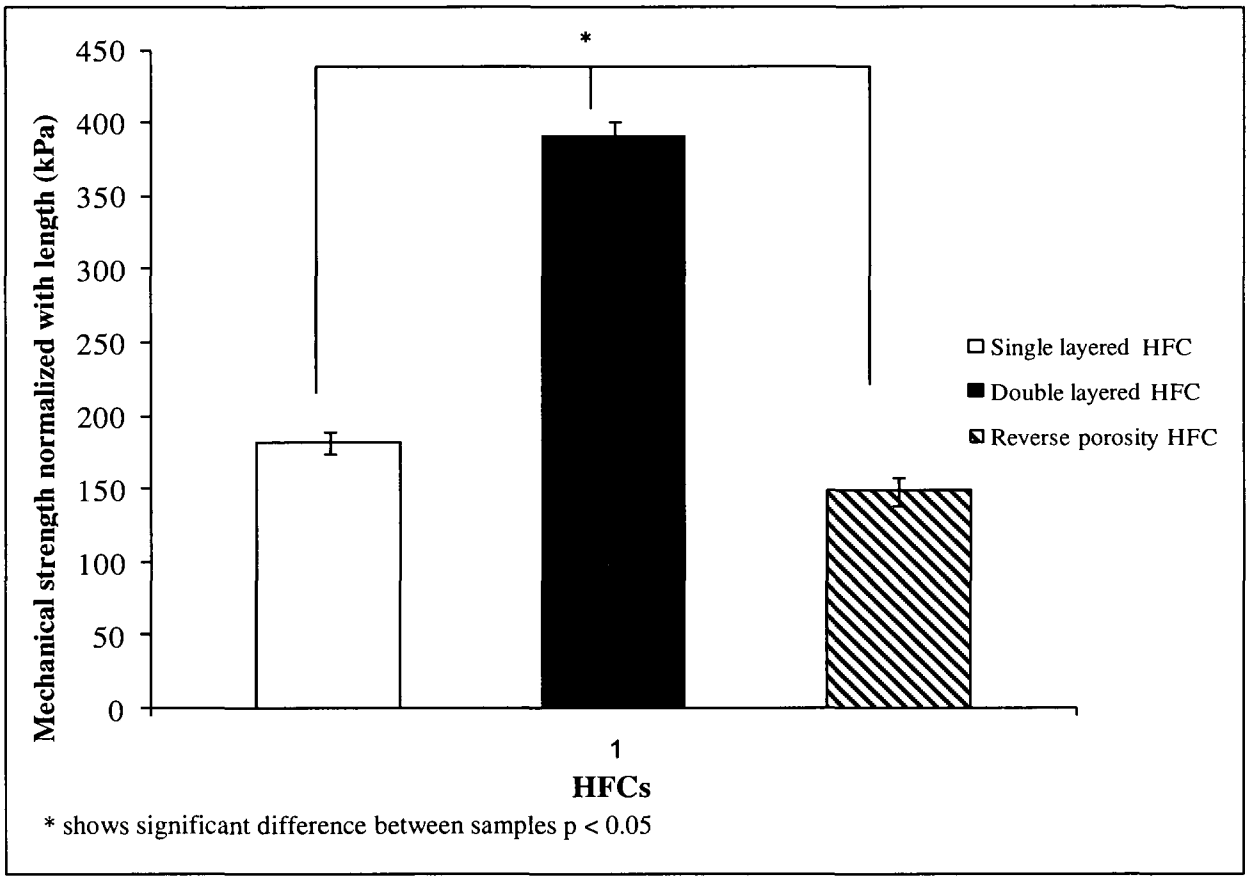

Figure 4.17 Comparison of mechanical strength normalized with length, for single layered, double layered and reverse porosity HFCs

The mechanical behaviour normalized with length and weight, for reverse porosity HFC, exhibited a lower trend as compared to that of double layered HFC, though it was improved as compared to single layered HFC. This means that for a given mass, it was the double layered HFC that exhibited the most superior mechanical behaviour as compared to reverse porosity or single layered HFCs as shown in Figure 4.18.

These results give a clear indication that fabricating a reverse porosity HFC does not provide us with similar mechanical strength as that of a double layered HFC. It further emphasizes the ability of the double layered HFC to provide enhanced mechanical behaviour by virtue of its structural and morphological layout, which principally mimics the design layout of the bone. This analysis regarding morphological structure of double layered HFC is discussed in detail in Discussion.

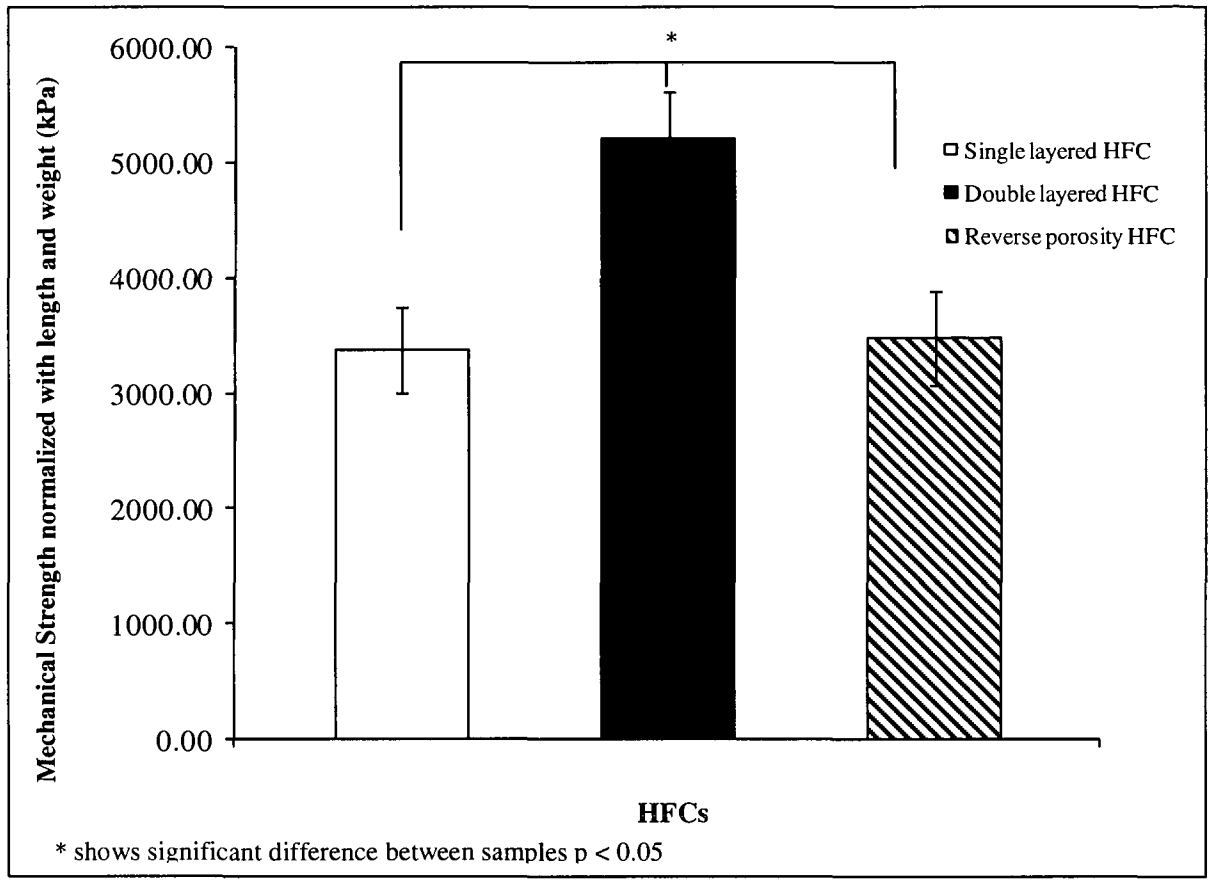

Figure 4.18 Comparison between mechanical strength normalized with length and weight, for single layered, double layered and reverse porosity HFCs

5. Discussion

5.1 Single and Double layered HFCs

During fabrication of the HFCs, it was necessary to fabricate the structure so that it possessed uniform morphology throughout its entire length. To achieve this, two approaches were used. Firstly, use of dip-coating technique ensured that polymer solution was evenly distributed on the glass mandrel. Secondly, a cylindrical teflon mold was used to encase the polymer tube during foaming in sub-critical CO_2 environment. Dimensions of teflon mold were large enough to allow the polymer tube to foam adequately while ensuring that its shape and dimensions were maintained. This fabrication technique was developed for both single and double layered HFCs.

In spite of following the above mentioned step wise approach, fabrication of double layered HFC was more complex than that of single layered HFC. This is because as per our design requirements we wanted to fabricate a double layered HFC with a porosity gradient, i.e. having different pore sizes in its inner and outer layers. This approach was challenging, especially in two ways. First, in order to provide such a porosity gradient each of the two layers was fabricated with a different polymer, to utilize their variable foaming ability. For designing a desirable porosity gradient, the foaming behaviour and pore sizes of each individual polymer and its blend with other polymers that had already been studied and utilized. Secondly, since a different polymer was used for each layer, each polymer had a different rate of expansion due to its specific foaming behaviour. Therefore it was imperative to maintain sufficient compatibility between the two layers so that they do not separate after being foamed and the overall HFC structure continues to retain its stability.

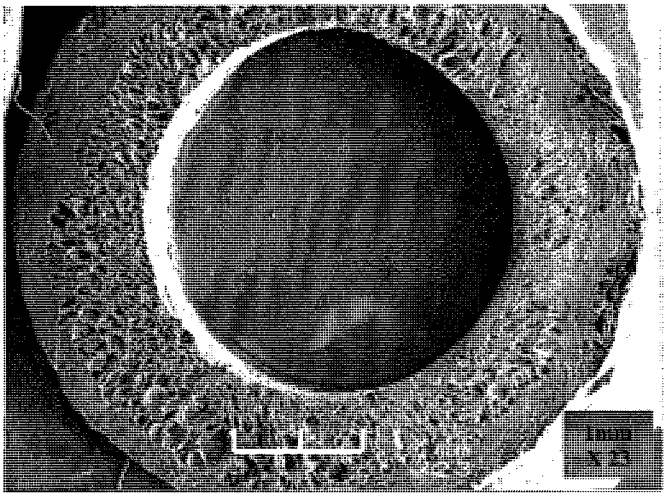

Figure 5.1 Porosity gradient between inner and outer layers in double layered HFC

The first challenge was achieved successfully by fabricating inner layer from PLGA 50:50 that foamed to provide large pores, and outer layer from a blend of PLCL/PCL_3/1 that foamed to provide smaller pores. As can be seen from Figure 5.1, a distinct gradient of porosity was obtained within the cross section of double layered HFC with this combination.

The ability of the inner layer to provide large pores can be explained by analyzing the physical and chemical properties of PLGA 50:50 that is an amorphous polymer with good solubility in sub-supercritical CO_2 [122] and low glass transition temperature (T_g) ranging between 45-50°C. Due to these characteristics at sub-supercritical operating conditions, CO_2 is dissolved into the polymer matrix and helps the molecules to relax, thereby further lowering its T_g [123]. As a result upon release of high pressure CO_2, and its conversion from supercritical to gaseous phase, a thermodynamic instability is rendered within the polymer matrix that leads to nucleation and growth of cells throughout the scaffold structure [111].

In the outer layer the formation of smaller pores as compared to the inner layer is due to combined foaming ability of PLCL and PCL. PLCL has a low T_g of -20°C and behaves quite similar to PLGA 50:50 under operating conditions of sub-supercritical CO_2. Given its semi-crystalline nature it does not enjoy a good solubility with sub-supercritical CO_2, thereby limiting its uptake in polymer matrix [124]. As a result upon release of the high pressure CO_2 and creation of thermodynamic instability, CO_2 molecules try to diffuse out and swell the polymer matrix but since the semi crystalline structure is not destroyed, the polymer cannot be foamed adequately. Therefore a combination of PLCL and PCL in the outer layer, in ratio 3/1 (w/w), gave rise to relatively smaller sized pores.

Considering our second challenging issue, to avoid separation of inner and outer layer of the double layered HFC due to different rates of expansion, it is necessary for the interface between the two layers to be strong enough to withstand the expansion forces. Choice of polymers for fabrication of the two layers played a very important role in resolving this issue. The inner layer of PLGA 50:50 and the outer layer of PLCL/PCL_3/1 (w/w) had different foaming behaviours. However presence of common segment of poly-d,l-lactic groups within the chemical structure of both PLGA 50:50 and PLCL, provided molecular entanglement and adhesion between the inner and outer layers after foaming. Also presence of common caprolactone segment chains between PLCL and PCL helped in providing homogeneity to the blend that constituted the outer layer. Thereby a stable structure with sufficient adherence between the inner and the outer layer could be successfully created. As can be seen from the SEM picture in Figure 5.2, the inner and outer layer of the double layered HFC displayed adhesion with no phase separation and hence a smooth interface between the two layers.

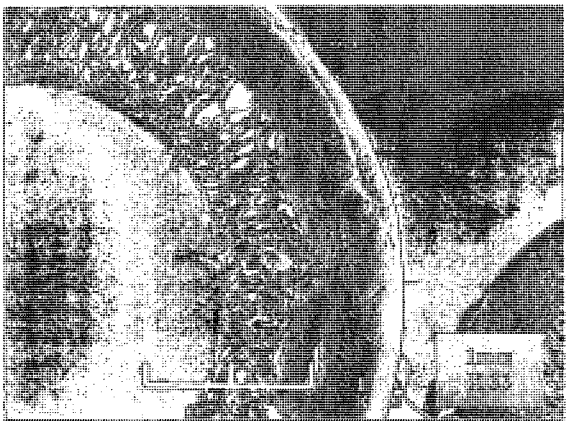

Figure 5.2 Interface between inner and outer layer of double layered HFC

5.2 Importance of Mechanical Strength of HFC

One of the main reasons for lack of functional recovery after spinal cord injury, given that various tubular strategies have been proposed for implantation, has been mismatch of mechanical strength of tubular implant with the surrounding spinal cord tissue. On one hand a weak tubular implant has been shown to collapse *in vivo*, due to thinning of the tubular wall brought about by combined action of compressive forces and phagocytosis leading to its collapse at site of injury [34]. On the other hand an excessively strong tubular implant can damage the surrounding tissue due to its undesirable rigidity. As shown by Nomura et al. [43] that the use of coil reinforced guidance channels led to formation of syringomyelic cyst formation causing further deterioration to the tissue regeneration process. In both circumstances, the process of nerve regeneration was adversely affected, due to mechanical strength mismatch.

Mechanical strength for a tubular implant is necessary to help maintain the patency of its lumen, during the nerve regeneration process [119]. To help establish the most desirable mechanical strength, we look at the mechanical properties of the surrounding spinal cord tissue that it should match. Literature states that the entire spinal cord, in different species, has an elastic modulus ranging between 230 to 600 kPa, including the membranous pia mater [35]. Mechanical strength of single and double layered HFCs was established, compared and analyzed by calculating their modulus of elasticity based on *in vitro* mechanical testing.

5.3 Directional aspect of Mechanical Testing of HFC

The two important aspects that were considered during *in vitro* mechanical testing of single and double layered HFCs were: 1) type of force being applied and 2) direction of application of force.

The type of force applied for mechanical testing was compressive in nature. Application of compressive force is the closest approximation to *in vivo* forces since the exact biomechanical conditions cannot be created *in vitro*. Studies dealing with *in vivo* implantation of tubular implants after the SCI have shown that it is the presence of constant and repetitive compressive biomechanical forces at site of injury that affect and compromise the patency of tubes [34, 35, 37, 41]. In light of the above, application of any other type of force e.g. tensile as done by some studies [35, 42], is not suggestible. A study by de Ruiter et al [37] also describes using bending loads to analyze the overall stiffness of the tubular implants designed for implantation after SCI. We have not incorporated that aspect within our testing methodology, since application of similar loads in *in vivo* environment has not been reported widely in literature.

There were two directions of application of force chosen for establishing the mechanical strength of the tubular implant. The first approach considered application of uniaxial force along the longitudinal direction of the tubular implant, referred to as 'Longitudinal direction' testing. This technique was used to establish the modulus of elasticity of single and double layered HFCs by considering both shape and morphological structure of the HFC. This type of testing was able to provide an estimation of material properties of the implant while also considering the cylindrical shape of the implant [34, 41].

As a secondary measure, mechanical testing with application of force along the transverse or radial direction of the HFC was undertaken. This approach was performed only to compare between the mechanical strength of single and double layered HFCs that had been fabricated in our lab. This technique was chosen to mimic the *in vivo* biomechanical forces as closely as possible. As has been shown by studies in this field [18, 34, 43, 45], during implantation, tubular implant is either inserted into or sutured to, rostral and caudal stump of the injured spinal cord. Consequently, a considerable impact of biomechanical forces *in vivo* is expected to be experienced along the length of tubular implant. Also we were interested in specifically analyzing the mechanical behaviour of the HFC when its length is compromised and its patency is at stake due to application of compressive force. To achieve the above, modifications were made to the theory postulated by Timoshenko et al. Application of force was considered on ring like section of the entire HFC structure and the compressive force applied was normalized against length of HFC. Within this approach, normalization of length for each HFC gave the added benefit of being able to compare HFC samples with different lengths.

We believe that by following the aforementioned approaches for *in vitro* mechanical testing, we were able to provide the closest estimate of biomechanical forces as are estimated to exist *in vivo*.

5.3.1 Mechanical Behaviour of HFC in Transverse Direction

As has been discussed above, a comparison between mechanical behaviour of single and double layered HFCs could be made.

The 'Force per unit length (F) versus the subsequent strain (ε)' curve was plotted for each HFC that was tested and the basic shape of the curve for both single and double layered HFCs, after testing, was similar. Figure 5.3 shows an example of type of curve obtained after testing of each HFC. The compressive behaviour exhibited by the curve is in agreement with the predicted behaviour of Elastic-Plastic foams [121]. By virtue of their foamed morphology, both single and double layered HFCs are characterized as cellular solid structures comprising of cells, generally referred to as pores. After neglecting initial toe-region, the curve can be divided into the following three regions as shown in Figure 5.3:

i) Linear Elasticity Region: This region within the cellular foamed structure arises due to application of uniaxial compressive force that causes the cell walls to bend.

ii) Plateau Region: This is the second part of the curve where the cells collapse due to continued application of force. As a result of the collapse there is formation of plastic hinges within the cells that causes the buckling of the foamed structure thus signifying its yield behaviour.

iii) Densification Region: This region is obtained due to continued application of load on the already collapsed foamed HFC structure. The opposite cell walls that touch each other result in compressing of the solid material itself by further application of force.

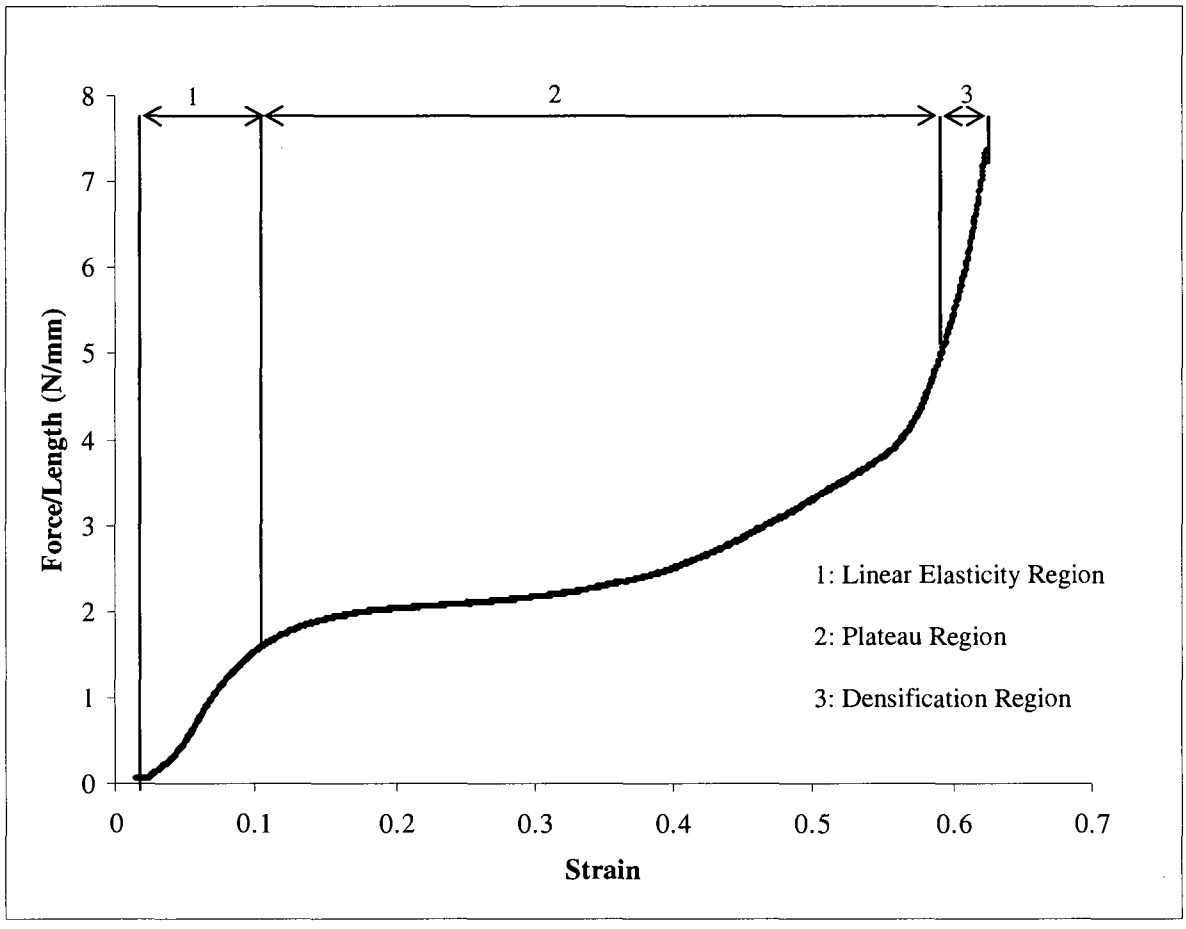

Figure 5.3 Curve obtained from 'Transverse Direction' testing

Even though the shape of the 'Force per unit length (F) versus the subsequent strain (ε)' curve was similar for both single and double layered HFCs, the slope of double layered HFC was higher than that of single layered HFC as shown in Figure 5.4. The steeper slope indicated that double layered HFC can withstand higher compressive load before deforming to the same extent as a single layered HFC. This indicates that double layered HFC exhibits a stronger mechanical behaviour than single layered HFC.

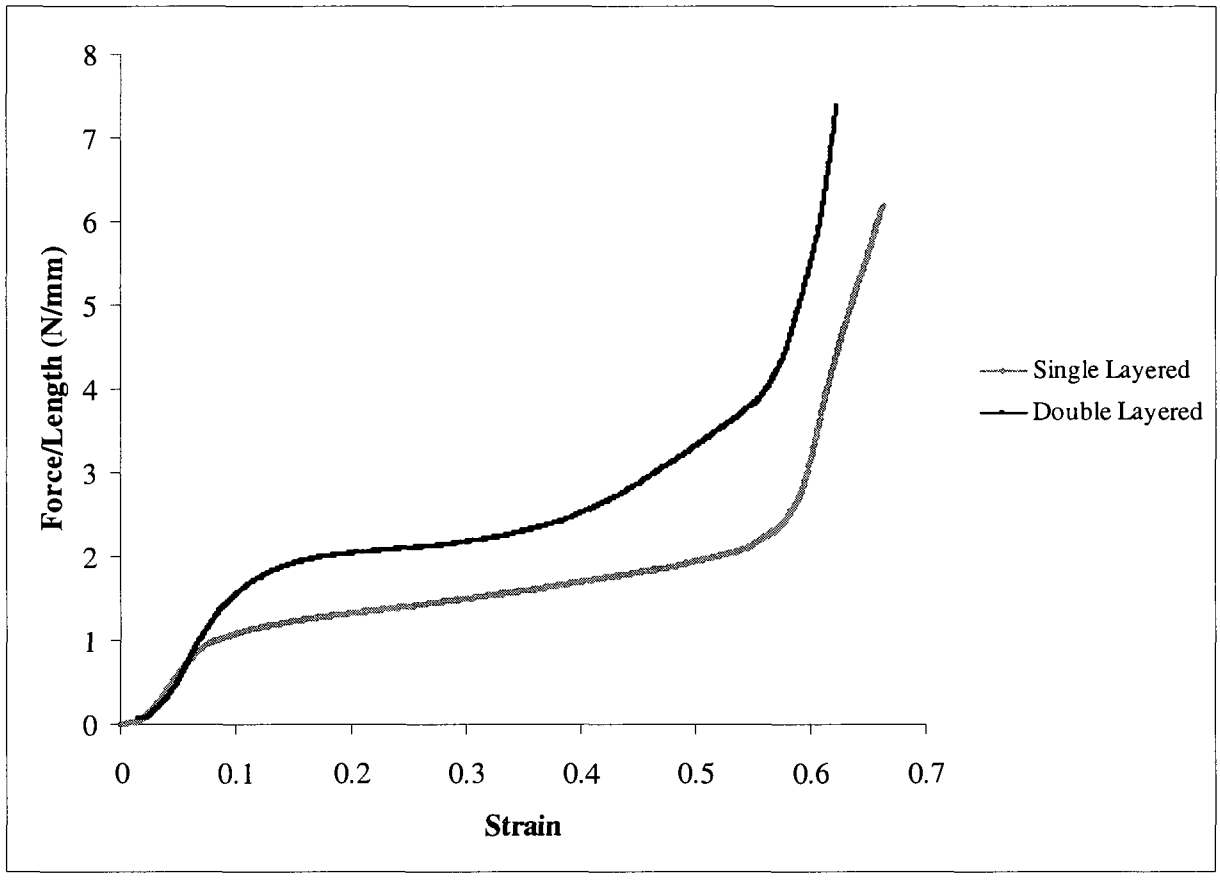

Figure 5.4 Comparison between slopes of single and double layered HFCs

5.3.2 Mechanical Strength comparison between single and double layered HFCs

The mechanical strength of single and double layered HFCs was analyzed by normalizing the compressive force applied by length of the HFC. Therefore mechanical behaviour has been denoted as normalized with length.

Our goal during the designing procedure was to develop an ideal HFC that provides optimum mechanical strength for its given mass. If increasing only the mechanical strength of HFC had been in question, it could have been achieved easily by increasing the mass of the material constituting the implant. However such an approach can prove to be detrimental since excessive HFC materials, once implanted *in vivo*, can cause damage to surrounding tissue at site due to overwhelmingly acid environment generated by the degradation products. In order to avoid this predicament, we developed a design of HFC that was capable of providing higher mechanical strength but still maintained a low mass. To achieve this requirement, we took inspiration from the structure of bone that provides high strength for an optimum weight [48]. In order to mimic the bone, we incorporated the conceptual design of porosity gradient within the double layered HFCs, the morphological details of which are discussed in the next section.

Therefore it was very important for us to establish the mechanical strength that was being offered by single and double layered HFCs for their given mass. To achieve this, mechanical behaviour of both types of HFCs was analyzed as 'normalized with length and weight'.

After comparing the mechanical behaviour as discussed above, it was observed that the double layered HFC was stronger than single layered HFC on both accounts. When

'normalized with length', double layered HFC had two times more mechanical strength than single layered HFC and when 'normalized with length and weight', it offered 1.5 times higher mechanical strength for a given mass when compared to single layered HFC.

The reason for higher mechanical strength of double layered HFC can be attributed to the presence of its outer layer that, besides increasing mechanical strength, ensures that mass of the HFC does not increase as much. We have tried to analyze the difference in mechanical strength of the two types of HFCs at a morphological level by performing image analysis on their SEM micrographs and discussed it in Section 5.3.4.

5.4 Mimicking Bone Structure: double layered HFC

As per our requirement, we were successful in being able to develop a distinct porosity gradient along the transverse cross-section of a double layered HFC. By providing such a porosity gradient, we wanted to achieve the aim of being able to mimic the bone structure. Bone is known for its unique ability to achieve a compromise between its load bearing capacity and weight, by providing high mechanical strength in face of local biomechanical loads that act on it, but still retaining an optimum mass [48]. Bone possesses a higher mechanical strength due to its structural layout that boasts of a double layered structure along its radius, with the outer layer of cortical bone, being solid and dense compared to the inner layer of cancellous bone that is spongy and porous with a typical honeycomb type foam structure [50, 121, 125] thus displaying a porosity gradient. Indeed by mimicking this design in form of a double layered HFC, we were able to show

experimentally that both its mechanical strength and ability to offer higher load bearing capacity for its given mass, increased as compared to single layered HFC.

5.5 Image analysis for Mechanical Strength of single and double layered HFCs

The Image Analysis was performed by measuring various parameters of individual cells from SEM pictures of the cross section of single and double layered HFCs. The purpose was to further understand the higher mechanical strength of double layered HFC based on its structural and material properties. Figure 5.5 depicts how the parameters from SEM pictures were calculated and Table 5.1 summarizes the average value of measured parameters and their ratios.

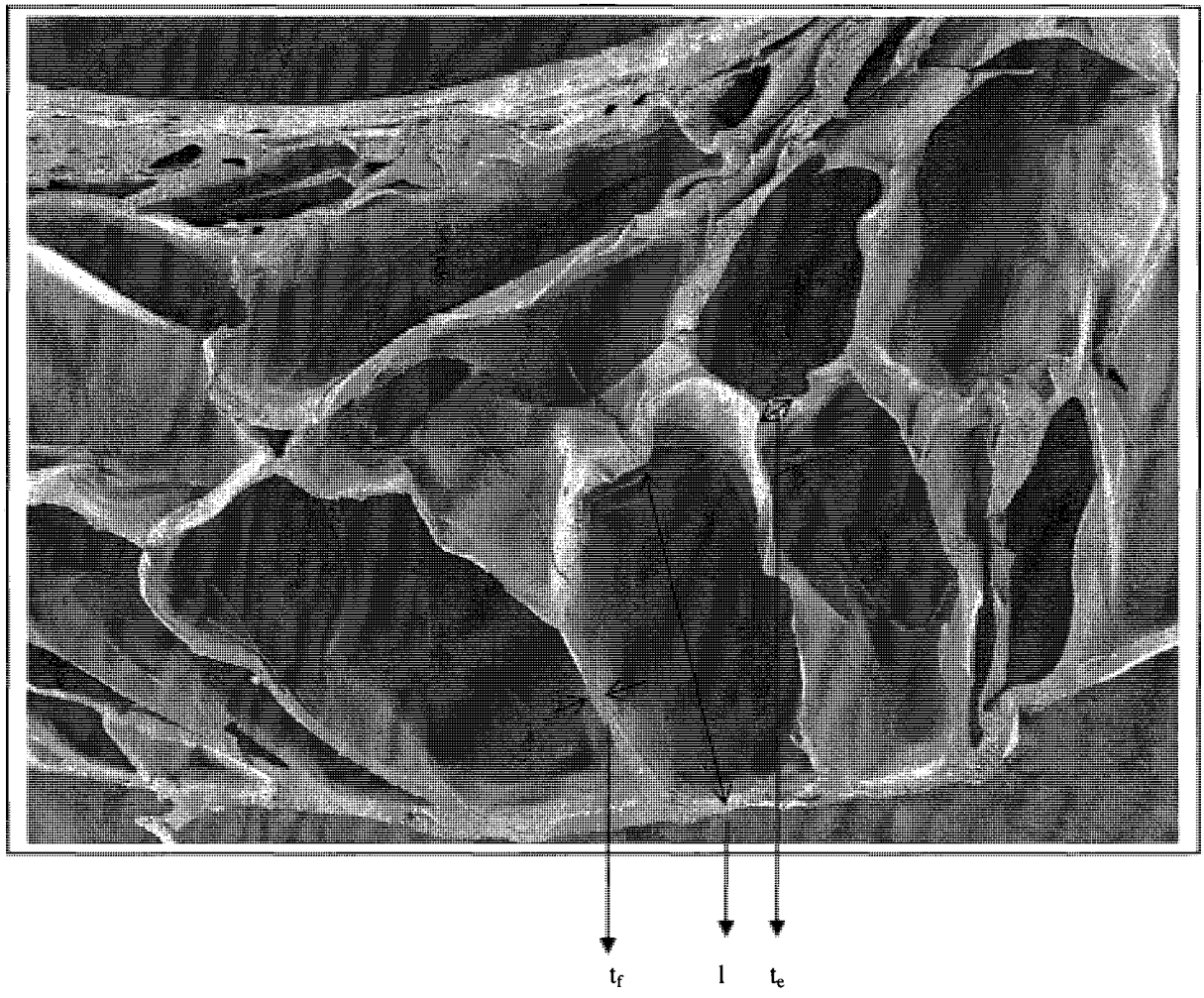

Figure 5.5 Parameters calculated from SEM pictures for image analysis

Table 5.1 Parameters for Image analysis of PLGA 50:50 and PLCL/PCL_3/1 blend layer

Parameters of PLGA 50:50 layer

l		(t_e^4/l^4)	t_f/l
Average Value (μm)	**Standard Deviation (μm)**		
65.03	12.51	0.00064	0.02519

Parameters of PLCL_PCL/3_1 blend layer

l		(t_e^4/l^4)	t_f/l
Average Value (μm)	**Standard Deviation (μm)**		
8.62	1.37	41.01856	0.38274

Note: Average value of each parameter was obtained from 10 measurements made from the sample group

where:

l: length of the cell member in the foamed structure of HFC

t_e: edge thickness of the cell member in the foamed structure of HFC

t_f: face thickness of the cell member in the foamed structure of HFC

Within the double layered HFC, average value of cell edge length parameter 'l' for inner layer (fabricated from PLGA 50:50), was 7 times greater than the average value of same parameter for the outer layer (fabricated from PLCL/PCL_3/1 blend). Also the dimensions of cell edge thickness and cell face thickness, 't_e' and 't_f' respectively, increased by almost two fold in outer layer as compared to inner layer. The relationship between modulus of elasticity of the foamed HFC (E^*) and modulus of elasticity of the solid polymer biomaterials (E_s) from which HFC has been fabricated, is defined as [121]:

$$E^* = E_s\left(\alpha' \frac{t_e^4}{l^4} + \beta' \frac{t_f}{l}\right) \qquad (9)$$

where α' and β' are constants of proportionality.

From the above mentioned relationship, two facts emerge. First, the value of modulus of elasticity of the foamed HFC, 'E^*', is directly proportional to the ratio '(t_e^4/l^4)' and secondly 'E^*' is directly proportional to the ratio '(t_f/l)'. Upon application of this relationship to the double layered HFC it becomes evident that the outer layer fabricated from PLCL/PCL_3/1 blend is mechanically stronger than the inner layer of PLGA 50:50. The higher value of cell edge length parameter 'l' of the inner layer is the main factor that compromises its mechanical strength. But it is the presence of outer layer of PLCL/PCL_3/1 blend, which enhances the overall mechanical strength of the double layered HFC. This reasoning also helps in understanding the lower mechanical strength of a standalone single layered HFC that is comprised only of the PLGA 50:50 when compared to the double layered HFC.

At this point it is worth mentioning that before being processed into foamed structures, the modulus of elasticity of raw materials (E_s) for PLGA 50:50 is approximately 3

times greater than that of blend of PLCL/PCL_3/1 [120]. But after the polymers have been foamed by soaking in sCO_2, by virtue of their morphological structure and pore size, within the double layered HFC, the outer layer of PLCL/PCL_3/1 blend imparts a higher mechanical strength when compared to the inner layer of PLGA 50:50. This is confirmed by mechanical testing and Image analysis of microstructure of the HFC samples. This change in micro structural dimensions of the two layers is observed due to unique foaming property of each polymer involved in creation of the HFC as has been shown by us with fabrication of single and multi layered scaffolds.

Thus, image analysis further helps in establishing the results that have been already shown experimentally, that of double layered HFC being mechanically stronger than single layered HFC.

5.6 Degradation Study

The importance of mechanical strength of the two types of HFCs has already been established and significant differences between them observed. The main aim of performing Degradation Study was to understand and compare the change in mechanical strength, of single and double layered HFCs, during *in vitro* degradation so that an insight into their *in vivo* behaviour could be obtained.

5.6.1 Changes in Mechanical Strength of single and double layered HFCs

During the study, mechanical strength of both types of HFCs was observed to reduce in magnitude with progression of time and an effective contrast could be observed between degradation behaviour of single and double layered HFCs. The single layered HFC showed a fast rate of degradation and all samples exhibited structural collapse by Week 4 but for double layered HFC such a structural collapse was observed by Week 8. This aspect also proved to be a limitation since calculation of shape dependent properties of HFCs such as volume, porosity and mechanical strength could not be done post to their collapse.

Both types of HFCs were fabricated from, either or all, biodegradable polyesters namely PLGA 50:50, PLCL & PCL. These polymers degrade by hydrolysis [83] when exposed to aqueous media, PBS in our case, that is being absorbed leads to cleavage of ester linkages within polymer chain thereby causing breakdown of the polymer backbone [47, 126, 127]. Degradation of these polymers, with time leads to formation of small chain low molecular weight fragments that have lower mechanical properties and as a result compromise the overall physical properties of the polymer [88].

At the beginning of the degradation study, mechanical strength of both types of HFCs first displayed an increase during Week 1, and then started to decline. This unexpected increase can be explained by analyzing other properties of the HFCs that were recorded at that timeline. As per their mathematical relationship, porosity of the HFC is directly related to its volume (the equations to this effect are provided in Chapter 3: Experimental, Section 3.5.2). For both types of HFCs, during Week 1, mass loss was not significant however a decrease in dimensions and hence reduction in volume, was observed. Theoretical

calculation of these parameters indicates a lowered value of porosity. From a morphological point of view, low porosity is indicative of diminishing some of the structural defects of porous HFCs by making their structure more dense and compact and as a result increasing their mechanical properties.

After Week 1, mechanical strength began to decline for both single and double layered HFCs. As has been discussed before, this can be attributed to hydrolysis that leads to formation of lower molecular weight by-products. The complete degradation of PLGA 50:50 layer at Week 4 was evident, with complete loss of cylindrical shape in case of single layered HFC samples and breaking of inner layer for double layered HFC samples, as shown in Figure 5.6. The double layered HFC seemed to be held together only due to the presence of outer layer of PLCL/PCL_3/1. At Week 6, for double layered HFC the inner layer completely broke down and obstructed its lumen thereby leading the samples to appear as 'solid cylindrical structures'. This integrity of double layered HFC was maintained till Week 8, after which the outer layer collapsed, thereby breaking down the cylindrical structure.

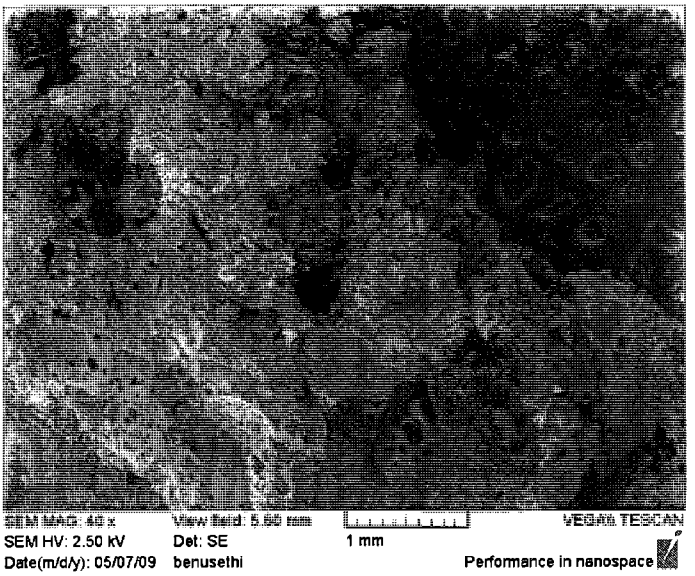

Single Layered HFC

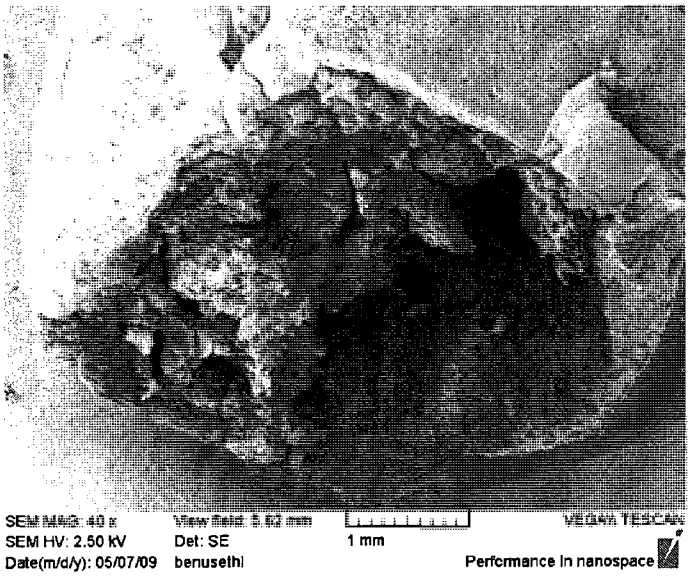

Double Layered HFC

Figure 5.6: Single and double layered HFCs at Week 4

5.6.2 Overall Degradation behaviour of single and double layered HFCs

The degradation behaviour shown both by single and double layered HFCs was in agreement with the model that has been proposed by Wu et al. [88]. The process of degradation could be divided into three stages for both HFCs, as shown in Figure 5.7 and 5.8, though time line for each stage was different:

i) Stage I- Quasi stable stage: During this stage (S1), mass loss of HFCs was not substantial, but a decrease in their dimensions was observed along with lowering of porosity. Also an increase in mechanical properties was observed at Week 1 that has already been explained above. This behaviour is consistent with other studies [128].

ii) Stage II-Loss-of-strength stage: This stage (S2) is marked by decrease in mechanical properties for both single and double layered HFCs however their dimensions and porosity did not decrease as much. As explained in literature [88] reduction in molecular weight of the degrading polymers leads to formation of low molecular weight by-products that have low mechanical properties

iii) Stage III-Loss of weight and disruption-of-scaffold stage: This stage (S3) is signified by substantial weight loss for both types of HFCs. Both volume and porosity continued to show a decline but at a very slow pace. The HFCs lost most of their mechanical strength and became fragile. For single and double layered HFCs, as in case of other stages this stage too arrived at different time points but for both, this stage was marked by complete collapse of their cylindrical structure.

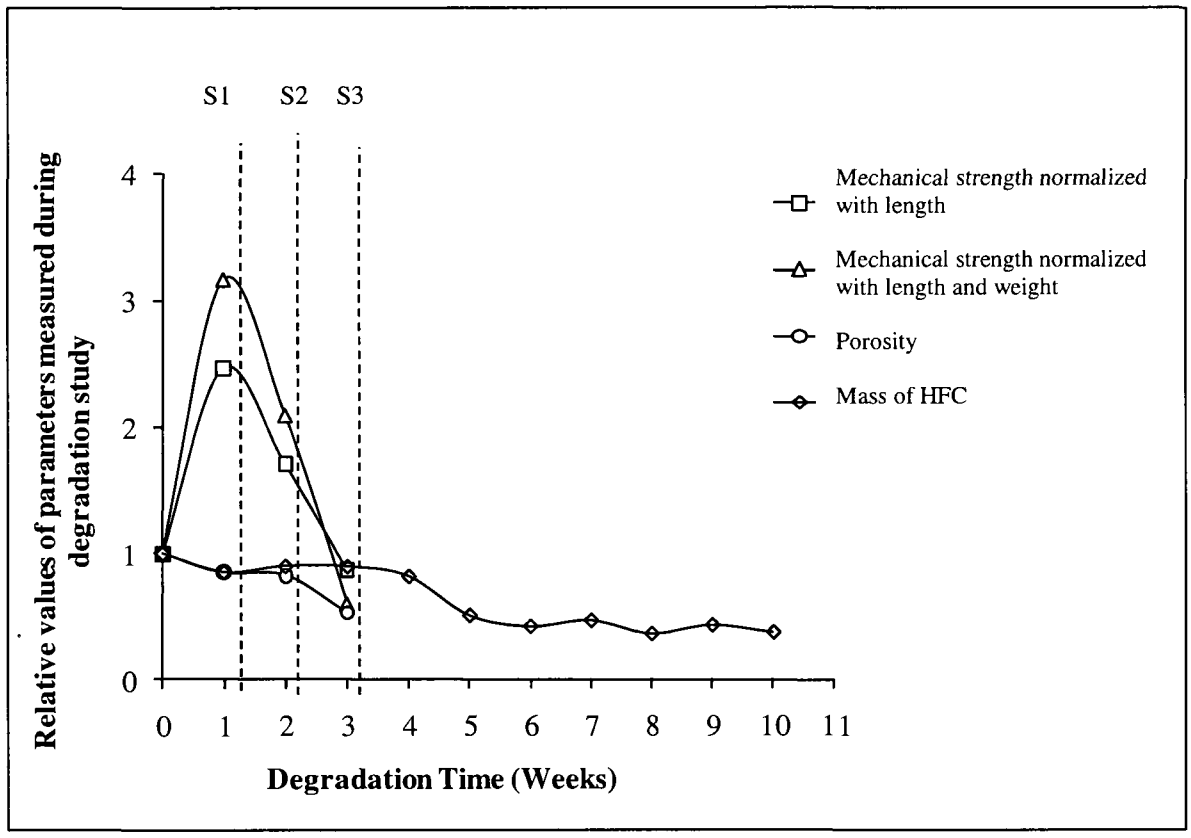

Figure 5.7 Degradation behaviour of single layered HFC

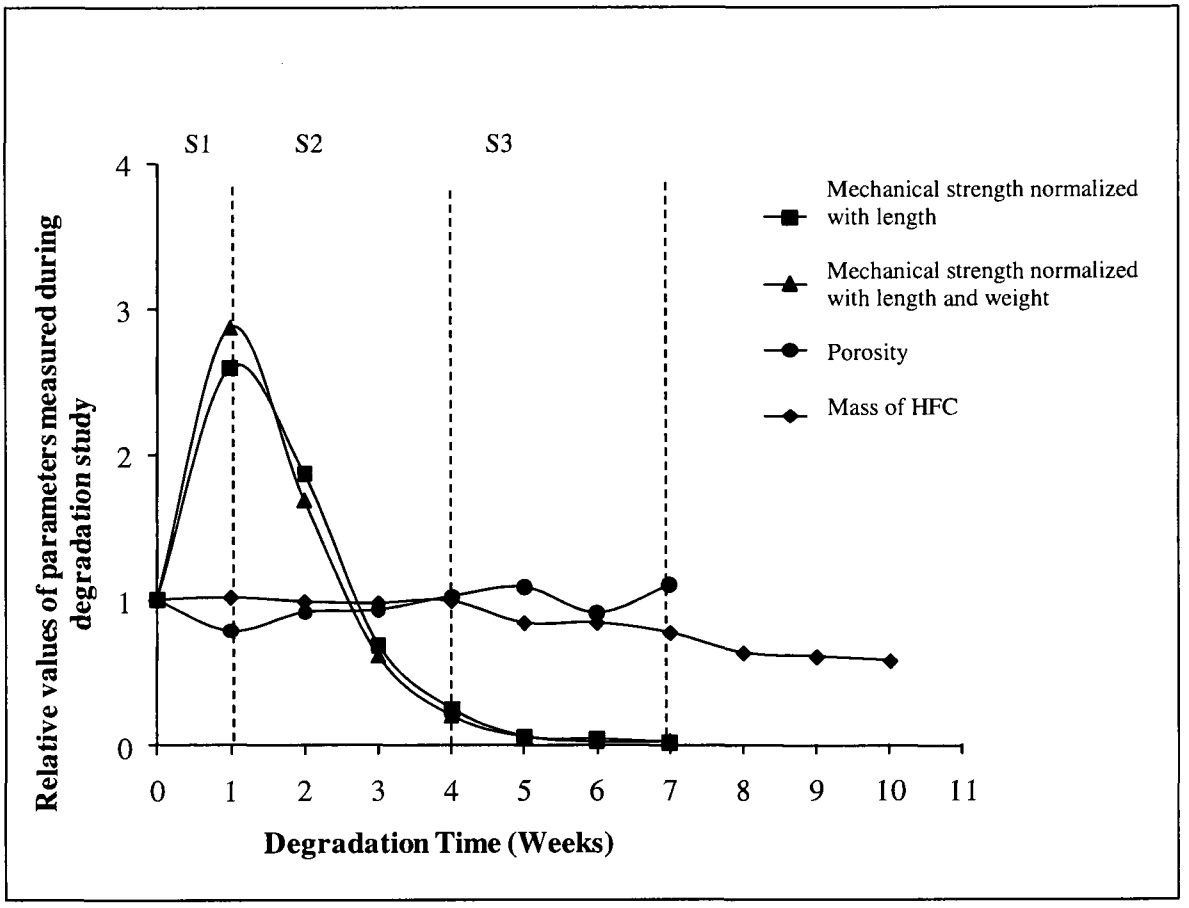

Figure 5.8 Degradation behaviour of double layered HFC

5.6.3 Rate of Degradation of HFC layers

Independent calculation of rate of mass loss for each of the two layers within the double layered HFC shows that outer layer had a lower rate as compared to inner layer. This lower rate helped the outer layer to retain its physical properties for a longer duration than the inner layer. Also on comparison of double layered HFC with single layered HFC, the former continued to exhibit higher mechanical strength due to its outer layer and cylindrical shape being intact.

The outer layer of the double layered HFC is comprised of PLCL/PCL_3/1 and the inner layer of the double layered HFC and entire single layered HFC are fabricated from PLGA 50:50. Upon comparison of rates of degradation of raw polymers [120], PLGA 50:50 has the highest degradation rate followed by PLCL and finally PCL [129]. This is in agreement with degradation behaviour that was observed in case of single and double layered HFCs. An explanation justifying these rates of degradation is given below.

PLGA 50:50 is a copolymer of poly (lactic acid) (PLA) and poly (glycolic acid) (PGA) and PLCL is a copolymer of PLA and ε-caprolactone (CL) in ratio 80/20. PCL is known to be semi-crystalline and amorphous nature of PLGA 50:50 and partially crystalline structure of PLCL are explained by the fact that crystallinity decreases as ratio of PLA decreases from 80% [83]. During hydrolysis amorphous regions of the polymer are known to degrade faster than the crystalline regions thus lowering mechanical properties, as seen for single layered HFC and inner layer of double layered HFC. In outer layer of double layered HFC, PLCL and PCL upon degradation create crystalline fragments as by-products that maintain mechanical strength for a longer duration until complete degradation.

Another factor that contributes to degradation of both types of HFCs during hydrolysis is hydrophilicity/hydrophobicity of the copolymers. When compared, PCL is more hydrophobic in nature than PGA. Within PLGA 50:50 and PLCL, PGA is more hydrophilic than CL [130]. Therefore PLGA 50:50 layer degrades faster than PLCL/PCL_3/1 layer.

5.6.4 Image analysis for Degradation Study

Image analysis was performed on SEM images of the single and double layered HFC taken during degradation study. By analyzing the changes in dimensions of parameters of pores that constituted foamed structure of single and double layered HFCs, the reduction in mechanical strength could be explained.

Table 5.2 lists the parameters that were measured from SEM pictures over the duration of 4 weeks during degradation study. After Week 4, due to collapse of single layered HFCs and inner layer of double layered HFCs, as discussed above, it became difficult to study their porous structure and layout from the SEM pictures.

The relationship between the ratio, '(t_e^4/l^4)' in the foamed structure of HFC, and mechanical strength of foamed HFC 'E^*', has already been defined and discussed at length in Section 5.3.4. Using the same argument it can be stated that as value of parameter 'l' increases for PLGA 50:50 layer, the layer becomes mechanically weak due to degradation of the biomaterial which makes the space within the cell size bigger as more and more material is degraded from it. As a result the ratio, '(t_e^4/l^4)' becomes smaller and finally at Week 4, it

acquires a value of 0.000133 as compared to 0.00122 at Week 1 leading to complete collapse of the structure of single layered HFC.

Similarly, the mechanical strength of double layered HFC is observed to decrease because the value of parameter 'l' is becoming larger for both inner and outer layer thereby leading to decrease in ratio '(t_e^4/l^4)' and compromising its overall mechanical strength. Between the duration of Week 4 and Week 6 due to rupturing of the inner layer, it was difficult to differentiate between inner and outer layer of double layered HFC samples, from the SEM pictures. Thus pore sizes could not be measured of specific layers. But it can be fairly estimated that mechanism of degradation in outer layer would have been similar in terms of further increase in pore size leading to its final collapse [121].

Table 5.2 Parameters for Image Analysis for PLGA 50:50 layer and PLCL/PCL_3/1 blend layer for HFC during Degradation Study

	PLGA 50:50 Layer		PLCL/PCL_3/1 blend Layer	
Week	**(t_e^4/l^4)**	**t_f/l**	**(t_e^4/l^4)**	**t_f/l**
0	0.00081	0.03020	30.48712	0.43814
1	0.00122	0.025093	9.52481	0.39499
2	0.00095	0.027145	4.37841	0.28080
3	0.00088	0.02515	1.61939	0.25103
4	0.000133	0.02035	0.86961	0.21327

Note: Average value of each parameter was obtained from 10 measurements made from the sample group

5.7 Reverse Porosity

It is evident from the above discussion that double layered HFC is mechanically stronger and as shown by the *in vitro* degradation study, it can retain its cylindrical structure for a longer duration than the single layered HFC. The mechanical strength enjoyed by the double layered HFC lies within the range, as recommended in literature, thereby being able to match the strength of surrounding spinal cord tissue. In exhibiting the above mentioned behaviour, presence of porosity gradient created as a result of morphological difference between inner and outer layers of the double layered HFC, plays a very crucial role. This porosity gradient in double layered HFC was created by seeking inspiration from design of bone and by mimicking its structural layout, as has been described in Section 5.3.3. It is based on the concept that the presence of a gradient with pore size becoming smaller moving from inner layer towards outer layer along radial direction of HFC provides increased strength.

To test a reverse scenario to the above mentioned design layout, a unique type of HFC with presence of a reverse porosity gradient layout compared to double layered HFC was created. This HFC, known as reverse porosity HFC, had outer layer with large sized pores and inner layer with small sized pores, thus reversing the structural design concept on which double layered HFCs were fabricated.

5.7.1 Mechanical Strength comparison for Reverse Porosity and other HFCs

Upon mechanical testing, reverse porosity HFCs exhibited lower mechanical strength, for both cases: normalized against length and normalized against length and weight

when compared with the double layered HFCs. This result effectively conveys that the direction of porosity gradient is very important. Even though reverse porosity HFC had a porosity gradient, in a reverse layout, the smaller pores in inner layer could not provide sufficient mechanical strength to the overall structure when compressive force was applied on the HFC. The first point of contact for the applied force was the outer surface of the HFC and presence of larger pores in the outer layer undermined the mechanical strength of the reverse porosity HFC as a whole.

To the best of my knowledge there are no models available in the literature providing information about mechanical strength of a structural layout that reverses the layout patters as observed in case of bone. Therefore it was difficult to compare the reverse porosity study that we had undertaken. Only one study, performed by Zeschky et al. [131], approached this issue in a remote manner by comparing the mechanical strength of asymmetric structures with their reverse layout. Their work involved fabrication of polysilsesquioxane derived ceramic foams, from which they were able establish that mechanical strength of the ceramic foamed structure was greater when it was tested with the outer layer consisting of small sized pores and the inner layer with large sized pores, as compared to the reverse scenario. This is in agreement with results shown by our mechanical testing of reverse porosity HFC and double layered HFC. Therefore we can confidently state that radial direction of porosity gradient, whereby the size of pores decreases from the inner layer towards the outer layer, provides enhanced mechanical strength to the HFC structure.

5.7.2 Image analysis for Mechanical Strength of Reverse Porosity HFC

Image analysis was performed with reverse porosity HFC too, as had been performed with single and double layered HFCs to analyze its mechanical strength. The average values of the parameters measured are shown in Table 5.3. The values reveal that the outer layer of PLCL/PCL blend had the average value of cell edge length parameter 'l' 6.8 times greater than the average value of same parameter for the inner layer of PLGA 50:50. As a result the ratios 't_e^4/l^4' and 't_f/l' decrease in the outer layer as compared to the inner layer. Using the same relationship as explained in Section 5.3.4, it becomes evident that the outer layer is weaker than the inner layer. Also when the value of modulus of elasticity of the solid polymer (E_s) is compared, value for PLGA 50:50 is approximately 3 times greater than each of PLCL and PCL [120]. As has been mentioned before, for reverse porosity HFCs the inner layer was fabricated from PLGA 50:50 and the outer layer from a different blend as compared to the double layered HFC, i.e. PLCL/PCL_9/1. After being soaked in sCO_2, the morphology of the outer layer was characterized by large sized pores. By virtue of foaming properties of the blend PLCL/PCL_9/1, modulus of elasticity (E^*) of the foamed outer layer did not improve as compared to the modulus of elasticity of raw material polymer (E_s) as had been observed in case of outer layer of double layered HFC. As a result low E_s value of PLCL/PCL_9/1 blend could not be enhanced due to foaming in sCO_2 environment. Consequently, this can be seen in the mechanical testing results that the presence of the weak outer layer does not contribute to the overall mechanical strength of the reverse porosity HFC.

Table 5.3 Image analysis parameters for reverse porosity HFCs

Parameters of PLGA 50:50 layer			
l		(t_e^4/l^4)	t_f/l
Average Value (μm)	**Standard Deviation (μm)**		
11.37	4.12	0.05026	0.31414

Parameters PLCL/PCL blend layer			
l		(t_e^4/l^4)	t_f/l
Average Value (μm)	**Standard Deviation (μm)**		
77.61	16.76	9.34818E-05	0.06916

Note: Average value of each parameter was obtained from 10 measurements made from the sample group

6. Conclusion

In conclusion, we were able to achieve the Project Goals that were stated in the beginning of the study. The summary is discussed below.

Two types of HFCs, single and double layered, were fabricated successfully using dip-coating technique. The desired morphology of HFCs, fabricated from biodegradable polymers, could be achieved by foaming the polymers in sub-critical CO_2 environment. The double layered HFC was designed to possess a porosity gradient, with the inner layer possessing larger pores and the outer layer designed with smaller pores. This was accomplished by using different polymers for fabrication of the inner and outer layers of the double layered HFC that successfully provided asymmetric structure along the cross-section of HFC.

The mechanical strength of HFC was an important criterion since it has been designed with proposed application at site of spinal cord injury. Comparison of mechanical properties *in vitro*, established that double layered HFC exhibited higher mechanical strength, as compared to single layered HFC. The double layered HFC proved to be stronger for its given mass as compared to single layered HFC. Thus we were successful in mimicking the design of porosity gradient as is observed within bone and also its concept of offering higher mechanical strength for its optimum mass.

Fabrication and mechanical testing of reverse porosity HFC, helped to establish the relationship between orientation of porosity gradient and mechanical strength, as has been observed successfully for double layered HFC. To obtain higher mechanical strength it was

necessary to have the layout within which inner layer had larger pores and outer layer had smaller pores, as in case of double layered HFC. A reverse layout with respect to this design, when incorporated within the HFC did not provide same magnitude of mechanical strength.

Finally, degradation study was able to exhibit the contrast in mechanical strengths, during degradation, between single and double layered HFCs. Single layered HFCs lost their mechanical strength and structural shape within 4 weeks during the study whereas the double layered HFC continued to maintain their structure for twice the duration of time, although its mechanical strength showed a step wise decline.

During this project, biodegradable double layered HFC were fabricated, using simple cost effective techniques, with a porosity gradient incorporated within the design that helped to increase its mechanical strength. The design of double layered HFC mimicked that of human bone by following a similar concept of higher load bearing ability being offered given an optimum mass. The Degradation Study performed *in vitro* exhibited step wise loss of mechanical strength of double layered HFC that was an improvement in comparison with the behaviour of single layered HFC. Therefore *in vitro* studies indicate double layered HFC to be a favourable candidate that can be proposed for implantation after SCI, based on its merits.

7. Future Work

This project was successful in establishing the difference in mechanical strength as tested *in vitro*, between two types of HFC, single layered HFC with a uniform morphology throughout the HFC and double layered HFC with presence of a porosity gradient mimicking the structural concept of the bone. Also, the different degradation rates of the two HFCs could be observed along with subsequent changes in their mechanical strength. These HFCs have been designed with the eventual purpose of in vivo implantation of bringing functional recovery after SCI. For accomplishing this task it is quite necessary, given the norms of tissue engineering, that the HFC behave as drug delivery vehicles. Further studies that can be conducted in this field are:

a) Investigate different mechanisms of loading therapeutic agents such as Neurotrophic Factors (NFs) within the HFC: Delivery of NFs at site after SCI can play an important role towards neuronal survival, proliferation and differentiation along with axonal regeneration. There are two main techniques that can be used for incorporation of these therapeutic agents within the HFC: firstly, by suspension or chemical linkage of therapeutic agent at fabrication stage and secondly, by using polymer based biodegradable microparticles, that encapsulate NF within them, for fabrication of HFC.

b) Study diffusion kinetics of therapeutic agents incorporated within each layer of double layered HFC: The two layers of double layered HFC have been designed with different porosities and when incorporated with therapeutic agents, each layer is expected to exhibit unique release behaviour. The different rates of release indicated

by each layer can be used to provide two different therapeutic agents in a stepwise manner, at the site of injury, each fulfilling its intended function.

c) Investigation of *in vivo* mechanical properties of HFCs loaded with therapeutic agents: After incorporation of therapeutic agents within the HFC it is necessary to test its mechanical properties *in vitro* to ensure its efficacy after implantation.

References

1. Schwab JM, Brechtel K, Mueller CA, Failli V, Kaps HP, Tuli SK, et al. Experimental strategies to promote spinal cord regeneration - an integrative perspective. Progress in Neurobiology 2006 Feb;78(2):91-116.
2. Tanaka S, Takigawa T, Ichihara S, Nakamura T. Mechanical properties of the bioabsorbable polyglycolic acid-collagen nerve guide tube. Polymer Engineering and Science 2006 Oct;46(10):1461-1467.
3. Timoshenko SP, Gere JM. Theory of Elastic Stability. Second ed. USA: McGraw-Hill Book Company, 1961.
4. Thuret S, Moon LDF, Gage FH. Therapeutic interventions after spinal cord injury. Nature Reviews Neuroscience 2006 Aug;7(8):628-643.
5. Talac R, Friedman JA, Moore MJ, Lu L, Jabbari E, Windebank AJ, et al. Animal models of spinal cord injury for evaluation of tissue engineering treatment strategies. Biomaterials 2004 Apr;25(9):1505-1510.
6. Silver J, Miller JH. Regeneration beyond the glial scar. Nature Reviews Neuroscience 2004 Feb;5(2):146-156.
7. Geller HM, Fawcett JW. Building a bridge: Engineering spinal cord repair. Experimental Neurology 2002 Apr;174(2):125-136.
8. Spilker MH, Yannas IV, Kostyk SK, Norregaard TV, Hsu HP, Spector M. The effects of tubulation on healing and scar formation after transection of the adult rat spinal cord. Restorative Neurology and Neuroscience 2001;18(1):23-38.
9. Teng YD, Lavik EB, Qu XL, Park KI, Ourednik J, Zurakowski D, et al. Functional recovery following traumatic spinal cord injury mediated by a unique polymer scaffold seeded with neural stem cells (vol 99, pg 3024, 2002). Proceedings of the National Academy of Sciences of the United States of America 2002 Jul;99(14):9606-9606.
10. Yang Y, De Laporte L, Rives CB, Jang JH, Lin WC, Shull KR, et al. Neurotrophin releasing single and multiple lumen nerve conduits. Journal of Controlled Release 2005;104(3):433-446.
11. Bunge MB. Bridging areas of injury in the spinal cord. Neuroscientist 2001 Aug;7(4):325-339.
12. Nomura H, Tator CH, Shoichet MS. Bioengineered strategies for spinal cord repair. Journal of Neurotrauma 2006 Mar-Apr;23(3-4):496-507.
13. Cohen BJ, Taylor JJ. The Nervous System: The Spinal Cord and Spinal Nerves. Memmler's structure and function of the human body. 9th Edition ed. Baltimore, MD: Wolters Kluwer Health/Lippincott William & Wilkins, 2009. p. 138-152.
14. Cohen BJ, Taylor JJ. The Nervous System: The Brain and Cranial Nerves. Memmler's structure and function of the human body. 9th Edition ed. Baltimore, MD: Wolters Kluwer Health/Lippincott William & Wilkins, 2009. p. 160-173.
15. Patton KT, Thibodeau GA. Nervous System Cells. Anatomy & Physiology 7th ed: St. Louis, Mo.: Mosby/Elsevier 2010. p. 372-404.
16. Patton KT, Thibodeau GA. Central Nervous System. Anatomy & Physiology 7th ed: St. Louis, Mo.: Mosby/Elsevier 2010. p. 412-445.

17. MayoFoundationforMedicalEducationandResearch. Spinal Cord Injury. 2009 [cited; Available from: http://www.mayoclinic.com/health/spinal-cord-injury/DS00460/DSECTION=causes
18. Tsai EC, Dalton PD, Shoichet MS, Tator CH. Synthetic hydrogel guidance channels facilitate regeneration of adult rat brainstem motor axons after complete spinal cord transection. Journal of Neurotrauma 2004 Jun;21(6):789-804.
19. Carmen J, Magnus T, Cassiani-Ingoni R, Sherman L, Rao MS, Mattson MR. Revisiting the astrocyte-oligodendrocyte relationship in the adult CNS. Progress in Neurobiology 2007 Jun;82(3):151-162.
20. Cao X, Shoichet MS. Tissue Engineering Strategies for Axonal Regeneration Following Spinal Cord Injury. In: DIllow AK, Lowman AM, editors. Biomimetic Materials and Design. New York: Marcel Dekker Inc., 2002. p. 417-442.
21. Pfister LA, Papaloizos M, Merkle HP, Gander B. Nerve conduits and growth factor delivery in peripheral nerve repair. Journal of the Peripheral Nervous System 2007 Jun;12(2):65-82.
22. Winter JO, Schmidt CE. Biomimetic Strategies and Applications in the Nervous System. In: DIllow AK, Lowman AM, editors. Biomimetic Materials and Design. New York: Marcel Dekker Inc., 2002. p. 375-415.
23. Bini TB, Gao SJ, Xu XY, Wang S, Ramakrishna S, Leong KW. Peripheral nerve regeneration by microbraided poly(L-lactide-co-glycolide) biodegradable polymer fibers. Journal of Biomedical Materials Research Part A 2004 Feb;68A(2):286-295.
24. Corey JM, Lin DY, Mycek KB, Chen Q, Samuel S, Feldman EL, et al. Aligned electrospun nanofibers specify the direction of dorsal root ganglia neurite growth. Journal of Biomedical Materials Research Part A 2007 Dec;83A(3):636-645.
25. Wells MR, Kraus K, Batter DK, Blunt DG, Weremowitz J, Lynch SE, et al. Gel matrix vehicles for growth factor application in nerve gap injuries repaired with tubes: A comparison of biomatrix, collagen, and methylcellulose. Experimental Neurology 1997 Aug;146(2):395-402.
26. Bini TB, Gao SJ, Wang S, Ramakrishna S. Development of fibrous biodegradable polymer conduits for guided nerve regeneration. Journal of Materials Science-Materials in Medicine 2005 Apr;16(4):367-375.
27. den Dunnen WFA, Meek MF, Grijpma DW, Robinson PF, Schakenraad JM. In vivo and in vitro degradation of poly[(50)/(50) ((85)/(L)(15)/(D))LA/epsilon-CL], and the implications for the use in nerve reconstruction. Journal of Biomedical Materials Research 2000 Sep;51(4):575-585.
28. Li JM, Shi RY. Fabrication of patterned multi-walled poly-L-lactic acid conduits for nerve regeneration. Journal of Neuroscience Methods 2007 Sep;165(2):257-264.
29. Long Y, Zhang N, Huang Y, Wen X. Formation of highly aligned grooves on inner surface of semipermeable hollow fiber membrane for directional axonal outgrowth. Journal of Manufacturing Science and Engineering-Transactions of the Asme 2008 Apr;130(2).
30. Meek MF, Jansen K, Steendam R, van Oeveren W, van Wachem PB, van Luyn MJA. In vitro degradation and biocompatibility of poly(DL-lactide-epsilon-caprolactone) nerve guides. Journal of Biomedical Materials Research Part A 2004 Jan;68A(1):43-51.

31. Zhang N, Zhang CH, Wen XJ. Fabrication of semipermeable hollow fiber membranes with highly aligned texture for nerve guidance. Journal of Biomedical Materials Research Part A 2005 Dec;75A(4):941-949.
32. Saltzman WM. Tissue Exchange and Tissue Development Tissue Engineering : Engineering Principles for the Design of Replacement Organs and Tissues: Oxford University Press, Incorporated 2004.
33. Meilander NJ, Bellamkonda RV. STANDARD HANDBOOK OF BIOMEDICAL ENGINEERING AND DESIGN. In: Kutz M, editor.: McGraw-Hill 2003.
34. Belkas JS, Munro CA, Shoichet MS, Johnston M, Midha R. Long-term in vivo biomechanical properties and biocompatibility of poly(2-hydroxyethyl methacrylate-co-methyl methacrylate) nerve conduits. Biomaterials 2005 May;26(14):1741-1749.
35. Dalton PD, Flynn L, Shoichet MS. Manufacture of poly(2-hydroxyethyl methacrylate-co-methyl methacrylate) hydrogel tubes for use as nerve guidance channels. Biomaterials 2002 Sep;23(18):3843-3851.
36. Dalton PD, Shoichet MS. Creating porous tubes by centrifugal forces for soft tissue application. Biomaterials 2001 Oct;22(19):2661-2669.
37. de Ruiter GC, Onyeneho IA, Liang ET, Moore MJ, Knight AM, Malessy MJA, et al. Methods for in vitro characterization of multichannel nerve tubes. Journal of Biomedical Materials Research Part A 2008 Mar;84A(3):643-651.
38. de Ruiter GC, Spinner RJ, Malessy MJA, Moore MJ, Sorenson EJ, Currier BL, et al. Accuracy of motor axon regeneration across autograft, single-lumen, and multichannel poly(lactic-co-glycolic acid) nerve tubes. Neurosurgery 2008 Jul;63(1):144-153.
39. Friedman JA, Windebank AJ, Moore MJ, Spinner RJ, Currier BL, Yaszemski MJ. Biodegradable polymer grafts for surgical repair of the injured spinal cord. Neurosurgery 2002 Sep;51(3):742-751.
40. Goraltchouk A, Freier T, Shoichet MS. Synthesis of degradable poly(L-lactide-co-ethylene glycol) porous tubes by liquid-liquid centrifugal casting for use as nerve guidance channels. Biomaterials 2005 Dec;26(36):7555-7563.
41. Katayama Y, Montenegro R, Freier T, Midha R, Belkas JS, Shoichet MS. Coil-reinforced hydrogel tubes promote nerve regeneration equivalent to that of nerve autografts. Biomaterials 2006;27(3):505-518.
42. Luo Y, Dalton PD, Shoichet MS. Investigating the properties of novel poly(2-hydroxyethyl methacrylate-co-methyl methacrylate) hydrogel hollow fiber membranes. Chemistry of Materials 2001 Nov;13(11):4087-4093.
43. Nomura H, Katayama Y, Shoichet MS, Tator CH. Complete spinal cord transection treated by implantation of a reinforced synthetic hydrogel channel results in syringomyelia and caudal migration of the rostral stump. Neurosurgery 2006 Jul;59(1):183-192.
44. Piotrowicz A, Shoichet MS. Nerve guidance channels as drug delivery vehicles. Biomaterials 2006 Mar;27(9):2018-2027.
45. Tsai EC, Dalton PD, Shoichet MS, Tator CH. Matrix inclusion within synthetic hydrogel guidance channels improves specific supraspinal and local axonal regeneration after complete spinal cord transection. Biomaterials 2006 Jan;27(3):519-533.
46. Houle JD. DEMONSTRATION OF THE POTENTIAL FOR CHRONICALLY INJURED NEURONS TO REGENERATE AXONS INTO INTRASPINAL PERIPHERAL-NERVE GRAFTS. Experimental Neurology 1991 Jul;113(1):1-9.

47. Lu L, Peter SJ, Lyman MD, Lai HL, Leite SM, Tamada JA, et al. In vitro and in vivo degradation of porous poly(DL-lactic-co-glycolic acid) foams. Biomaterials 2000 Sep;21(18):1837-1845.
48. Rubin CT. SKELETAL STRAIN AND THE FUNCTIONAL-SIGNIFICANCE OF BONE ARCHITECTURE. Calcified Tissue International 1984;36:S11-S18.
49. Harley BA, Hastings AZ, Yannas IV, Sannino A. Fabricating tubular scaffolds with a radial pore size gradient by a spinning technique. Biomaterials 2006 Feb;27(6):866-874.
50. Leong KF, Chua CK, Sudarmadji N, Yeong WY. Engineering functionally graded tissue engineering scaffolds. Journal of the Mechanical Behavior of Biomedical Materials 2008 Apr;1(2):140-152.
51. Oh SH, Park IK, Kim JM, Lee JH. In vitro and in vivo characteristics of PCL scaffolds with pore size gradient fabricated by a centrifugation method. Biomaterials 2007 Mar;28(9):1664-1671.
52. Zein I, Hutmacher DW, Tan KC, Teoh SH. Fused deposition modeling of novel scaffold architectures for tissue engineering applications. Biomaterials 2002 Feb;23(4):1169-1185.
53. Oudega M, Xu XM. Schwann cell transplantation for repair of the adult spinal cord. Journal of Neurotrauma 2006 Mar-Apr;23(3-4):453-467.
54. Bunge MB, Pearse DD. Transplantation strategies to promote repair of the injured spinal cord. 2003; 2003. p. 55-62.
55. Oudega M, Gautier SE, Chapon P, Fragoso M, Bates ML, Parel JM, et al. Axonal regeneration into Schwann cell grafts within resorbable poly(alpha-hydroxyacid) guidance channels in the adult rat spinal cord. Biomaterials 2001 May;22(10):1125-1136.
56. Meek MF, Coert JH. US Food and Drug Administration/Conformit Europe-approved absorbable nerve conduits for clinical repair of peripheral and cranial nerves. Annals of Plastic Surgery 2008 Apr;60(4):466-472.
57. Meek MF, Coert JH. US Food and Drug Administration/Conformit Europe-approved absorbable nerve conduits for clinical repair of peripheral and cranial nerves. Annals of Plastic Surgery 2008 Jan;60(1):110-116.
58. Cai J, Ziemba KS, Smith GM, Jin Y. Evaluation of cellular organization and axonal regeneration through linear PLA foam implants in acute and chronic spinal cord injury. Journal of Biomedical Materials Research Part A 2007 Nov;83A(2):512-520.
59. Li XG, Yang ZY, Zhang AF, Wang TL, Chen WC. Repair of thoracic spinal cord injury by chitosan tube implantation in adult rats. Biomaterials 2009 Feb;30(6):1121-1132.
60. Novikova LN, Pettersson J, Brohlin M, Wiberg M, Novikov LN. Biodegradable poly-beta-hydroxybutyrate scaffold seeded with Schwann cells to promote spinal cord repair. Biomaterials 2008 Mar;29(9):1198-1206.
61. Novikov LN, Novikova LN, Mosahebi A, Wiberg M, Terenghi G, Kellerth JO. A novel biodegradable implant for neuronal rescue and regeneration after spinal cord injury. Biomaterials 2002 Aug;23(16):3369-3376.
62. Yoshii S, Oka M, Shima M, Akagi M, Taniguchi A. Bridging a spinal cord defect using collagen filament. Spine 2003 Oct;28(20):2346-2351.
63. Liu S, Said G, Tadie M. Regrowth of the rostral spinal axons into the caudal ventral roots through a collagen tube implanted into hemisected adult rat spinal cord. Neurosurgery 2001 Jul;49(1):143-150.

64. Patist CM, Mulder MB, Gautier SE, Maquet V, Jerome R, Oudega M. Freeze-dried poly(D,L-lactic acid) macroporous guidance scaffolds impregnated with brain-derived neurotrophic factor in the transected adult rat thoracic spinal cord. Biomaterials 2004 Apr;25(9):1569-1582.
65. Fouad K, Schnell L, Bunge MB, Schwab ME, Liebscher T, Pearse DD. Combining Schwann cell bridges and olfactory-ensheathing glia grafts with chondroitinase promotes locomotor recovery after complete transection of the spinal cord. Journal of Neuroscience 2005 Feb;25(5):1169-1178.
66. Novikova LN, Novikov LN, Kellerth JO. Biopolymers and biodegradable smart implants for tissue regeneration after spinal cord injury. Current Opinion in Neurology 2003 Dec;16(6):711-715.
67. Xu XM, Chen A, Guenard V, Kleitman N, Bunge MB. Bridging Schwann cell transplants promote axonal regeneration from both the rostral and caudal stumps of transected adult rat spinal cord. Journal of Neurocytology 1997 Jan;26(1):1-16.
68. Xu XM, Zhang SX, Li HY, Aebischer P, Bunge MB. Regrowth of axons into the distal spinal cord through a Schwann-cell-seeded mini-channel implanted into hemisected adult rat spinal cord. European Journal of Neuroscience 1999 May;11(5):1723-1740.
69. Goraltchouk A, Scanga V, Morshead CM, Shoichet MS. Incorporation of protein-eluting microspheres into biodegradable nerve guidance channels for controlled release. Journal of Controlled Release 2006 Jan;110(2):400-407.
70. Jain A, Kim YT, McKeon RJ, Bellamkonda RV. In situ gelling hydrogels for conformal repair of spinal cord defects, and local delivery of BDNF after spinal cord injury. Biomaterials 2006 Jan;27(3):497-504.
71. Nimni ME, Cheung D, Strates B, Kodama M, Sheikh K. CHEMICALLY MODIFIED COLLAGEN - A NATURAL BIOMATERIAL FOR TISSUE REPLACEMENT. Journal of Biomedical Materials Research 1987;21(6):741-771.
72. Stokols S, Tuszynski MH. The fabrication and characterization of linearly oriented nerve guidance scaffolds for spinal cord injury. Biomaterials 2004;25(27):5839-5846.
73. Stokols S, Sakamoto J, Breckon C, Holt T, Weiss J, Tuszynski MH. Templated agarose scaffolds support linear axonal regeneration. Tissue Engineering 2006 Oct;12(10):2777-2787.
74. Freier T, Montenegro R, Koh HS, Shoichet MS. Chitin-based tubes for tissue engineering in the nervous system. Biomaterials 2005 Aug;26(22):4624-4632.
75. Huang YC, Huang YY, Huang CC, Liu HC. Manufacture of porous polymer nerve conduits through a lyophilizing and wire-heating process. Journal of Biomedical Materials Research Part B-Applied Biomaterials 2005 Jul;74B(1):659-664.
76. Madihally SV, Matthew HWT. Porous chitosan scaffolds for tissue engineering. Biomaterials 1999 Jun;20(12):1133-1142.
77. Temtem M, Silva LMC, Andrade PZ, dos Santos F, da Silva CL, Cabral JMS, et al. Supercritical CO2 generating chitosan devices with controlled morphology. Potential application for drug delivery and mesenchymal stem cell culture. Journal of Supercritical Fluids 2009 Apr;48(3):269-277.
78. Freier T, Kunze C, Nischan C, Kramer S, Sternberg K, Sass M, et al. In vitro and in vivo degradation studies for development of a biodegradable patch based on poly(3-hydroxybutyrate). Biomaterials 2002 Jul;23(13):2649-2657.

79. Kunze C, Bernd HE, Androsch R, Nischan C, Freier T, Kramer S, et al. In vitro and in vivo studies on blends of isotactic and atactic poly (3-hydroxybutyrate) for development of a dura substitute material. Biomaterials 2006 Jan;27(2):192-201.
80. Bender MD, Bennett JM, Waddell RL, Doctor JS, Marra KG. Multi-channeled biodegradable polymer/CultiSpher composite nerve guides. Biomaterials 2004 Mar-Apr;25(7-8):1269-1278.
81. Wong DY, Leveque JC, Brumblay H, Krebsbach PH, Hollister SJ, LaMarca F. Macro-architectures in spinal cord scaffold implants influence regeneration. Journal of Neurotrauma 2008 Aug;25(8):1027-1037.
82. He LM, Zhang YQ, Zeng CG, Ngiam M, Liao S, Quan DP, et al. Manufacture of PLGA Multiple-Channel Conduits with Precise Hierarchical Pore Architectures and In Vitro/Vivo Evaluation for Spinal Cord Injury. Tissue Engineering Part C-Methods 2009 Jun;15(2):243-255.
83. Huang SJ. Handbook of Biodegradable Polymers. In: Bastioli C, editor. Poly(Lactic Acid) and Copolyesters: Smithers Rapra Technology, 2005.
84. Valmikinathan CM, Tian JJ, Wang JP, Yu XJ. Novel nanofibrous spiral scaffolds for neural tissue engineering. Journal of Neural Engineering 2008 Dec;5(4):422-432.
85. Wen XJ, Tresco PA. Fabrication and characterization of permeable degradable poly(DL-lactide-co-glycolide) (PLGA) hollow fiber phase inversion membranes for use as nerve tract guidance channels. Biomaterials 2006 Jul;27(20):3800-3809.
86. Widmer MS, Gupta PK, Lu LC, Meszlenyi RK, Evans GRD, Brandt K, et al. Manufacture of porous biodegradable polymer conduits by an extrusion process for guided tissue regeneration. Biomaterials 1998 Nov;19(21):1945-1955.
87. Davies OR, Lewis AL, Whitaker MJ, Tai HY, Shakesheff KM, Howdle SM. Applications of supercritical CO2 in the fabrication of polymer systems for drug delivery and tissue engineering. Advanced Drug Delivery Reviews 2008 Feb;60(3):373-387.
88. Wu LB, Ding JD. In vitro degradation of three-dimensional porous poly(D,L-lactide-co-glycolide) scaffolds for tissue engineering. Biomaterials 2004 Dec;25(27):5821-5830.
89. Wu LB, Zhang JC, Jing DY, Ding JD. "Wet-state" mechanical properties of three-dimensional polyester porous scaffolds. Journal of Biomedical Materials Research Part A 2006 Feb;76A(2):264-271.
90. Leung L, Chan C, Baek S, Naguib H. Comparison of morphology and mechanical properties of PLGA bioscaffolds. Biomedical Materials 2008 Jun;3(2).
91. Thomson RC, Yaszemski MJ, Powers JM, Mikos AG. Hydroxyapatite fiber reinforced poly(alpha-hydroxy ester) foams for bone regeneration. Biomaterials 1998 Nov;19(21):1935-1943.
92. Vaquette C, Frochot C, Rahouadj R, Muller S, Wang X. Mechanical and biological characterization of a porous poly-L-lactic acid-co-epsilon-caprolactone scaffold for tissue engineering. Soft Materials 2008;6(1):25-33.
93. Zhang JC, Wu LB, Jing DY, Ding JD. A comparative study of porous scaffolds with cubic and spherical macropores. Polymer 2005 Jun;46(13):4979-4985.
94. Gupta D, Tator CH, Shoichet MS. Fast-gelling injectable blend of hyaluronan and methylcellulose for intrathecal, localized delivery to the injured spinal cord. Biomaterials 2006 Apr;27(11):2370-2379.

95. Lesny P, De Croos J, Pradny M, Vacik J, Michalek J, Woerly S, et al. Polymer hydrogels usable for nervous tissue repair. 2002; 2002. p. 243-247.
96. Nisbet DR, Moses D, Gengenbach TR, Forsythe JS, Finkelstein DI, Horne MK. Enhancing neurite outgrowth from primary neurones and neural stem cells using thermoresponsive hydrogel scaffolds for the repair of spinal cord injury. Journal of Biomedical Materials Research Part A 2009 Apr;89A(1):24-35.
97. Woerly S, Doan V, Evans-Martin F, Paramore CG, Peduzzi JD. Spinal cord reconstruction using NeuroGel (TM) implants and functional recovery after chronic injury. Journal of Neuroscience Research 2001 Dec;66(6):1187-1197.
98. Woerly S, Pinet E, de Robertis L, Van Diep D, Bousmina M. Spinal cord repair with PHPMA hydrogel containing RGD peptides (NeuroGel (TM)). Biomaterials 2001 May;22(10):1095-1111.
99. Carone TW, Hasenwinkel JM. Mechanical and morphological characterization of homogeneous and bilayered poly(2-hydroxyethyl methacrylate) scaffolds for use in CNS nerve regeneration. Journal of Biomedical Materials Research Part B-Applied Biomaterials 2006 Aug;78B(2):274-282.
100. Bamber NI, Li HY, Lu XB, Oudega M, Aebischer P, Xu XM. Neurotrophins BDNF and NT-3 promote axonal re-entry into the distal host spinal cord through Schwann cell-seeded mini-channels. European Journal of Neuroscience 2001 Jan;13(2):257-268.
101. Xu XM, Guenard V, Kleitman N, Aebischer P, Bunge MB. COMBINATION OF BDNF AND NT-3 PROMOTES SUPRASPINAL AXONAL REGENERATION INTO SCHWANN-CELL GRAFTS IN ADULT-RAT THORACIC SPINAL-CORD. Experimental Neurology 1995 Aug;134(2):261-272.
102. Sander EA, Alb AM, Nauman EA, Reed WF, Dee KC. Solvent effects on the microstructure and properties of 75/25 poly(D,L-lactide-co-glycolide) tissue scaffolds. Journal of Biomedical Materials Research Part A 2004;70A(3):506-513.
103. Moore MJ, Friedman JA, Lewellyn EB, Mantila SM, Krych AJ, Ameenuddin S, et al. Multiple-channel scaffolds to promote spinal cord axon regeneration. Biomaterials 2006;27(3):419-429.
104. Rowlands AS, Lim SA, Martin D, Cooper-White JJ. Polyurethane/poly(lactic-co-glycolic) acid composite scaffolds fabricated by thermally induced phase separation. Biomaterials 2007;28(12):2109-2121.
105. Sundback C, Hadlock T, Cheney M, Vacanti J. Manufacture of porous polymer nerve conduits by a novel low-pressure injection molding process. Biomaterials 2003;24(5):819-830.
106. Wan ACA, Mao HQ, Wang S, Leong KW, Ong L, Yu H. Fabrication of poly(phosphoester) nerve guides by immersion precipitation and the control of porosity. Biomaterials 2001 May;22(10):1147-1156.
107. Khang G, Kim MS, Lee HB. A Manual for Biomaterials/Scaffold Fabrication Techology. Singapore: World Scientific Publishing Co. Pte. Ltd, 2007.
108. Tuzlakoglu K, Reis RL. Biodegradable Polymeric Fiber Structures in Tissue Engineering. Tissue Engineering Part B-Reviews 2009;15(1):17-27.
109. Murugan R, Ramakrishna S. Nano-featured scaffolds for tissue engineering: A review of spinning methodologies. Tissue Engineering 2006;12(3):435-447.

110. Jessop P, Leitner W. Chemical Synthesis using supercritical fluids: Weinheim: Wiley-VCH, 1999.
111. Goel SK, Beckman EJ. GENERATION OF MICROCELLULAR POLYMERIC FOAMS USING SUPERCRITICAL CARBON-DIOXIDE .1. EFFECT OF PRESSURE AND TEMPERATURE ON NUCLEATION. Polymer Engineering and Science 1994 Jul;34(14):1137-1147.
112. Sun XH, Liu HJ, Li G, Liao X, He JS. Investigation on the cell nucleation and cell growth in microcellular foaming by means of temperature quenching. Journal of Applied Polymer Science 2004 Jul;93(1):163-171.
113. Mooney DJ, Baldwin DF, Suh NP, Vacanti LP, Langer R. Novel approach to fabricate porous sponges of poly(D,L-lactic-co-glycolic acid) without the use of organic solvents. Biomaterials 1996;17(14):1417-1422.
114. Quirk RA, France RM, Shakesheff KM, Howdle SM. Supercritical fluid technologies and tissue engineering scaffolds. Current Opinion in Solid State & Materials Science 2004;8(3-4):313-321.
115. Koegler WS, Patrick C, Cima MJ, Griffith LG. Carbon dioxide extraction of residual chloroform from biodegradable polymers. Journal of Biomedical Materials Research 2002 Oct;63(5):567-576.
116. FDA. Guidance for Industry Q3C Impurities: Residual Solvents. 2003 [cited; Available from: http://www.fda.gov/cber/gdlns/q3cresolvent.htm
117. Dillow AK, Dehghani F, Hrkach JS, Foster NR, Langer R. Bacterial inactivation by using near- and supercritical carbon dioxide. Proceedings of the National Academy of Sciences of the United States of America 1999 Aug;96(18):10344-10348.
118. Wang W, Itoh S, Matsuda A, Aizawa T, Demura M, Ichinose S, et al. Enhanced nerve regeneration through a bilayered chitosan tube: The effect of introduction of glycine spacer into the CYIGSK sequence. Journal of Biomedical Materials Research Part A 2008 Jun;85A(4):919-928.
119. Kawaguchi S, Nakamura T, Shimizu Y, Masuda T, Takigawa T, Liu Y, et al. Mechanical properties of artificial tracheas composed of a mesh cylinder and a spiral stent. Biomaterials 2001 Dec;22(23):3085-3090.
120. Durect. Chemical and Physical Properties. 2009 [cited; Available from: http://www.absorbables.com/properties.htm
121. Gibson LJ AM. Cellular Solids: structure and properties. Second ed. Cambridge: Cambridge University Press, 1999.
122. Liu DH, Tomasko DL. Carbon dioxide sorption and dilation of poly(lactide-co-glycolide). Journal of Supercritical Fluids 2007 Jan;39(3):416-425.
123. Pini R, Storti G, Mazzotti M, Tai HY, Shakesheff KM, Howdle SM. Sorption and swelling of poly(DL-lactic acid) and poly(lactic-co-glycolic acid) in supercritical CO2: An experimental and modeling study. Journal of Polymer Science Part B-Polymer Physics 2008 Mar;46(5):483-496.
124. Reverchon E, Cardea S. Production of controlled polymeric foams by supercritical CO2. Journal of Supercritical Fluids 2007 Feb;40(1):144-152.
125. Watkins J. Structure and Function of the Musculoskeletal System: Human Kinetics, 1999.

126. Holy CE, Dang SM, Davies JE, Shoichet MS. In vitro degradation of a novel poly(lactide-co-glycolide) 75/25 foam. Biomaterials 1999 Jul;20(13):1177-1185.
127. Lu L, Garcia CA, Mikos AG. In vitro degradation of thin poly(DL-lactic-co-glycolic acid) films. Journal of Biomedical Materials Research 1999 Aug;46(2):236-244.
128. Zhang R, PX M. Composite scaffolds for bone tissue engineering:degradation. 47th Annual Meeting,Orthopaedic Research Society; 2001; San Francisco, CA; 2001. p. 632.
129. Batich C, Leamy P. Standard Handbook of Biomedical Engineering and Design. In: Kutz M, editor. Biopolymers: McGraw-Hill, 2003.
130. Williams DF. BIODEGRADATION OF SURGICAL POLYMERS. Journal of Materials Science 1982;17(5):1233-1246.
131. Zeschky J, Lo JSH, Scheffler M, Hoeppel HW, Arnold M, Greil P. Polysiloxane-derived ceramic foam for the reinforcement of Mg alloy. Zeitschrift Fur Metallkunde 2002 Aug;93(8):812-818.
132. Athanasiou KA, Agrawal CM, Barber FA, Burkhart SS. Orthopaedic applications for PLA-PGA biodegradable polymers. Arthroscopy-the Journal of Arthroscopic and Related Surgery 1998 Oct;14(7):726-737.
133. Borgens RB, Shi RY, Bohnert D. Behavioral recovery from spinal cord injury following delayed application of polyethylene glycol. Journal of Experimental Biology 2002 Jan;205(1):1-12.
134. Cai J, Peng XJ, Nelson KD, Eberhart R, Smith GM. Permeable guidance channels containing microfilament scaffolds enhance axon growth and maturation. Journal of Biomedical Materials Research Part A 2005 Nov;75A(2):374-386.
135. Chang CJ, Hsu SH. The effect of high outflow permeability in asymmetric poly(DL-lactic acid-co-glycolic acid) conduits for peripheral nerve regeneration. Biomaterials 2006 Oct;27(7):1035-1042.
136. Chang CJ, Hsu SH, Yen HJ, Chang H, Hsu SK. Effects of unidirectional permeability in asymmetric poly(DL-lactic acid-co-glycolic acid) conduits on peripheral nerve regeneration: An in vitro and in vivo study. Journal of Biomedical Materials Research Part B-Applied Biomaterials 2007 Oct;83B(1):206-215.
137. Duerstock BS, Borgens RB. Three-dimensional morphometry of spinal cord injury following polyethylene glycol treatment. Journal of Experimental Biology 2002 Jan;205(1):13-24.
138. Evans GRD, Brandt K, Katz S, Chauvin P, Otto L, Bogle M, et al. Bioactive poly(L-lactic acid) conduits seeded with Schwann cells for peripheral nerve regeneration. Biomaterials 2002;23(3):841-848.
139. Falk RF, Randolph TW. Process variable implications for residual solvent removal and polymer morphology in the formation of gentamycin-loaded poly(L-lactide) microparticles. Pharmaceutical Research 1998 Aug;15(8):1233-1237.
140. Goel SK, Beckman EJ. GENERATION OF MICROCELLULAR POLYMERIC FOAMS USING SUPERCRITICAL CARBON-DIOXIDE .2. CELL-GROWTH AND SKIN FORMATION. Polymer Engineering and Science 1994 Jul;34(14):1148-1156.
141. Grizzi I, Garreau H, Li S, Vert M. HYDROLYTIC DEGRADATION OF DEVICES BASED ON POLY(DL-LACTIC ACID) SIZE-DEPENDENCE. Biomaterials 1995;16(4):305-311.

142. Guan LM, Davies JE. Preparation and characterization of a highly macroporous biodegradable composite tissue engineering scaffold. Journal of Biomedical Materials Research Part A 2004 Dec;71A(3):480-487.
143. Herberger J, Murphy K, Munyakazi L, Cordia J, Westhaus E. Carbon dioxide extraction of residual solvents in poly(lactide-co-glycolide) microparticles. Journal of Controlled Release 2003 Jun;90(2):181-195.
144. Huang YY, Qi M, Zhang M, Liu HZ, Yang DZ. Degradation mechanisms of poly (lactic-co-glycolic acid) films in vitro under static and dynamic environment. 2006; 2006. p. S293-S297.
145. Ikada Y. Scope of Tissue Engineering. Tissue Engineering: Fundamentals and Applications. The Netherlands: Elsevier Ltd, 2006.
146. Kataoka K, Suzuki Y, Kitada M, Hashimoto T, Chou H, Bai HL, et al. Alginate enhances elongation of early regenerating axons in spinal cord of young rats. Tissue Engineering 2004 Mar-Apr;10(3-4):493-504.
147. Kataoka K, Suzuki Y, Kitada M, Ohnishi K, Suzuki K, Tanihara M, et al. Alginate, a bioresorbable material derived from brown seaweed, enhances elongation of amputated axons of spinal cord in infant rats. Journal of Biomedical Materials Research 2001 Mar;54(3):373-384.
148. Kohama I, Lankford KL, Preiningerova J, White FA, Vollmer TL, Kocsis JD. Transplantation of cryopreserved adult human Schwann cells enhances axonal conduction in demyelinated spinal cord. Journal of Neuroscience 2001;21(3):944-950.
149. Leung L, Chan C, Song J, Tam B, Naguib H. A parametric study on the processing and physical characterization of PLGA 50/50 bioscaffolds. Journal of Cellular Plastics 2008 May;44(3):189-202.
150. Li XK, Cai SX, Liu B, Xu ZL, Dai XZ, Ma KW, et al. Characteristics of PLGA-gelatin complex as potential artificial nerve scaffold (vol 57, pg 198, 2007). Colloids and Surfaces B-Biointerfaces 2007 Oct;59(2):224-224.
151. Lu P, Tuszynski MH. Growth factors and combinatorial therapies for CNS regeneration. Experimental Neurology 2008 Feb;209(2):313-320.
152. Luo Y, Shoichet MS. A photolabile hydrogel for guided three-dimensional cell growth and migration. Nature Materials 2004 Apr;3(4):249-253.
153. Ma PX, Zhang RY. Microtubular architecture of biodegradable polymer scaffolds. Journal of Biomedical Materials Research 2001 Sep;56(4):469-477.
154. Menei P, Montero-Menei C, Whittemore SR, Bunge RP, Bunge MB. Schwann cells genetically modified to secrete human BDNF promote enhanced axonal regrowth across transected adult rat spinal cord. European Journal of Neuroscience 1998;10(2):607-621.
155. Mikos AG, Lyman MD, Freed LE, Langer R. WETTING OF POLY(L-LACTIC ACID) AND POLY(DL-LACTIC-CO-GLYCOLIC ACID) FOAMS FOR TISSUE-CULTURE. Biomaterials 1994 Jan;15(1):55-58.
156. Müller R-J. Handbook of Biodegradable Polymers. In: Bastioli C, editor. Biodegradation Behaviour of Polymers in Liquid Environments: Smithers Rapra Technology, 2005.
157. Ngo TTB, Waggoner PJ, Romero AA, Nelson KD, Eberhart RC, Smith GM. Poly(L-lactide) microfilaments enhance peripheral nerve regeneration across extended nerve lesions. Journal of Neuroscience Research 2003 Apr;72(2):227-238.

158. Pasquali I, Bettini R. Are pharmaceutics really going supercritical? International Journal of Pharmaceutics 2008 Dec;364(2):176-187.
159. Roark Raymond J YWC. Formulas for Stress and Strain. Fifth ed: McGraw-Hill Book Company, 1975.

160. Rolls A, Shechter R, Schwartz M. NEURON - GLIA INTERACTIONS - OPINION The bright side of the glial scar in CNS repair. Nature Reviews Neuroscience 2009 Mar;10(3):235-U291.
161. Rosner BI, Siegel RA, Grosberg A, Tranquillo RT. Rational design of contact guiding, neurotrophic matrices for peripheral nerve regeneration. Annals of Biomedical Engineering 2003 Dec;31(11):1383-1401.
162. Suzuki K, Suzuki Y, Ohnishi K, Endo K, Tanihara M, Nishimura Y. Regeneration of transected spinal cord in young adult rats using freeze-dried alginate gel. Neuroreport 1999 Sep;10(14):2891-2894.
163. Suzuki Y, Kitaura M, Wu SF, Kataoka K, Suzuki K, Endo K, et al. Electrophysiological and horseradish peroxidase-tracing studies of nerve regeneration through alginate-filled gap in adult rat spinal cord. Neuroscience Letters 2002 Feb;318(3):121-124.
164. Temtem M, Casimiro T, Aguiar-Ricardo A. Solvent power and depressurization rate effects in the formation of polysulfone membranes with CO2-assisted phase inversion method. Journal of Membrane Science 2006 Oct;283(1-2):244-252.
165. Tsai EC, Krassioukov AV, Tator CH. Corticospinal regeneration into lumbar grey matter correlates with locomotor recovery after complete spinal cord transection and repair with peripheral nerve grafts, fibroblast growth factor 1 fibrin glue, and spinal fusion. Journal of Neuropathology and Experimental Neurology 2005 Mar;64(3):230-244.
166. Wen XJ, Tresco PA. Effect of filament diameter and extracellular matrix molecule precoating on neurite outgrowth and Schwann cell behavior on multifilament entubulation bridging device in vitro. Journal of Biomedical Materials Research Part A 2006;76A(3):626-637.
167. Willerth SM, Sakiyama-Elbert SE. Approaches to neural tissue engineering using scaffolds for drug delivery. Advanced Drug Delivery Reviews 2007 May;59(4-5):325-338.
168. Wu LB, Ding JD. Effects of porosity and pore size on in vitro degradation of three-dimensional porous poly(D,L-lactide-co-glycolide) scaffolds for tissue engineering. Journal of Biomedical Materials Research Part A 2005 Dec;75A(4):767-777.
169. Xu Q, Ren XW, Chang YN, Wang JW, Yu L, Dean K. Generation of microcellular biodegradable polycaprolactone foams in supercritical carbon dioxide. Journal of Applied Polymer Science 2004 Oct;94(2):593-597.
170. Yang F, Cui WJ, Xiong Z, Liu L, Bei JZ, Wang SG. Poly(L,L-lactide-co-glycolide)/tricalcium phosphate composite scaffold and its various changes during degradation in vitro. Polymer Degradation and Stability 2006 Dec;91(12):3065-3073.
171. Yang F, Murugan R, Ramakrishna S, Wang X, Ma YX, Wang S. Fabrication of nano-structured porous PLLA scaffold intended for nerve tissue engineering. Biomaterials 2004 May;25(10):1891-1900.

172. Yang F, Murugan R, Wang S, Ramakrishna S. Electrospinning of nano/micro scale poly(L-lactic acid) aligned fibers and their potential in neural tissue engineering. Biomaterials 2005 May;26(15):2603-2610.
173. Yang SF, Leong KF, Du ZH, Chua CK. The design of scaffolds for use in tissue engineering. Part 1. Traditional factors. Tissue Engineering 2001 Dec;7(6):679-689.
174. Yu LMY, Leipzig ND, Shoichet MS. Promoting neuron adhesion and growth. Materials Today 2008 May;11(5):36-43.
175. Zee Mvd. Handbook of Biodegradable Polymers. In: Bastioli C, editor. Biodegradability of Polymers – Mechanisms and Evaluation Methods: Smithers Rapra Technology, 2005.
176. Zhang J, Davis TA, Matthews MA, Drews MJ, LaBerge M, An YHH. Sterilization using high-pressure carbon dioxide. Journal of Supercritical Fluids 2006 Oct;38(3):354-372